8-16-2013 12:00 AM

# Reduced Order Estimation of Time Varying Wireless Channels in Real Life Scattering Environment

Elena Uchiteleva
*The University of Western Ontario*

Supervisor
Dr. S. Primak
*The University of Western Ontario*

Graduate Program in Electrical and Computer Engineering
A thesis submitted in partial fulfillment of the requirements for the degree in Master of Engineering Science

# Reduced Order Estimation of Time Varying Wireless Channels in Real Life Scattering Environment

(Thesis format: Monograph)

by

Elena Alexandrovna Uchiteleva

Graduate Program
in
Electrical and Computer Engineering
Department of Electrical and Computer Engineering

A thesis submitted in partial fulfillment
of the requirements for the degree of
Master of Engineering Science

School of Graduate and Postdoctoral Studies
The University of Western Ontario
London, Ontario, Canada

# Abstract

This thesis deals with theoretical study and numerical simulation of $2 \times 1$ MISO system with Alamouti coding and imperfect channel estimation at the receiver. We adopt two channel models to represent scattering environment. One is Sum of Sinusoids model, which is simple, but does not properly reflect the geometry of scattering environment. The second model uses a set of Modulated Discrete Prolate Spheroidal Sequences to represent the channel in a scenario with scattering from one or more clusters with predefined geometry. The effect of clusters location on estimation quality is examined. Furthermore, we derive reduced complexity Wiener filters for slow flat fading channel estimation in pilot aided receiver. Our approach is based on the approximation of the channel covariance function to zero and second order Taylor series to reduce computational effort of the filter design. Theoretical MMSE is developed, verified through simulation and compared to one of a full Wiener filter.

**Keywords**: Alamouti coding, MIMO channels, scattering, DPSS, channel estimation, Wiener filter, STTD, STBC

# Acknowledgements

I would like to thank my supervisor Dr. S. Primak for inviting me into his research group in 2011. I am grateful for his valuable guidance, advice, motivation and financial support throughout the program, which made this thesis possible. I had really great time during the course of this work and I really appreciate the priceless knowledge that he shared with me, his dedication and generosity with his time in helping me. I have learned a lot, I have increased my research abilities, and I have professionally grown during my Master's degree. Thank you Dr. Primak.

I would also like to thank the Examining Board, Dr. A. Shami, Dr. R. K. Rao and Dr. H. Hong, for their time to review and examine my thesis work, and Dr. X. Wang for being the Chair of Examining Board during my defense.

I would also like to thank my amazing family, Nadia and Alexander, Sveta, Dan and Junior Dan for their love and believing in me throughout these not easy times, for all they do and for always being ready to help. Please do not ever change. After all these years of living apart in different countries on different continents it was wonderful to finally have all my family all together at the same city of London. I love you.

I would also like to extend my thanks to Lyudmil Marinov and Dr. H. Ladak for being great mentors during my Teaching Assistance work. Your guidance and instructions were always of a great help, which I sincerely appreciate.

I would especially like to thank my colleague and a friend Oscar Filio ("Bro Oscar") for having such a great and positive personality, for his friendship and support through this time. Also, timely little coffee breaks with peers are very important for the progress of the research as they give not only the essential mind rest and recharge (which in turn increase productivity) but also an opportunity to share the knowledge and ideas with others. Thank you Oscar for all that good advice and pointers you gave me during our coffee breaks and for always being such an interesting and fun companion. I am glad to have a friend like you.

I would also like to thank all other colleagues and friends from the Engineering Department: Dan Dechene ("The Bro"), Marco Luccini ("Fratello"), Mohamad Kalil ("Bro Mohamad"), Siamack Ghadimi ("Bro Siamack"), Maysam Mirahmadi ("Bro Maysam"), Jason Gejie Liu ("Bro Jason"), Elham Dolatabadi, Duane Jacques, Aidin

Reyhani, Eric Southern, Brigitte Kok Madsen, Mohammad Abusharkh, Karim Hammad, Dan Wallace, Manar Jammal and Kevin Mi. Thank you guys for creating such a nice and warm work environment.

And let me not forget to thank Western Student Recreation Centre for providing excellent sport facilities, which helped me to maintain my good health and shape during my research work at Western. As an old saying goes, *a sound mind in a sound body*.

*To my loving parents Nadia and Alexander*

# Table of Contents

# List of Tables

# List of Figures

# Acronyms

| | |
|---|---|
| **AFD** | *Average Fade duration* |
| **AoA** | *Angle of Arrival* |
| **AoD** | *Angle of Departure* |
| **AWGN** | *Additive White Gaussian Noise* |
| **BEP** | *Bit Error Probability* |
| **BER** | *Bit Error Rate* |
| **BS** | *Base Station* |
| **BPSK** | *Binary Phase Shift Keying* |
| **CSI** | *Channel State Information* |
| **FIR** | *Finite Impulse Response* |
| **IIR** | *Infinite Impulse Response* |
| **LCR** | *Level Crossing Rate* |
| **LoS** | *Line of Sight* |
| **LSE** | *Least-Squares Estimate* |
| **MDPSS** | *Modulated Discrete Prolate Spheroidal Sequences* |
| **MIMO** | *Multiple Input Multiple Output* |
| **MISO** | *Multiple Input Single Output* |
| **ML** | *Maximum Likelihood* |
| **MMSE** | *Minimum Mean Square Error* |
| **MS** | *Mobile Station* |
| **MSS** | *Moderate Spatial Scale* |
| **MVU** | *Minimum Variance Unbiased* |
| **PDF** | *Probability Density Function* |
| **PDP** | *Power Delay Profile* |
| **PSAM** | *Pilot Symbol Assisted Modulation* |
| **PSD** | *Power Spectrum Density* |

| | |
|---|---|
| **Rx** | *Receiving Side* |
| **RMS** | *Root Mean Square* |
| **RS-GBM** | *Regular-Shaped Geometry Based Stochastic Model* |
| **SISO** | *Single Input Single Output* |
| **SNR** | *Signal to Noise Ratio* |
| **SoS** | *Sum of Sinusoids* |
| **SSS** | *Small Spatial Scale* |
| **STBC** | *Space-Time Block Coding* |
| **STTD** | *Space-Time Transmit Diversity* |
| **Tx** | *Transmitting Side* |
| **V2I** | *Vehicle to Infrastructure* |
| **V2V** | *Vehicle to Vehicle* |
| **WSS** | *Wide-Sense Stationary* |

# Chapter 1
# Introduction

Radio transmission system simulators play a very important role in development of wireless communications. They allow us to perform numerous tests in lab conditions with fewer time and cost demands than field experiments [1]. While significant efforts have been invested in this problem, increasing sophistication of systems and different conditions of their deployment call for continuous additional efforts in modeling of every single stage of communication stage: from channel modeling and its estimation to information coding and modulation schemes.

## 1.1 Channel Simulators

Proper simulation of characteristics of wireless channels is of a great interest and relevance for design of communication systems. Numerous techniques and models have been proposed to describe fading channels in different scenarios. We consider the case of communication in the urban area, where the received signal is a combination of rays reflected/diffracted from the different obstacles and rough objects, which is called multipath [2]. Rayleigh fading is one of the most popular models for description of rich scattering environments [3]. The family of Sum of Sinusoids (SoS) simulators is frequently used to emulate flat-fading Rayleigh channels [4] - [5]. More about these channel simulators can be found in Chapter 2 of the thesis.

One of our goals is to simulate a complex scenario, with one or more rough clusters in scattering environment, which is characteristic to communication sites with different objects in surroundings, for example city or countryside streets. This scenarios feature the presence of specular components along with those of Line of Sight (LoS) and diffusive ones. The geometry-based model, which was adopted for this work, is described in Chapter 2. This model is represented by 4-dimensional

tensor of the channel response using Modulate Discrete Prolate Spheroidal Sequences (MDPSS) [6]. By modulation of the bandwidth of a set of DPSS [7] we achieve different scattering scenarios with parameters defined by theoretical models or/and measurements [6]. Application of this channel model allows us to evaluate the performance of different modulation schemes in different fading scenarios. Moreover aforementioned channel model is very flexible in definition of the geometry and location of different clusters what enables us to analyze various scattering scenarios of interest. At the same time, it allows us to define number of antennas along with velocities and movement directions of each communication side.

## 1.2 Space-Time Transmit Diversity Systems

The idea of Space-Time Block Coding (STBC) systems is to code modulated data stream in time and space (*i.e.* across different transmit antennas) and to transmit it block-wise via several complex symbol streams. At the receiver side these streams are detected, decoded and demodulated and the information is recovered. Such schemes increase system diversity what results in lower bit error rates, [2], [8]. At the same time, they firmly rely on the channel information at the receiver side. Therefore high quality channel estimation is of a great importance for these systems. Over the past two decades linear STBC have become very popular in both research and industrial communities and it is widely adopted in a number of global standards. Multiple Input Single Output (MISO) is a very common scenario in the downlink of a cellular system. Therefore in our project we focus on simple but yet one of the most elegant coding techniques for $2 \times 1$ MISO system, Alamouti scheme [9], which is used in some third/fourth generation wireless mobile standards and whose concept played an important role in consequent development of wireless communication industry. Linear combining scheme suggested by Alamouti is used for symbol detection and the Wiener filter is used as a pilot filter for channel gains estimation [10]. Detailed analysis of Alamouti coding is given in Chapter 3.

## 1.3 Channel Estimation

As it has been mentioned above, the Alamouti scheme (and many others) relies on accurate channel knowledge at the receiver side during the decoding stage, therefore channel estimation is essential for reliable performance of any such scheme. Channel estimation could be performed by sending a known signal (or pilot tone) parallel to the data sequence [11] - [12]. This technique utilizes a pilot tone to provide the receiver with explicit information about the phase and amplitude reference for the detection. However, it requires complex signal processing or an expensive spectrum allocation for the tone. Use of such technique is unpractical. Another method is to use previously detected symbols in order to estimate channel fluctuations [2], [13]. This technique does not need any pilot sequences for estimation, however it is prone to mistakes which can affect blocks and even frames of detected information. The most popular approach nowadays is estimation via training sequences (pilots) which are periodically inserted into the data stream. At the receiver pilots are accumulated and are used for calculation of channel gains via different pilot filters. The most common scheme in use is called Pilot Symbol Assisted Modulation (PSAM) [14], [10], [8]. In this work pilot-assisted estimation scheme is utilized and the estimation is done by means of the Wiener filter at the receiver side [10], [15]. Detailed analysis of the Wiener filter and its performance evaluation in different channel conditions are shown in Chapter 3.

## 1.4 Summary of Contribution

One of the goals of this work is to apply MDPSS channel model to simulate real environment containing several different clusters in vicinity of the mobile movement. As the outcome we expect to gain a deeper insight into performance of systems in different scatering environments. This approach is useful in Vehicle to Infrastructure (V2I) and, most importantly, in Vehicle to Vehicle (V2V) communication scenarios, as new channel models for precise emulation of complex urban environment are still on demand [16]. We show in Chapter 3 how one can use available online tools (like

Google Maps ©) in order to provide the mobile with accurate channel tracking as it moves through altering city environment. Several common real-life street scenarios are presented and analyzed. Extension to any other site geometries are straight forward.

The second main contribution of this thesis is development of reduced order Wiener filters for estimation of narrow-band slowly fading channels. It is well-known that if the observation of the process is made in Additive White Gaussian Noise (AWGN), Wiener filter is the optimal linear filter in minimum mean square root sense [17], [15]. However, full Wiener filter is difficult to implement especially for slow fading and uncertainty in knowledge of channel statistics, because it requires implementation of auto-covariance function of the channel process in order to calculate filter taps coefficients. Moreover, it is difficult to estimate channel auto-covariance function, and, once we know it, it is computationally inefficient to apply it for filter coefficients calculation, which is wasteful of battery energy of the mobile. Our approach is to suggest a reduced order (light) Wiener filter, which is based only on a partial knowledge of channel covariance function. More specifically, we develop a framework for analysis and design of filter coefficients for channel estimation by providing the theoretical performance, validated by the simulation, of $2 \times 1$ MISO Space-Time Transmit Diversity (STTD) system assuming imperfect Channel State Information (CSI) at the receiver in slowly varying channels, whilst we conjecture that in cases of highly correlated pilot signals, there is no need to calculate full covariance function of the process, in order to achieve good performance, and it is sufficient to provide its low order polynomial approximation. This assumption allows us to work with partially unknown channel statistics at the receiver and reduces computational effort, decreasing the delay and increasing a battery life of the devise. Analytical expressions for tap coefficients and Minimum Mean Square Error (MMSE) are derived for zero and second order Light Wiener filters, the results are validated by the simulation and compared.

## 1.5 Thesis Organization

The remainder of this thesis is organized as follows. In Chapter 2 SoS and MDPSS channel models and their implementations are discussed and verified. The description of STTD system with Alamouli coding and pilot-assisted channel estimation via full Wiener filter is provided in Chapter 3. At the same chapter the simulation of movement of mobile, equipped with aforementioned system, through an urban area is presented and analyzed. Several different scenarios of V2I and V2V communications are taken into consideration. In Chapter 4 theoretical derivation of Light Wiener filters is shown and verified by the simulation. The performances of both filters are compared to each other and to a full Wiener filter case. Finally in Chapter 5 conclusions are derived and future work directions are discussed.

# Chapter 2
# Channel Models

Wireless channel simulators are widely used for reproducing channel behavior during the signal transmission over propagation medium. They gained popularity because they allow us to evaluate systems in lab conditions, which is much easier and cheaper than running field experiments. There are many statistical models known nowadays for description of multi-path fading behavior of channels. For example, Rayleigh fading model is the most frequently used one due to its simplicity. This model is based on the assumption that the signal arrives to the receiver via many independent paths, which are uniformly distributed around the receiver, with random phase and gain. According to Central Limit Theorem in this case the channel impulse response converges to a circularly symmetric complex Gaussian process with zero mean [2]. A more complex statistical model for this scenario is Nakagami-m distribution [18], which is more flexible and accurate in matching the statistics of the channel. Another frequently used exemplar is Rician fading model, in which along with large number of scuttered components, there is not negligible specular path (or Line of Sight component), which has some known magnitude. A statistical model due to Clarke, which is widely used to describe flat fading Rayleigh distributed channels whose autocorrelation function is Bessel function of first kind and zero order, and its simplified version Jake's simulation model. Weichselberger model which describes Multiple Input Multiple Output (MIMO) link with cross-correlation between antenna's elements and both link sides as well, Bello's model, Key-hole model, etc. All of these models are built to depict different types of channel environments.

In our work we use two different models: SoS model for representing Rayleigh flat fading channels [4] and MDPSS model for representing non-uniform scattering from one or more clusters or rough surfaces [6]. These models are sufficient to describe the most common real life scattering scenarios.

## 2.1 Sum of Sinusoids Model

Let us assume that the received signal can be represented in a baseband form as follows [2]:

$$y[m] = h[m]x[m] + w[m] \tag{2.1}$$

where $x[m]$ is an information bit, that one is interested to transmit, $w[m]$ is an additive Gaussian White noise, *i.e.* $w[m] \sim CN(0, N_0)$, $h[m]$ is a flat fading channel gain sample. The purpose of this section is to introduce simulational model which reproduces statistical properties of Clarke's mathematical reference model with a finite number of sinusoids. This model is used throughout our work to simulate flat-fading channels. The main characteristics, *i.e.* autocorrelations and cross-correlations of the quadrature components, autocorrelation of the complex envelope, Probability Density Functions (PDF) of envelope and phase, Level Crossing Rate (LCR), Average Fade Duration (AFD) and autocorrelation of the squared envelope of this model are discussed, compared to those of theoretical model and confirmed by the simulation. These characteristics are important to simulate as they represent major statistical properties of random channels, which are deduced from measurements of real life environment. Therefore an important purpose of channel simulators is to represent these statistical characteristics.

### 2.1.1 Rayleigh Fading and Clarke's model

One of the most common communication scenarios which might be found in urban and sub-urban areas is described by Mobile Station (MS) surrounded by rich scattering environment [1], see Fig. 2.1. In this kind of scenario there is no LoS component and scattered signal is seen by a MS as arriving from all directions Fig. 2.2.

According to Clarke's model [2], if number of scattered signal waves $N$ impinging on the receiver is very big, i.e. $N \to \infty$, channel gains process converges to Complex Circularly Symmetric Gaussian Process:

$$h(t) = h_R(t) + jh_I(t) \tag{2.2}$$

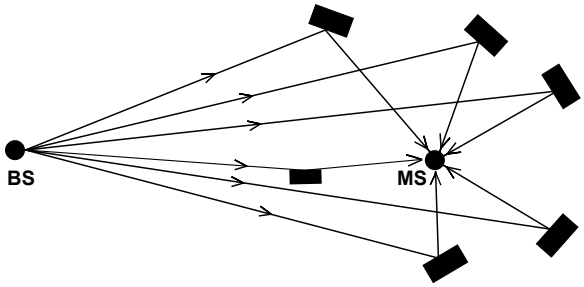


Figure 2.1: *Example of a rich scattering environment near MS*

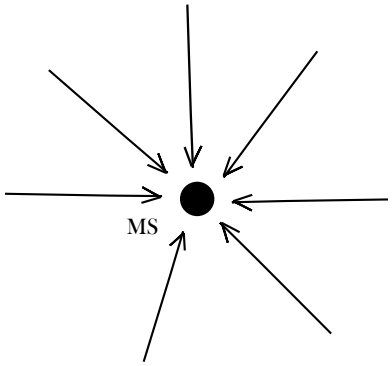


Figure 2.2: *A signal is seen by a MS as arriving from all directions*

Here the real and imaginary parts $h_R(t), h_I(t)$ are real Gaussian distributed processes with auto-correlation and cross-correlation functions described by:

$$R_{h_R h_R}(\tau) = \mathbb{E}\left[h_R(t) h_R(t+\tau)\right] = J_0(\omega_d \tau) \tag{2.3}$$

$$R_{h_R h_I}(\tau) = \mathbb{E}\left[h_R(t) h_I(t+\tau)\right] = 0 \tag{2.4}$$

Where $\mathbb{E}[\cdot]$ denotes expectation and $J_0(\cdot)$ denotes zero-order Bessel function of the first kind. Fading envelope of $h$ is Rayleigh distributed:

$$f_{|h|}(x) = \begin{cases} \frac{x}{\sigma^2} \exp\left(-\frac{x^2}{2\sigma^2}\right), & (0 \le x \le \infty) \\ 0, & (x < 0) \end{cases} \tag{2.5}$$

where $\sigma^2$ is the time-average of the received signal before envelope detection. The phase $\Theta_h(t)$ of the complex envelope is Uniformly distributed:

$$f_{\Theta_h}(\theta_h) = \frac{1}{2\pi}, \qquad -\pi \leq \theta_h < \pi \tag{2.6}$$

#### 2.1.1.1 Simulation Reference Model

According to [19] and [3] one may build a simulator for a frequency-nonselective Rayleigh fading channels as a sum of a finite number of periodic components with random phase and gain:

$$g(t) = E_0 \sum_{n=1}^{N} C_n \exp\left[j(\omega_d t \cos\alpha_n + \phi_n)\right] \tag{2.7}$$

Here $C_n$, $\alpha_n$ and $\phi_n$ are real valued random gain, angle and initial phase of the $n$'s path, $\omega_d$ is the maximum radian Doppler frequency, $E_0$ is a scaling constant and $N$ is a number of propagation paths. Then (2.7) might be written as a sum of a sine and cosine parts:

$$g(t) = g_c(t) + jg_s(t) \tag{2.8a}$$

$$g_c(t) = E_0 \sum_{n=1}^{N} C_n \cos\left(\omega_d t \cos\alpha_n + \phi_n\right) \tag{2.8b}$$

$$g_s(t) = E_0 \sum_{n=1}^{N} C_n \sin\left(\omega_d t \cos\alpha_n + \phi_n\right) \tag{2.8c}$$

According to Central Limit Theorem $g_c(t)$ and $g_s(t)$ converge to a Gaussian distributed random processes for large $N$. Assuming, that $\alpha_n$ and $\phi_n$ are Uniformly distributed over $[-\pi, \pi)$ for all $n$ and independent variables (according to Clark's model), one may derive the following desired second-order statistics (autocorrelation

and cross-correlation functions of sine and cosine terms) [19], [20]:

$$R_{g_c g_c}(\tau) = \mathbb{E}\left[g_c(t) g_c(t+\tau)\right] = J_0(\omega_d \tau) \tag{2.9a}$$

$$R_{g_s g_s}(\tau) = J_0(\omega_d \tau) \tag{2.9b}$$

$$R_{g_c g_s}(\tau) = 0 \tag{2.9c}$$

$$R_{g_s g_c}(\tau) = 0 \tag{2.9d}$$

$$R_{gg}(\tau) = \mathbb{E}\left[g(t) g^*(t+\tau)\right] = 2J_0(\omega_d \tau) \tag{2.9e}$$

$$R_{|g|^2|g|^2}(\tau) = 4 + 4J_0(\omega_d \tau) \tag{2.9f}$$

Without loss of generality we assume that $\sum_{n=1}^{N} \mathbb{E}\left[C_n^2\right] = 1$ and $E_0 = \sqrt{2}$. Hence it might be shown that PDFs of fading envelope $|g(t)|$ and the phase $\Theta_g(t)$ equal to:

$$f_{|g|}(x) = x \cdot \exp\left(-\frac{x^2}{2}\right), \qquad x \geqslant 0 \tag{2.10a}$$

$$f_{\Theta_g}(\theta_g) = \frac{1}{2\pi}, \qquad \theta_g \in [-\pi, \pi) \tag{2.10b}$$

Hence, the above model is clearly Rayleigh fading channel with Rayleigh distributed envelope and Uniformly distributed phase.

### 2.1.2 Jake's Model

In Jake's model it is assumed that [4]:

$$C_n = \frac{1}{\sqrt{N}} \tag{2.11a}$$

$$\alpha_n = \frac{2\pi n}{N}, \qquad n = 1, 2, \ldots, N \tag{2.11b}$$

$$\phi_n = 0, \qquad n = 1, 2, \ldots, N \tag{2.11c}$$

This simplifies the model and makes it deterministic [21]. Nevertheless, this model is wide sense non-stationary, when averaged over many channel realizations or non-ergodic [22]. Other issue is higher order statistics, which do not match the theoretical desired higher order statistics, even though infinitely large number of sinusoids is

taken. Hence, many other models were proposed as an improvement of Jake's model, what gave rise to a family of Jake's simulators (see [4] for more examples). Although some of these models succeed to eliminate the non-stationarity, they still did not match higher-order statistics (like autocorrelations and cross-correlations of the quadrature components or squared envelope) even when the number of sinusoids approaches infinity.

According to [4] with several modifications of Jake's model it is possible to achieve desired statistical requirements with quick convergence to a Rayleigh fading channel while using as small number of sinusoids as a single-digit integer and with only 50 random trials. This model might be used to generate not correlated waveforms for MIMO channel scenario.

### 2.1.3 Sum of Sinusoids Model with Correct Statistical Properties

The authors of [4] proposed a different approach by representing the definition of random variables $\alpha_n$, $\phi_n$ and $C_n$ as follows:

$$\tilde{C}_n = \frac{\exp(j\psi_n)}{\sqrt{N}}, \qquad n = 1, 2, \ldots, N \tag{2.12a}$$

$$\tilde{\alpha}_n = \frac{2\pi n - \pi + \theta}{N}, \qquad n = 1, 2, \ldots, N \tag{2.12b}$$

$$\tilde{\phi}_n = -\tilde{\phi}_{\frac{N}{2}+n} = \phi, \qquad n = 1, 2, \ldots, \frac{N}{2} \tag{2.12c}$$

Therefore simulation prototype function takes a form of:

$$\tilde{g}(t) = E_0 \sum_{n=1}^{N} \tilde{C}_n \exp\left[j(\omega_d t \cos\tilde{\alpha}_n + \tilde{\phi}_n)\right] \tag{2.13}$$

Here $\psi_n$, $\phi$ and $\theta$ uniformly distributed over $[-\pi, \pi)$ and mutually independent, $\frac{N}{2}$ is an integer. It might be shown that this model is Wide-Sense Stationary (WSS) model for Rayleigh fading channel. Then (2.13) is rearranged and simplified by choosing

$M = N/4$, and $\omega_n = \omega_d \cos\tilde{\alpha}_n$:

$$\hat{g}(t) = \frac{E_0}{\sqrt{N}} \sum_{n=1}^{M} \sqrt{2} e^{j\psi_n} \left[ e^{j(\omega_n t + \phi)} + e^{-j(\omega_n t + \phi)} \right] \tag{2.14}$$

Hence, the normalized low-pass fading process of SoS model might be written as:

$$X(t) = X_c(t) + jX_s(t) \tag{2.15a}$$

$$X_c(t) = \frac{2}{\sqrt{M}} \sum_{n=1}^{M} \cos(\psi_n) \cdot \cos(\omega_d t \cos\alpha_n + \phi) \tag{2.15b}$$

$$X_s(t) = \frac{2}{\sqrt{M}} \sum_{n=1}^{M} \sin(\psi_n) \cdot \cos(\omega_d t \cos\alpha_n + \phi) \tag{2.15c}$$

with

$$\alpha_n = \frac{2\pi n - \pi + \theta}{4M}, \qquad n = 1, 2, \ldots, N \tag{2.16}$$

It is shown in [4], that the theoretical values of auto-correlation and cross-correlation functions of imaginary and real parts of X(t), complex envelope and squared envelope are:

$$R_{X_c X_c}(\tau) = J_0(\omega_d \tau) \tag{2.17a}$$

$$R_{X_s X_s}(\tau) = J_0(\omega_d \tau) \tag{2.17b}$$

$$R_{X_c X_s}(\tau) = 0 \tag{2.17c}$$

$$R_{X_s X_c}(\tau) = 0 \tag{2.17d}$$

$$R_{XX}(\tau) = 2J_0(\omega_d \tau) \tag{2.17e}$$

$$\begin{aligned} R_{|X|^2|X|^2}(\tau) &= 4 + 4J_0^2(\omega_d \tau) + \frac{4 + 2J_0(2\omega_d \tau)}{M} \\ &= 4 + 4J_0^2(\omega_d \tau), \qquad \text{if } M \to \infty \end{aligned} \tag{2.17f}$$

As we may see, auto-correlation and cross-correlation functions (2.17a) - (2.17e) do not depend on number of sinusoids $M$ used in the model and match exactly the statistics of the reference model. Fourth order statistics (2.17f) match the desired ones when M approaches the infinity, and have a good approximation even when M

is as small as 8.

Then the PDFs of a fading envelope $|X(t)|$ and the phase $\Theta_X(t) = \arctan[X_c(t), X_s(t)]$ are presented, and it is also shown, that when $M$ approaches infinity, the envelope's PDF converges to Rayleigh distribution, and phase's PDF converges to Uniform over $[-\pi, \pi)$. Hence:

$$f_{|X|}(x) = x \cdot \exp\left(\frac{-x^2}{2}\right), \qquad x \geqslant 0 \tag{2.18a}$$

$$f_{\Theta_X(\theta_X)} = \frac{1}{2\pi}, \qquad \theta_X \in [-\pi, \pi) \tag{2.18b}$$

LCR is defined as the expected rate at which the Rayleigh fading envelope, normalized to the local Root Mean Square (RMS) signal level, crosses a specified threshold level $\rho$ in a positive slope, and the AFD is defined as an average time duration for which the fading envelope remains below some specified threshold $\rho$. Both these functions allow us to evaluate error statistics to provide an appropriate error-correction techniques. When $M$ approaches infinity, the LCR (or $L_{|X|}$) and AFD (or $T_{|X|}$) are described by:

$$L_{|X|} = \sqrt{2\pi}\rho f_d e^{-\rho^2} \tag{2.19a}$$

$$T_{|X|} = \frac{e^{\rho^2} - 1}{\rho f_d \sqrt{2\pi}} \tag{2.19b}$$

where $\rho$ is the normalized fading envelope level, $\rho = \dfrac{|X|}{|X|_{rms}}$, $|X|_{rms}$ is a root mean square envelope level.

### 2.1.4 Simulation Evaluation of SoS Model With Correct Higher Order Statistics

The evaluation of the properties of the proposed channel model (2.15) is based on the comparison with theoretical curves of a Rayleigh fading channel (2.7). We chose $M = 8$, the number of sinusoids, $f_d T_s = 0.025$, the normalized sampling period, and ensemble averages $K = 10, 50, 100$ of random trials, as indicated in plots below.

#### 2.1.4.1 Autocorrelation and Cross-correlation Functions

The simulation results of auto-correlation of real and imaginary parts are shown in Figs. 2.3-2.4, cross-correlation between imaginary and real parts of the simulator are shown in Fig. 2.5. Then real and imaginary parts of the auto-correlation function of the complex fading channel are shown in Figs. 2.6-2.7. The auto-correlation of the squared envelope, $R_{|X|^2|X|^2}$ is plotted in Fig. 2.8. As we may see, there is a good agreement between the simulated results and the reference even though the number of sinusoids used in simulation is only 8 and number of random trials is only 50. With greater number of trials for averaging we may achieve better match with theoretical curves.

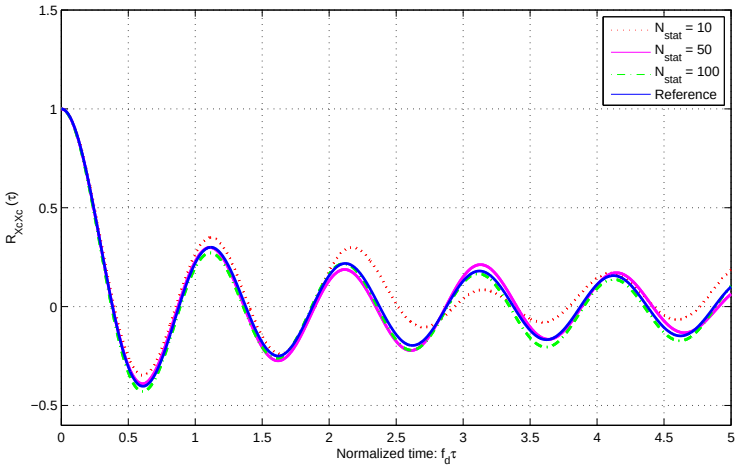


Figure 2.3: *Autocorrelation of the simulated real part of $X(t)$, $X_c(t)$. $N_{stat}$ denote the number of random trials*

#### 2.1.4.2 PDF of the Envelope and the Phase

The Probability Density Functions of the envelope $|X(t)|$ and the phase of the fading simulator are shown in figures (2.9) and (2.10). As we may see in case of the fading envelope there is a very good convergence to the theoretical curve, when the number of random trials is only 10. The PDF of the phase though is more sensitive to the number of trials.

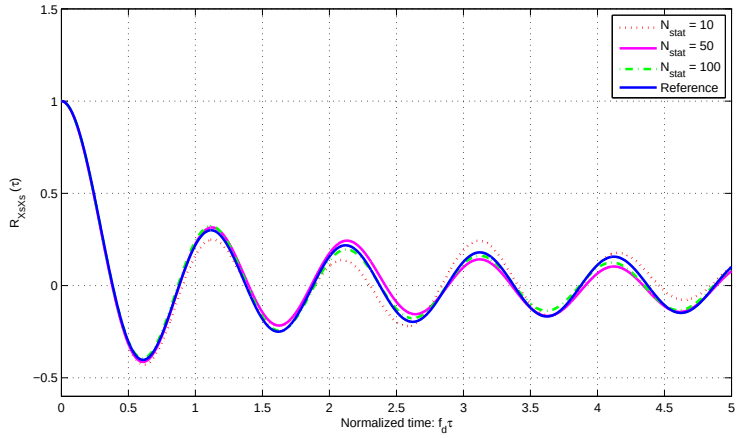


Figure 2.4: *Autocorrelation of the imaginary part of the simulated channel,* $X_s(t)$.

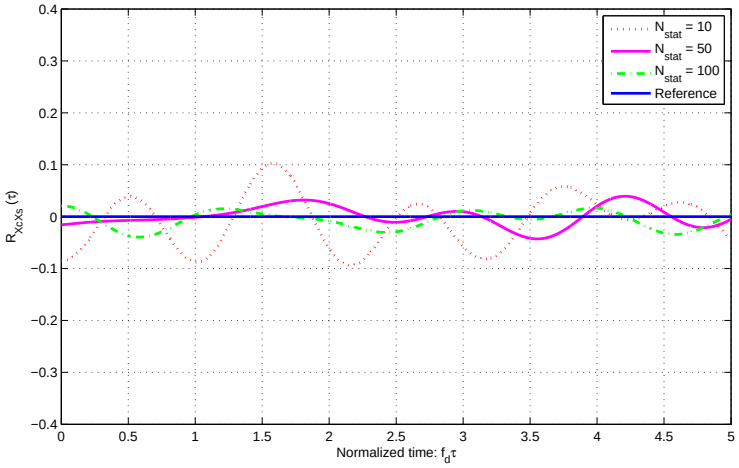


Figure 2.5: *Cross-correlation of the real and imaginary parts of the simulated channel.*

#### 2.1.4.3 LCR and AFD evaluation

LCR and AFD are shown in Figs. 2.11 - 2.12. Again we may observe a very good agreement with the theory for already 10 random trials.

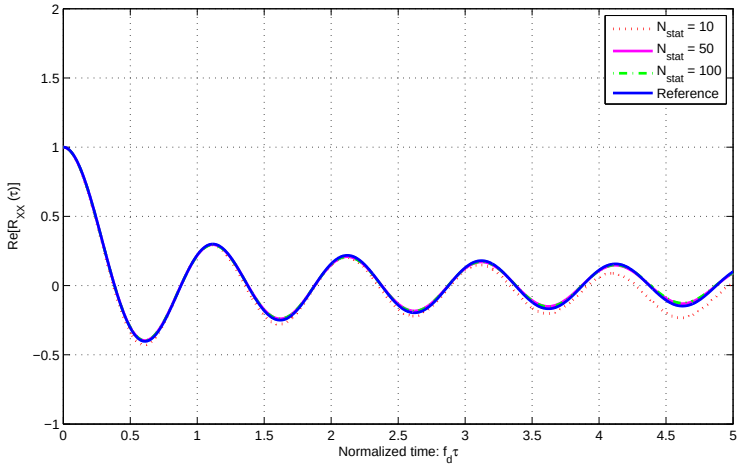


Figure 2.6: *The real part of the autocorrelation of the complex envelope* $X(t)$*,* $Re[R_{XX}]$*.*

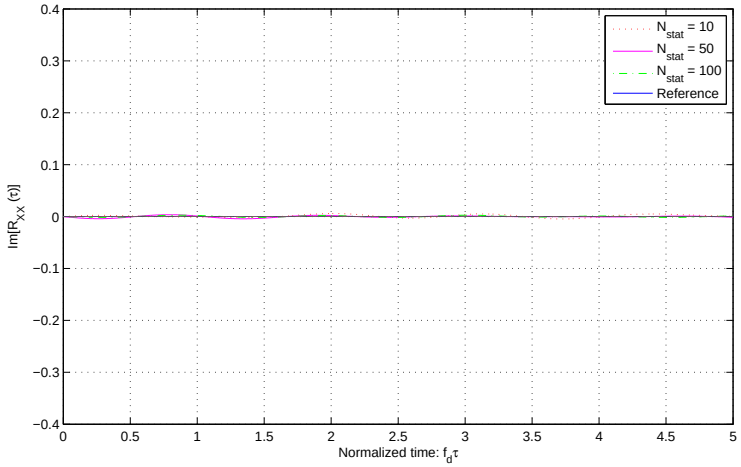


Figure 2.7: *The imaginary part of the autocorrelation of the complex channel envelope* $X(t)$*,* $Im[R_{XX}]$*.*

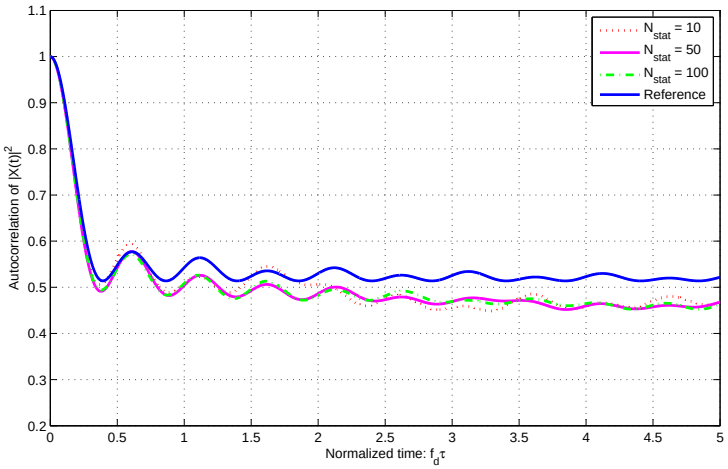


Figure 2.8: *The autocorrelation of a squared envelope of the fading channel* $X(t)$, $R_{|X|^2|X|^2}$.

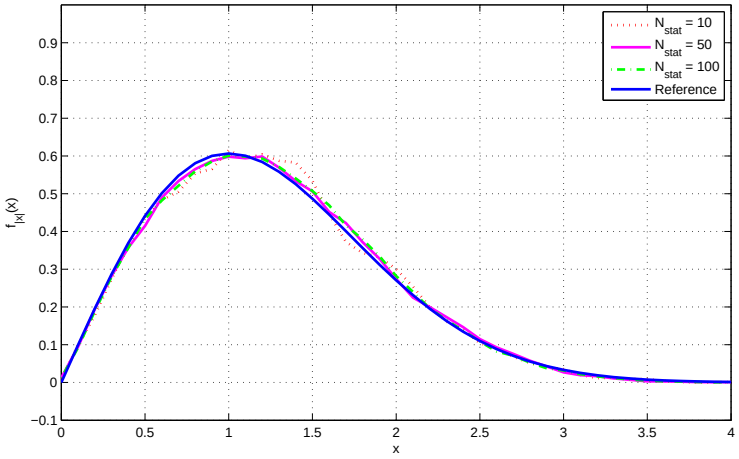


Figure 2.9: *The PDF of the envelope of the fading channel simulator* $X(t)$, $f_{|X|(x)}$.

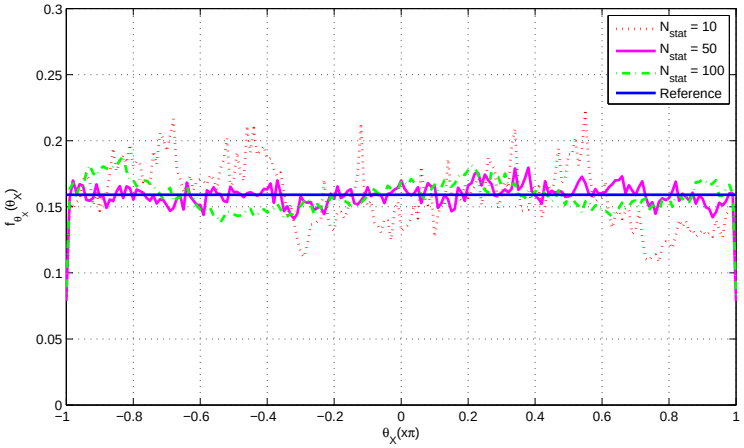


Figure 2.10: *The PDF of the phase of the fading channel simulator* $X(t)$, $f_{\Theta_x(\Theta_x)}$.

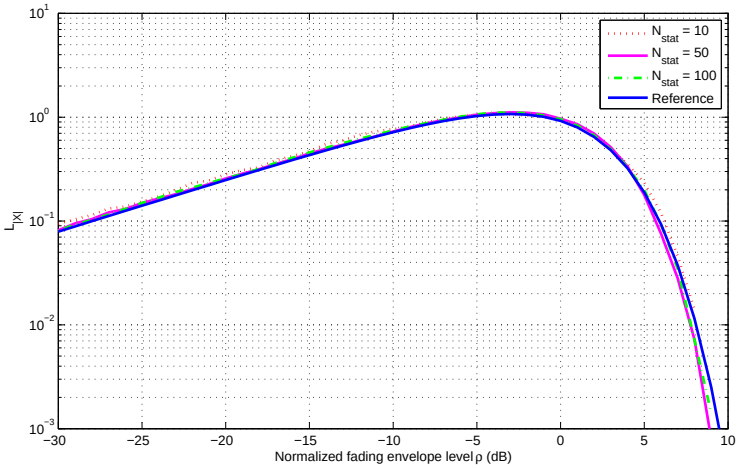


Figure 2.11: *The LCR of the simulated envelope* $|X(t)|$

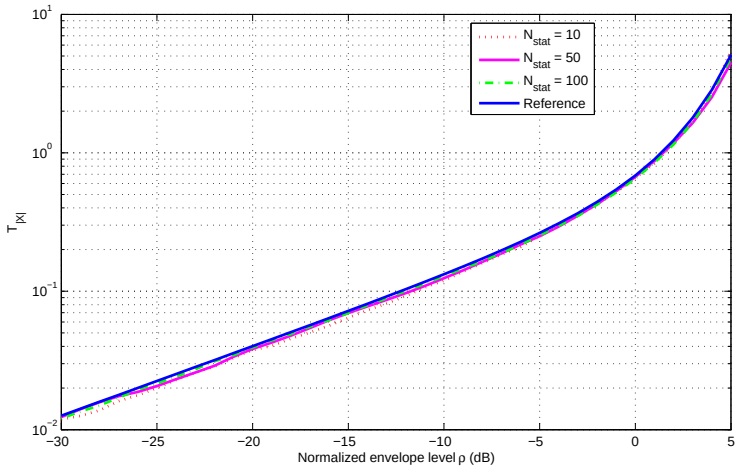


Figure 2.12: *The AFD of the simulated envelope* $|X(t)|$.

## 2.2 Modulated Discrete Prolate Spheroidal Sequences Model

SoS is a very popular model for MIMO channel modeling and simulation, but when we want to evaluate some specific features of a communication system such as prediction and estimation, use of this model may mislead by overmuch optimistic results since the received signal is a sum of periodic components. Moreover, this model describes uniform scattering around the mobile, hence it is not appropriate when non-uniform scattering is required to be modeled for some particular scenarios.

A different approach for channel modeling was reviewed in [23]. This approach utilizes Thomson Multitaper analysis in communication problems like channel modeling, prediction or estimation. The set of MDPSS might be applied for accurate representation of a bandlimited channel in scenario of scattering from one or more clusters. Discrete Prolate Spheroidal sequences form a set of orthogonal functions which might be used as a basis. An example of first four DPSS are shown in Fig. 2.13.

As described in [23], $n_t \times n_r$ MIMO channel matrix could be composed of

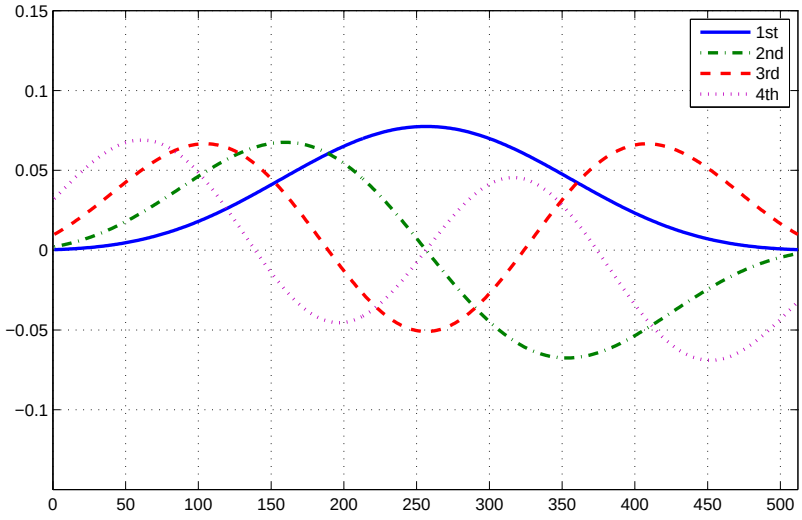


Figure 2.13: *An example of first four Discreet Prolate Spheroidal Sequences*

three components: Line of Sight ($\mathbf{H_{LoS}}$), Diffusive ($\mathbf{H_{diff}}$) and Specular ($\mathbf{H_{sp}}$):

$$\mathbf{H} = \mathbf{H_{LoS}} + \mathbf{H_{diff}} + \mathbf{H_{sp}} \tag{2.20}$$

LoS component is represented by:

$$\mathbf{H_{LoS}} = \sqrt{\frac{P_{LoS}}{n_t n_r}} a_L b_L^H \exp\left(j\phi_{LoS}\right) \tag{2.21}$$

Here $a_L$ and $b_L$ are receiving and transmitting antenna manifold vectors with unity amplitude describing phase shifts with respect to some reference point. $P_{LoS}$ is a power of LoS component, $\phi_{LoS}$ is a constant deterministic phase of angle of arrival of LoS component.

$\mathbf{H_{diff}}$ component is composed of zero-mean complex circularly symmetric Gaussian variables. This component is due to a composition of large amount of reflected and scattered from large rough surfaces waves with uniformly distributed and uncorrelated phases.

Last component, $\mathbf{H_{sp}}$, is an intermediate case between *LoS* and diffusive components, which caused by the scattering from mildly rough surfaces (or First Fresnel zones), resulting in strong correlation of phases of upcoming waves and a certain angular spread of the received signal. For a singular specular component:

$$\mathbf{H_{sp}} = \sqrt{\frac{P_{sp}}{n_t n_r}} \left[\mathbf{a} \odot \mathbf{w_a}\right] \left[\mathbf{b} \odot \mathbf{w_b}\right]^H \xi \tag{2.22}$$

Where $P_{sp}$ is a power of a specular component, $\xi$ is a random complex Gaussian variable with parameters: $m_I + jm_Q$, $\sigma_I^2$, $\sigma_Q^2$ and independent in-phase and quadrature components. Angular spread is depicted by window terms $w_a$ and $w_b$, which are shown to be well-approximated by known Discrete Prolate Spheroidal Sequences. For multiple specular components case the resulting matrix is a weighted sum of contributions (2.22) from different clusters what results in different angles of arrival and

departure:

$$\mathbf{H_{sp}} = \sum_{k=1} \sqrt{\frac{P_{sp,k}}{n_t n_r}} \left[a_k \odot w_{a,k}\right] \left[b_k \odot w_{b,k}\right]^H \xi_k \tag{2.23}$$

Moreover, different elements of (2.23) are not i.i.d. since they have different absolute mean value, which have to be estimated individually. Nevertheless, in case of a very narrow angular spread of each component, windows $w_{a,k}$, $w_{b,k}$ have only unity elements, resulting in equivalent variances of in-phase and quadrature elements of all elements of matrix $\mathbf{H_{sp}}$.

### 2.2.1 Geometry of Scattering Environment

For simulation of a single cluster environment we use a geometry description from Fig. 2.14: there are two horizontal multi-element linear antenna arrays on both receiving and transmitting sides, the space between antennas contains a single scattering cluster. Impulse response $h(\tau, t)$ is assumed to be sampled at the rate $F_{st}$ ($\tau = n/F_{st} = nT_{st}$) and the channel is sounded at the rate $F_s$ ($t = m/F_s = mT_s$). The carrier frequency is $f_c$; $n_r$, $n_t$, $d_r$, $d_t$ are the number of isotropic elements and

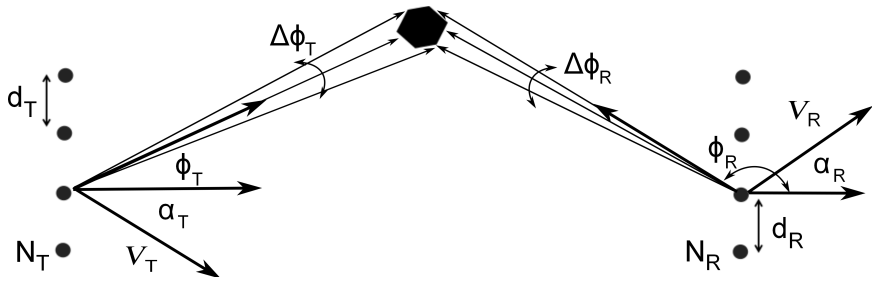


Figure 2.14: *Geometry of a single cluster problem*

the distance between them at receiving and transmitting antennas respectively; $v_r$ and $v_t$ are velocities at which receiver and transmitter move making angles $\alpha_t$ and $\alpha_r$ with corresponding broadside vectors; $\phi_t$, $\phi_r$ are azimuthal angles at which a cluster center is seen from receiving and transmitting sides. For simplicity it is assumed that co-elevation angles $\theta_t = \theta_r = \frac{\pi}{2}$ and there is no spread at this direction. Due to a large distance between antennas and a scatterer, the angular spread in horizontal

direction might be assumed very small comparing to the angular resolution of arrays:

$$\Delta\phi_t \ll \frac{2\pi\lambda}{(n_t-1)d_t}, \quad \Delta\phi_r \ll \frac{2\pi\lambda}{(n_r-1)d_r} \tag{2.24}$$

Also the cluster produces small delay spread $\Delta\tau$, which is assumed to be no greater than a few samples interval $T_{st} = 1/F_{st}$.

### 2.2.2 Statistics of the Channel

It is well known, that angular and spatial domains are dual to each other, hence angular spread results into a spatial selectivity which could be expressed by the following covariance function (which is inverse Fourier Transform of Angle of Arrival (AoA) or Angle of Departure (AoD) spread PDF):

$$\rho(d) = \int_{-\pi}^{\pi} \exp\left(j2\pi\frac{d}{\lambda}\phi\right)\rho(\phi)\mathrm{d}\phi \tag{2.25}$$

As we have assumed before, the angular size of a cluster is much smaller than antennas angular resolutions, therefore AoA and AoD spreads might be considered uniform and not correlated, and the joint distribution becomes:

$$p_{\phi_t,\phi_r}(\phi_t,\phi_r) = p_{\phi_t}(\phi_t)p_{\phi_r}(\phi_r) = \frac{1}{\Delta_{\phi_t}}\cdot\frac{1}{\Delta_{\phi_r}} \tag{2.26}$$

The spatial covariance function might be approximated then by:

$$\rho(d) \approx \exp\left(j\frac{2\pi d}{\lambda}\sin\phi_0\right)\mathrm{sinc}\left(\Delta\phi\frac{d}{\lambda}\cos\phi_0\right) \tag{2.27}$$

The correlation matrix between antennas elements might be decomposed then in terms of frequency MDPSS:

$$R \approx \mathbf{W}\mathbf{U}_{\mathbf{D_A}}\mathbf{\Lambda}_{\mathbf{D_A}}\mathbf{U}^{\mathbf{H}}_{\mathbf{D_A}}\mathbf{W}^{\mathbf{H}} = \sum_{k=1}^{D_A}\lambda_k u_k u_k^H \tag{2.28}$$

where $N$ is a number of antennas, $D_A \approx \lceil 2\Delta\phi \frac{d_A}{\lambda} \cos\phi_0 \rceil + 1$ (an effective number of degrees of freedom generated by the process with correlation matrix R), $d_A$ is a distance between antenna elements, $\Lambda_{D_A}$ is a diagonal matrix of size $D_A \times D_A$, $\mathbf{U}$ is $N \times D_A$ matrix of the DPSS and $\mathbf{W} = \text{diag}\left\{\exp\left(j2\pi \frac{d_A}{\lambda} n \sin\phi_0\right)\right\}$, $1 \leq n \leq N$. It might be shown that for a case of a narrow cluster number of degrees of freedom, $D_A$, is much smaller than the number of antennas, $N$, hence the transfer function, $H(\omega, t)$, takes a form:

$$H(\omega, t) = \sum_{n_t}^{D_t} \sum_{n_r}^{D_r} \sqrt{\lambda_{n_t} \lambda_{n_r}} u_{n_r}^{(r)} {u_{n_t}^{(t)}}^H h_{n_t, n_r}(\omega, t) \tag{2.29}$$

This equation is Karhunen-Loeve series in spatial domain which is known to require the smallest number of terms needed for representation of a spatial selective process [7]. From the equation (2.29) we may conclude, that by modulating the spatial response of the channel from both receiving and transmitting sides we may achieve angular spread, which represents scattering from the cluster. The same procedure might be performed in Frequency and Doppler domains: let us assume that we want to represent bandlimited process $[-W : W]$ using $N_F$ equally spaced samples in Frequency domain. We also assume, that cluster produces a certain delay spread in time $\Delta\tau$ ($\tau$ is a mean delay associated with the cluster). Hence, if the variation of power is relatively small during the $\Delta\tau$ delay window, we may again represent the frequency channel variations as a sum of MDPSS:

$$h(\omega, t) = \sum_{n_f=1}^{D_f} \sqrt{\lambda_{n_f}} u_{n_f}^{(\omega)} h_{n_f}(t) \tag{2.30}$$

where $D_f = \lfloor 2W\Delta\tau \rfloor + 1$. In Doppler domain, the resulting Doppler shift is calculated by:

$$f_D = \frac{f_c}{c} \left[ v_t \cos\left(\phi_{t0} - \alpha_t\right) + v_r \cos\left(\phi_{r0} - \alpha_r\right) \right] \tag{2.31}$$

The widening of the Doppler spectrum as a result of cluster angular spread is expressed by:

$$\Delta f_D = \frac{f_c}{c}\left[v_t \Delta\phi_t |\sin(\phi_{t0} - \alpha_t)| + v_r \Delta\phi_r |\sin(\phi_{r0} - \alpha_r)|\right] \tag{2.32}$$

And the variation of the spectrum in this expansion (due to a very narrow cluster angular extent) is small, so that again we may use MDPSS to describe channel response in Doppler domain:

$$h_d = \sum_{n_d=1}^{D} \xi_{n_d} \sqrt{\lambda_{n_d}} u_{n_d}^{(d)} \tag{2.33}$$

Here $D = \lfloor \Delta f_D T_{max} \rfloor + 1$ is a number of MDPSS needed, $T_{max}$ is the duration of the simulation and $\xi_{n_d}$ are complex Gaussian i.i.d. variables with unit variance. Therefore a sample of a complete frequency selective MIMO channel representation takes a form of four dimensional tensor:

$$\begin{aligned}\mathcal{H}_4 = \mathcal{W}_4 \odot \sum_{n_r}^{D_r}\sum_{n_t}^{D_t}\sum_{n_f}^{D_f}\sum_{n_d}^{D} \sqrt{\lambda_{n_r}^{(r)}\lambda_{n_t}^{(t)}\lambda_{n_f}^{(\omega)}\lambda_{n_d}^{(d)}}\,\xi_{n_r,n_t,n_f,n_d} \cdot \\ \cdot\ {}_1u_{n_r}^{(r)} \times_2 u_{n_t}^{(t)} \times_3 u_{n_f}^{(\omega)} \times_4 u_{n_d}^{(d)}\end{aligned} \tag{2.34}$$

where $u_{n_r}^{(r)}$, $u_{n_t}^{(t)}$, $u_{n_f}^{(\omega)}$, $u_{n_d}^{(d)}$ are DPSS representing dimensions of a signal at the receive, transmit, frequency and Doppler domains with "domain-dual domain" products: $|\Delta\phi_r \frac{N_r d_r}{\lambda}\cos\phi_{r0}|$, $|\Delta\phi_t \frac{N_t d_t}{\lambda}\cos\phi_{t0}|$, $W\Delta\tau$, $T_{max}\frac{\Delta f_D}{2}$ respectively. $\mathcal{W}_4$ is a tensor of modulating sinusoids described as follows:

$$\mathcal{W}_4 = {}_1w^{(r)} \times_2 w^{(t)} \times_3 w^{(\omega)} \times_4 w^{(d)} \tag{2.35}$$

$$
\begin{aligned}
w^{(r)} &= \left[1, \exp\left(j2\pi\frac{d_r}{\lambda}\right), \cdots, \exp\left(j2\pi\frac{d_r}{\lambda}\sin\phi_{r0}(N_r-1)\right)\right]^T \\
w^{(t)} &= \left[1, \exp\left(j2\pi\frac{d_t}{\lambda}\right), \cdots, \exp\left(j2\pi\frac{d_t}{\lambda}\sin\phi_{t0}(N_t-1)\right)\right]^T \\
w^{(\omega)} &= \left[1, \exp\left(j2\pi\Delta F\tau\right), \cdots, \exp\left(j2\pi\Delta F\tau(N_f-1)\right)\right]^T \\
w^{(d)} &= \left[1, \exp\left(j2\pi f_D T_s\right), \cdots, \exp\left(j2\pi f_D(T_{max}-T_s)\right)\right]^T
\end{aligned} \tag{2.36}
$$

Here $\Delta F = \dfrac{2W}{N_f - 1}$, $T_{max} = LT_s$, and $\odot$ is element-wise (Hadamard) product of two tensors.

### 2.2.3 Multi-Cluster Environment

In general, one may simulate channel representing scattering from several clusters (multi-cluster environment). In this case the total channel response is a superposition of independently generated single-cluster responses:

$$
\mathcal{H}_4 = \sum_{k=1}^{N_c} \sqrt{P_k}\mathcal{H}_4(k), \quad \sum_{k=1}^{N_c} \sqrt{P_k} = P \tag{2.37}
$$

Where $N_c$ is the total number of clusters and $\mathcal{H}_4(k)$ is a normalized response from $k$-th cluster with relative power $P_k$; $E\left[\|\mathcal{H}_4(k)\|_F^2\right] = 1$, $P$ is a total power. This representation depicts composition signals with different delays arriving from different directions, rather than real location of the clusters. Thus it is possible to have two clusters with the same AoA and AoD but different excess delay or same excess delay but different angles of arrival and departure.

### 2.2.4 Auto-Covariance Function

Spectrum analysis of the problem shows that Power Spectrum Density (PSD) of one-cluster problem is approximately a window around $f = f_D$ with width $\Delta f_D$ and height $\dfrac{P}{\Delta f_D}$, when $P$ is a total power of the channel or its variance $\sigma_c^2$, see Fig. 2.15 for description. Therefore one may calculate the covariance function of the channel

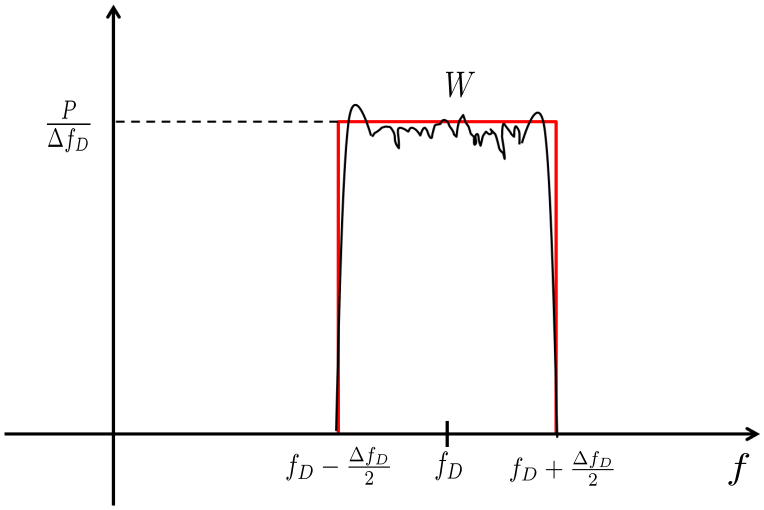


Figure 2.15: *Example of PSD of one-cluster environment*

process applying Fourier Analysis. Assume that PSD is a perfect window function $W(f)$ which is located around $f_D$. Then it might be expressed as:

$$W(f) = \frac{P}{\Delta f_D} \cdot \text{rect}\left(\frac{f}{\Delta f_D}\right) * \delta\left(f - f_D\right) \tag{2.38}$$

When $\delta(\cdot)$ is Kronecker Delta function and Rectangle function is defined as follows:

$$\text{rect}\left(f\right) = \begin{cases} 1 & \text{if} \quad -\frac{1}{2} \leq f \leq \frac{1}{2} \\ 0 & \text{else} \end{cases} \tag{2.39}$$

As well known, covariance function is an inverse Fourier Transform of PSD:

$$\begin{aligned} R(\tau) = \mathcal{F}^{-1}\left\{W(f)\right\} = \frac{P}{\Delta f_D} \exp\left(j2\pi f_D \tau\right) \Delta f_D \cdot \text{sinc}\left(\Delta f_D \tau\right) = \\ = P \exp\left(j2\pi f_D \tau\right) \text{sinc}\left(\Delta f_D \tau\right), \end{aligned} \tag{2.40}$$

here sinc function of variable $x$ is defined as $\text{sinc}(x) = \dfrac{\sin(x)}{x}$. Therefore auto-covariance function of the channel process is a multiplication of an exponent and a sinc functions:

$$R(\tau) = P \exp\left(j2\pi f_D \tau\right) \text{sinc}(\Delta f_D \tau) \tag{2.41}$$

In a case of multi-cluster environment with $N_c$ clusters, each cluster produces a window $W_k$ around frequency $f_{Dk}$ (corresponding to cluster $k$), $k = 1, \ldots, N_c$ at PSD profile. Hence PSD takes a form of a sum of $N_c$ independent windows and auto-covariance function $R_{tot}(\tau)$ is a sum of $N_c$ auto-covariance functions $R_k(\tau)$ corresponding to each cluster (due to linearity of Fourier Transform operation):

$$\begin{aligned} R_{tot}(\tau) &= R_1(\tau) + R_2(\tau) + \ldots + R_{N_c}(\tau) = \\ &= P_1 \exp\left(j2\pi f_{D_1}\tau\right) \operatorname{sinc}\left(\Delta f_{D_1}\tau\right) + \\ &+ P_2 \exp\left(j2\pi f_{D_2}\tau\right) \operatorname{sinc}\left(\Delta f_{D_2}\tau\right) + \ldots + \\ &+ P_{N_c} \exp\left(j2\pi f_{D_{N_c}}\tau\right) \operatorname{sinc}\left(\Delta f_{D_{N_c}}\tau\right) = \\ &= \sum_{k=1}^{N_c} P_k \exp\left(j2\pi f_{D_k}\tau\right) \operatorname{sinc}\left(\Delta f_{D_k}\tau\right) \end{aligned} \tag{2.42}$$

Where $P_k \geq 0$ is a relative power of cluster $k$, $\sum_{k=1}^{N_c} P_k = P$. Total power $P$ is usually normalized to unity, $P = 1$.

### 2.2.5 Simulation Evaluation of the MDPSS Model

In this section we show an example of simulation of one and two clusters environments and compare the results to theoretical derivations, discussed previously.

#### 2.2.5.1 One Cluster Environment

Example of simulation of a sample of one-cluster flat fading channel is given in Figs. 2.16 - 2.18. See Tab.2.1 for simulation parameters summary. Fig. 2.16 shows an absolute value of time-varying frequency response of a channel sample. Black areas indicate deep fading whereas white areas indicate a good channel quality. In Fig. 2.17 the normalized Power Delay Profile (PDP) of the channel sample is plotted, where we clearly see a peak at delay associated with a particular cluster delay $\tau = 0.3\mu sec$ with delay spread of $0.1\mu sec$, and at Fig. 2.18 we may see resulting widened Doppler spectrum at frequency $f_D \approx 54.7[Hz]$ with Doppler spread of $4.8Hz$ (calculated from

equations (2.31) - (2.32)).

Theoretical and simulated auto-correlation functions are plotted in Figs. 2.19 - 2.21 as functions of normalized time $f_{D_0}\tau$, when $f_{D_0} = f_c\frac{|v_t| + |v_r|}{c}$. One may find the real part of auto-correlation function $Re\{R(\tau)\}$ in Fig. 2.19, the imaginary part of auto-correlation function $Im\{R(\tau)\}$ in Fig. 2.20 and the fading envelope $|R(\tau)|$ in Fig. 2.21. In all cases there is a very good convergence of simulation to the theoretical curve.

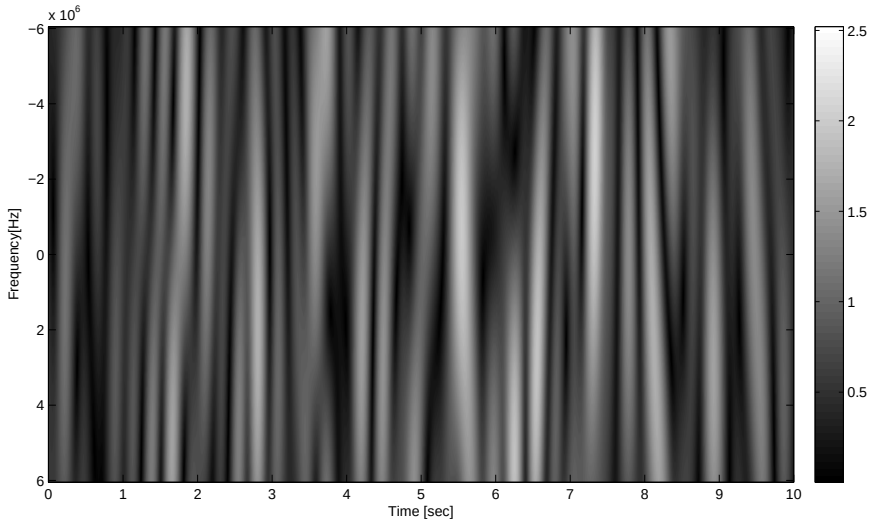


Figure 2.16: *Absolute value of time varying frequency response $H(f,t)$ of a channel sample*

| *Param.* | *Value* | *Description* |
|---|---|---|
| $N_r$ | 8 | *Number of antennas on the receiving side* |
| $N_t$ | 8 | *Number of antennas on the receiving side* |
| $v_r$ | 30 $[km/h]$ | *Speed of the receiver* |
| $v_t$ | 0 $[km/h]$ | *Speed of the transmitter* |
| $W$ | 6 $[MHz]$ | *Required channel half-bandwidth* |
| $f_c$ | 2 $[GHz]$ | *Carrier frequency* |
| $d_r$, $d_t$ | 0.5 | *Receive/transmit antenna spacing normalized to wave length* |
| $P_c$ | 0.8 | *Power weights for clusters* |
| $\phi_{0r}$ | $10^o$ | *Azimuthal angle at which center of the cluster is seen to the receiver* |
| $\phi_{0t}$ | $20^o$ | *Azimuthal angle at which center of the cluster is seen to the transmitter* |
| $\alpha_r, \alpha_t$ | $0^o$ | *The angle between broadside vector and movement direction* |
| $\Delta\phi_r$ | $5^o$ | *Angular spread seen from receiving side* |
| $\Delta\phi_t$ | $8^o$ | *Angular spread seen from transmitting side* |
| $\tau$ | 0.3 $[\mu sec]$ | *A mean delay associated with the cluster* |
| $\Delta\tau$ | 0.1 $[\mu sec]$ | *Corresponding delay spread* |
| $F_{st}$ | 50 $[MHz]$ | *Sampling frequency in delay domain* |
| $F_s$ | 250 $[Hz]$ | *Rate of sampling in Doppler domain* |
| $irL$ | 142 | *Length of the impulse response (num of samples)* |
| $L$ | 1024 | *Number of samples (in Doppler domain)* |
| $Nf$ | 128 | *Number of equally spaced samples for process representation at bandwidth [-W,W]* |
| $rate$ | $10^5$ $[bps]$ | *The transmission rate, bits per second* |

Table 2.1: *Example of simulation parameters for the channel with one scattering cluster*

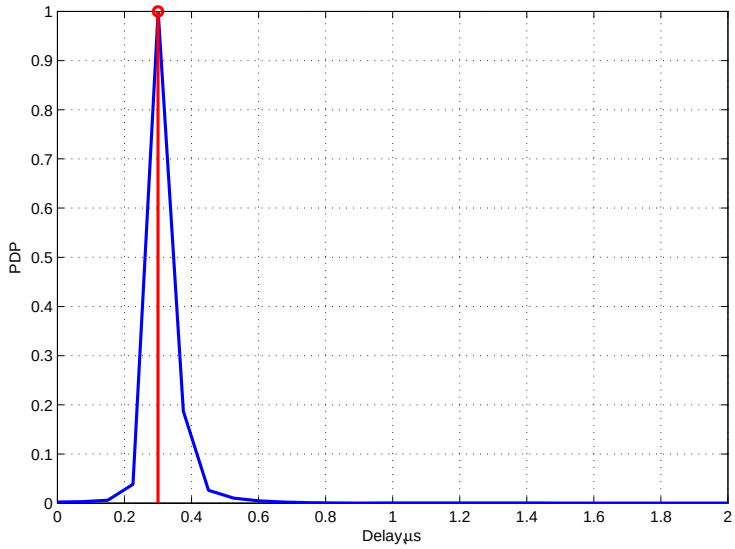


Figure 2.17: *PDP of one-cluster channel response,* $\tau = 0.3$ $\mu sec$

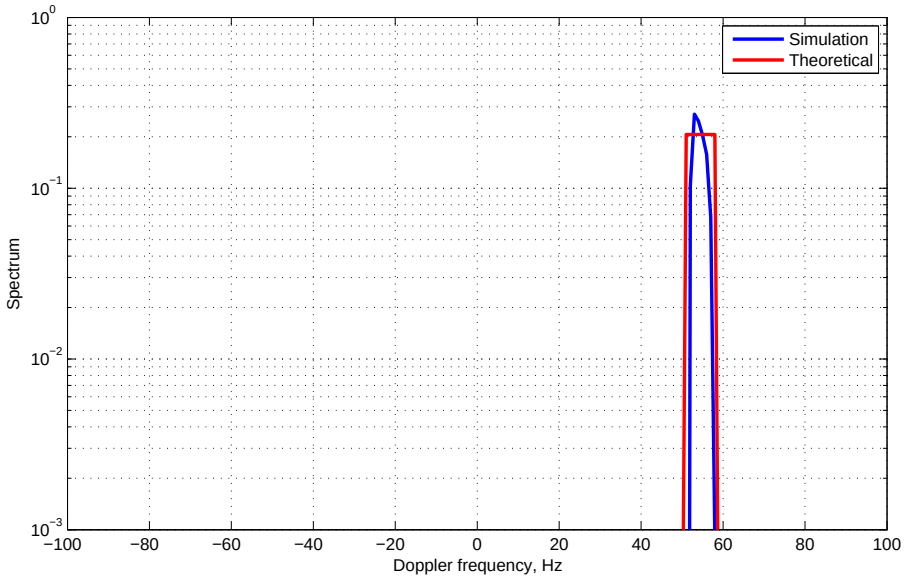


Figure 2.18: *Doppler PSD of one-cluster channel response,* $f_D \approx 54.7Hz$

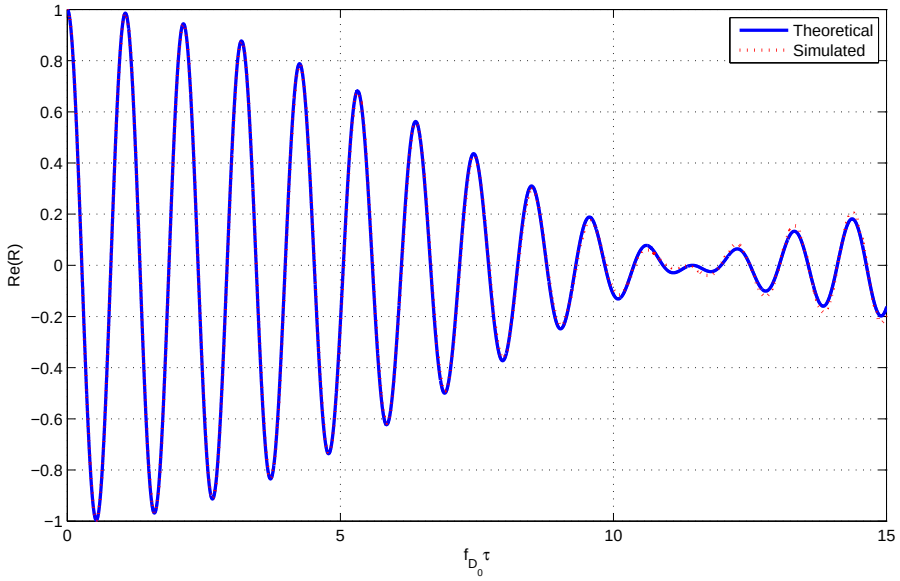


Figure 2.19: *Real part of auto-covariance function of the channel process,* $Re\{R(\tau)\}$

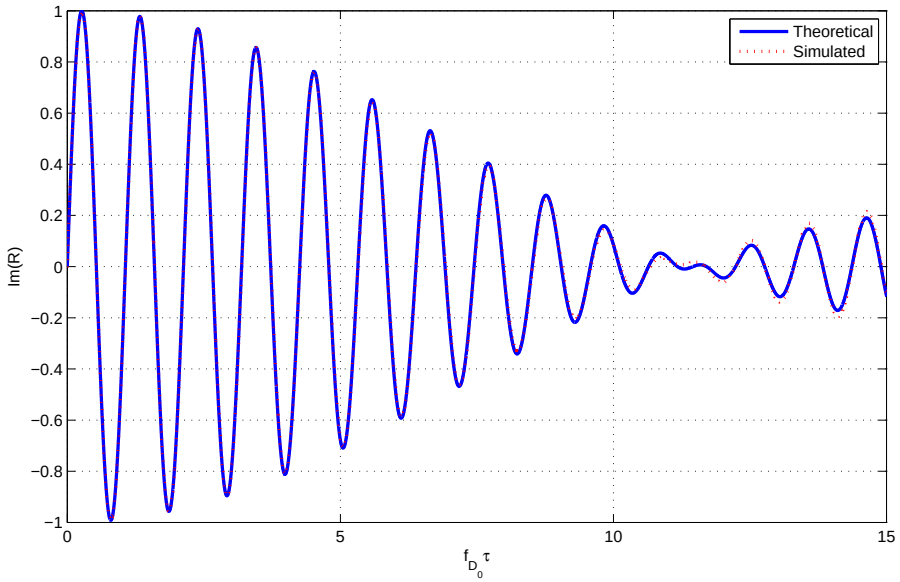


Figure 2.20: *Imaginary part of auto-covariance function of the channel process,* $Im\{R(\tau)\}$

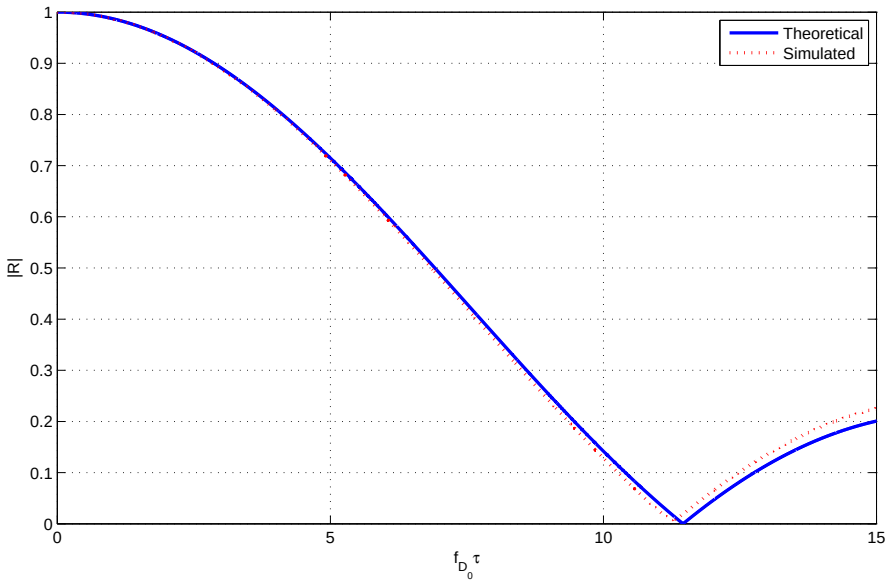


Figure 2.21: *Fading envelope of auto-covariance function of the channel process,* $|R(\tau)|$

### 2.2.5.2 Two Clusters Environment

A two clusters case is depicted in Fig. 2.22. Parameters of two clusters are given in Tab.2.2. If some parameters are not mentioned in the table, they remain the same as for one cluster case and equal for both clusters. Simulation results are plotted in Figs. 2.23 - 2.24. Real and imaginary parts of auto-correlation function are plotted in Figs. 2.25 - 2.26, as well as its envelope in Fig. 2.27.

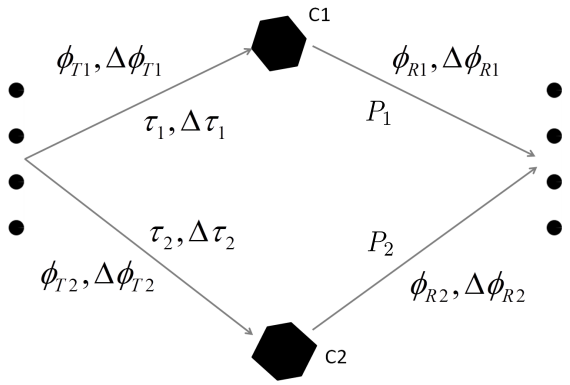


Figure 2.22: *Two-clusters environment example*

| *Cluster* | *Parameter* | *Value* |
|---|---|---|
| *Cluster1* | $\phi_{0r_1}$ | $10^o$ |
| | $\tau_1$ | 0.3 $\mu sec$ |
| | $P_1$ | 0.6 |
| *Cluster2* | $\phi_{0r_2}$ | $120^o$ |
| | $\tau_2$ | 0.8 $\mu sec$ |
| | $P_2$ | 0.4 |

Table 2.2: *Two-clusters environment parameters*

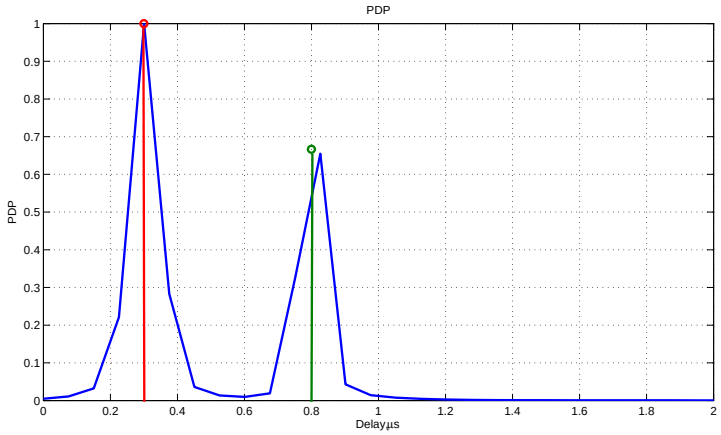


Figure 2.23: *PDP of two-clusters case,* $\tau_1 = 0.3$ $\mu sec$, $\tau_2 = 0.8$ $\mu sec$

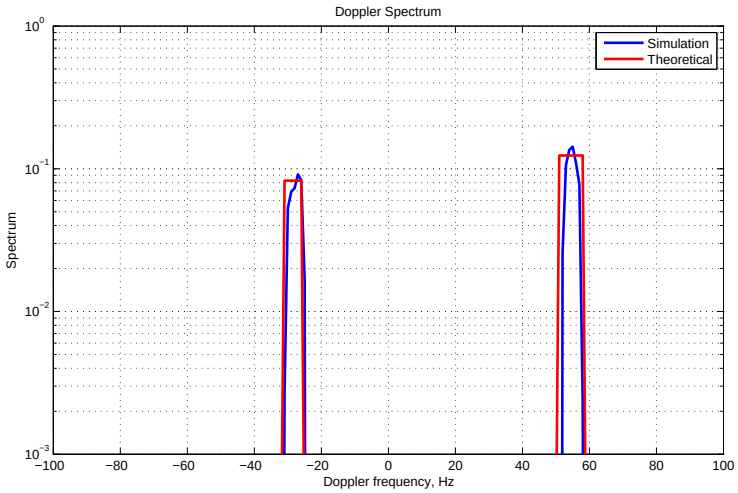


Figure 2.24: *Doppler PSD of two-clusters channel,* $f_{D_1} \approx 55.7$ $Hz$, $f_{D_2} \approx -27.8$ $Hz$

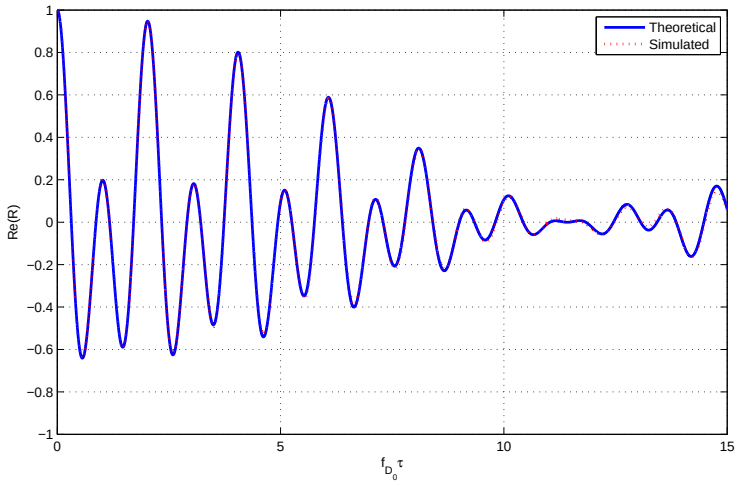


Figure 2.25: *Real part of auto-covariance function of two-clusters channel process,* $Re\{R(\tau)\}$

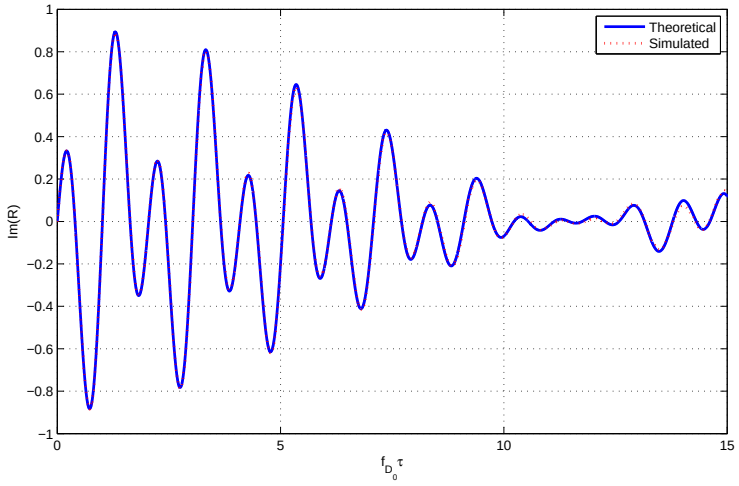


Figure 2.26: *Imaginary part of auto-covariance function of two-clusters channel process,* $Im\{R(\tau)\}$

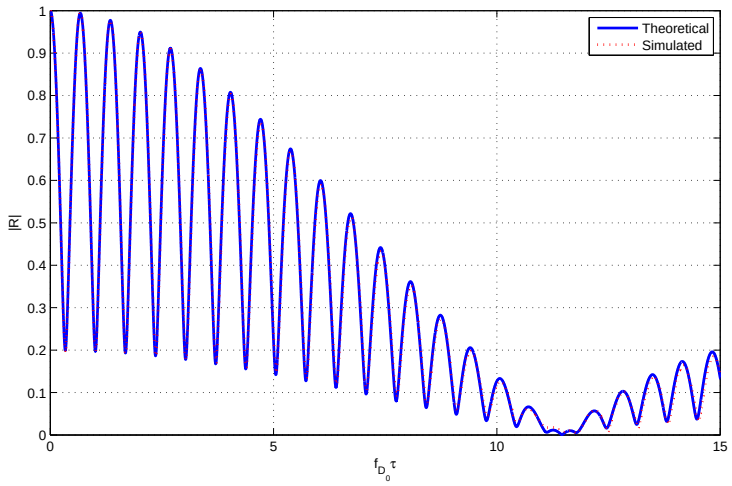


Figure 2.27: *Fading envelope of auto-covariance function of two-clusters channel process,* $|R(\tau)|$

## 2.3 Summary

- Channel simulators are widely used to test a variety of different communication systems in laboratory conditions what reduces time and financial expenses of experiments.
- One of the most famous channel models is Rayleigh fading model, which assumes that signal comes to the receiver in infinitely large number of independent paths (uniform scattering of the signal around the mobile). This assures that channel tap gains are complex circularly symmetric Gaussian processes, and their magnitude is Rayleigh distributed and phase is Uniformly distributed. This scenario is a very common in urban and suburban environments.
- A family of SoS channel simulators is built to mock flat fading Rayleigh channels behaviour, and is very popular due to its simplicity. These simulators are a sum of sinusoidal and cosinusoidal terms with random phase, AoA and amplitude. One of the most common problems with this kind of simulators is higher order statistics (such as covariance function of a squared envelope of the channel), which very often do not match desired one. In this chapter we reviewed a special SoS model with a proper higher order statistics, which we use throughout our work.
- Another common scenario in urban area is scattering from one ore more clusters, affecting the signal to come to the receiver from particular angels with narrow angular spreads (contrary to uniform distribution of paths in the previous scenario). MDPSS-based multi-cluster model for MIMO link, discussed in this chapter, is very flexible in determination of clusters geometry and hence is suitable to describe any site of interest. Moreover, it enables one to determine number of antennas on each side of communication and whether one or both sides are in motion, what allows to apply this model either for infrastructure to mobile or mobile to mobile cases.
- Combination of these two models is sufficient to generalize all common scenarios in urban and suburban areas.

# Chapter 3
# Simulation of a Transmission System

A general block scheme of a digital communication system is shown in Fig. 3.1, [24]. In

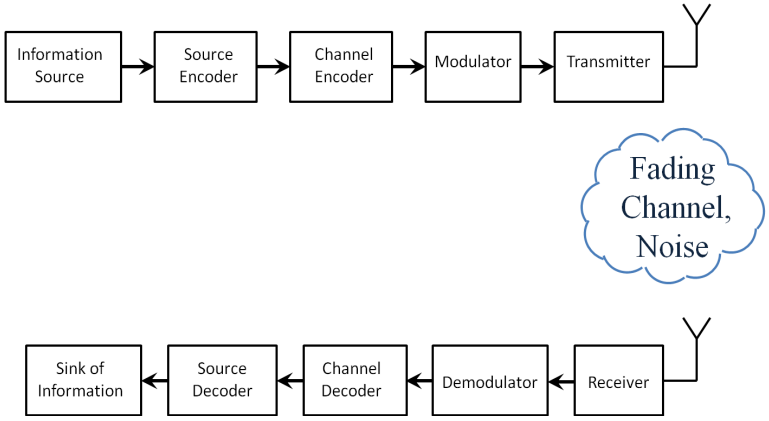


Figure 3.1: *A general block diagram of a digital transmission system*

general, information is coded, modulated and sent via one or more antennas through a fading channel, then it is detected at the receiver (again, via one or multiple antennas) along with Additive White Gaussian noise, demodulated and decoded. A channel is viewed as a linear time and space varying filter, what allows us to use a concept of system transfer/impulse response functions, which is well-studied for both wide band and narrow band channels.

Since in the process of transmission the information is corrupted by fading effect of a channel and the noise, it is a subject to errors. Therefore one of the central criteria of evaluation of the system is Bit Error Probability (BEP) or Bit Error Rate (BER) as a function of Signal to Noise Ratio (SNR). In this chapter we examine the effect of a fading channel on the system performance. We adopt Alamouti space-time coding scheme to improve BER. As the next step we discuss full CSI, no CSI and incomplete CSI (*i.e.* with channel estimation) cases at the receiver side and how it

affects the performance of the whole system. We also discuss methods of obtaining the information about channel gains during the transmission.

## 3.1 Perfect CSI at the Receiver

First of all, we would like to observe the effects of presence of different adverse factors, like noise or fading channel, on the the quality of communications, and what are the possible ways to improve the system's performance.

### 3.1.1 AWGN channel

It is instructive to compare performance of the communication system over a fading channel with AWGN channel, which introduces no channel fading, but only additive Gaussian noise distortion to a signal. Thus AWGN performance is the limiting performance (the best case) for scenarios involving channel fading. The discrete-time baseband equivalent model of the received signal in Single Input Single Output (SISO) system is:

$$y[m] = x[m] + w[m] \tag{3.1}$$

Here $x[m]$ is a signal with amplitude $\sqrt{E_b}$ at time $m$ and $w[m] \sim \mathcal{CN}(0, \frac{N_0}{2})$ is complex circularly symmetric Gaussian white noise. It is well known, that for antipodal signals in AWGN scenario with Maximum Likelihood (ML) detector at the receiver, BER is given by [17]:

$$p_e = \frac{1}{\sqrt{2\pi N_0/2}} \int_{\sqrt{E_b}}^{\infty} e^{-\frac{t^2}{2N_0/2}} \mathrm{d}t = \tag{3.2}$$

$$= Q\left(\sqrt{\frac{E_b^2}{N_0/2}}\right) = Q\left(\sqrt{2\gamma}\right) = \tag{3.3}$$

$$= \frac{1}{2}\mathrm{erfc}\left(\sqrt{\gamma}\right), \tag{3.4}$$

where $\gamma = \frac{E_b}{N_0}$ is the received signal to noise ratio per symbol time. $Q(\cdot)$ is the complementary cumulative distribution function of normally distributed random variable. $Q(x)$ function decays exponentially with $\frac{x^2}{2}$, hence the upper bound of the performance is [2]:

$$Q\left(\sqrt{2\gamma}\right) < e^{-\gamma}, \qquad \gamma > 0 \tag{3.5}$$

The lower bound might be found as well:

$$Q\left(\sqrt{\gamma}\right) > \frac{1}{\sqrt{4\pi\gamma}}\left(1 - \frac{1}{2\gamma}\right)e^{-\gamma}, \quad \gamma > 1 \tag{3.6}$$

The simulation results are presented in Figure(3.2).

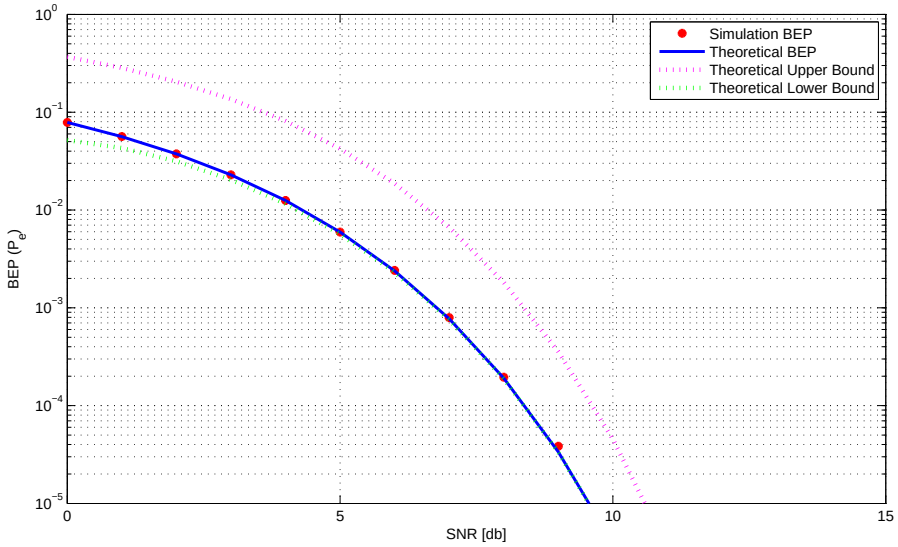


Figure 3.2: *BEP in AWGN channel as a limiting case*

### 3.1.2 Detection in Rayleigh Fading Channel

Now we add the fading effect to our communication system. Let us consider first the simplest example of Rayleigh fading channel process, where channel gains are complex Gaussian *i.i.d.* random variables. We consider the discrete-time baseband equivalent model at the receiver as follows [10]:

$$y[m] = h[m]x[m] + w[m] \tag{3.7}$$

where $w[m]$ is the sampled low-pass filtered Complex White Gaussian noise, $w[m] \sim \mathcal{CN}(0, N_0)$, $h[m]$ is a flat-fading Rayleigh channel gain with normalized variance, *i.e.* $h[m] \sim \mathcal{CN}(0, 1)$. $x[m]$ is a Binary Phase Shift Keying (BPSK) modulated signal, $x[m] = \pm\sqrt{E_b}$, where $E_b$ is an energy of one bit sent.

Non-coherent detection is the scenario when the receiver does not have any information or prior knowledge about the channel state. In this case due to randomness in the phase of the received signal the detection of uncoded BPSK modulation scheme completely fails. Since the channel gains are Rayleigh distributed, their phase is Uniform in $[-\pi, \pi)$, therefore the phase of the received signal is also Uniformly distributed regardless of the transmitted symbol. Thus the binary phase modulation, as well as any other phase modulation scheme will be flawed. Moreover, in [2] it was shown that non-coherent detection is energetically non-efficient for other modulation schemes, therefore usually coherent detection is used.

Now we assume that there is full CSI (channel state information) at the receiver side (we will discuss no CSI case later). Knowledge of channel gains allows us to perform coherent detection of the signal [2]. Since the decoding of the received signal is performed symbol by symbol, we may drop time index:

$$y = hx + w \tag{3.8}$$

For antipodal signals (BPSK) with bit amplitude $a$, the detection is similar to AWGN case, where we evaluate the symbol of real part of the sufficient statistics:

$$r = Re\left\{\left(\frac{h}{|h|}\right)^{*} y\right\} = |h|x + z \tag{3.9}$$

where $z \sim G(0, N_0/2)$. Conditioned on $h$, the error probability is:

$$Q\left(\frac{a|h|}{\sqrt{N_0/2}}\right) = Q\left(\sqrt{2|h|^2\gamma}\right) \tag{3.10}$$

Overall error probability might be calculated by averaging over random channel gain $|h|$, hence:

$$p_e = \mathbb{E}\left[Q\left(\sqrt{2|h|^2\gamma}\right)\right] = \frac{1}{2}\left(1 - \sqrt{\frac{\gamma}{1+\gamma}}\right) \tag{3.11}$$

Here $\mathbb{E}[x]$ denotes mean value of random variable $x$. Fig. 3.3 compares between performance of the system in Rayleigh fading channel with coherent detection and at AWGN channel. We can clearly see, that the performance significantly degrades in

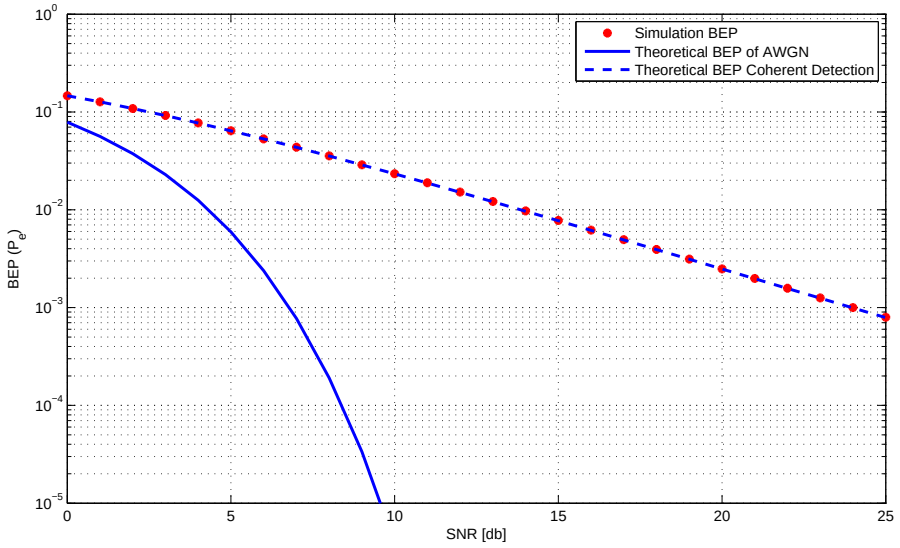


Figure 3.3: *Bit error probability of coherent detection in Rayleigh fading channel*

presence of a fading channel even when CSI is known. For high SNR and coherent

detection (in SISO case):

$$p_e \approx \frac{1}{4\gamma} \tag{3.12}$$

is inversely proportional to SNR, in contrast to AWGN case when the probability decays exponentially with SNR. Hence, we may conclude that the reason for poor performance of the system in fading channel is not because the receiver does not have knowledge about channel gains or the noise is high, but because the gains are random and there is a probability, that the channel is in deep fade. The probability of the channel to be in a deep fade is given by [2]:

$$p_{\text{deep fade}} \approx \frac{1}{\gamma} \tag{3.13}$$

In contrast, the the performance at AWGN channel is corrupted only by noise, hence the performance over this channel is better.

The solution for this problem is to exploit different diversity techniques, which operate over time, frequency and/or space. It is desired to send information not over only one path, but over several independent signal paths, each of which fades independently, what ensures us that if one of the paths is in a deep fade, we would still have a reliable communication over other signal paths. The simplest diversity technique is repetition coding. More complex techniques exploit channel diversity and its degrees of freedom, providing coding gains as well. In this work we concentrate on space-time Alamouti Coding scheme for $2 \times 1$ MISO channel.

### 3.1.3 Space-time Coding: Alamouti Scheme

Multiple Input Single Output (MISO) is a very common scenario in the downlink of a cellular system, because it has one base station and multiple antennas at every handset. Consider a system with $L$ transmitting antennas and one receiving. We may get a diversity gain of $L$, if we transmit the same symbol over $L$ symbol times: every time only one antenna is transmitting and others are silent. This is the simplest case of coding: repetition code over space, which is shown to be wasteful of degrees of freedom at the system [2]. There is a lot of research done in the area of time-space

coding, and here we focus on one of the most elegant coding techniques: Alamouti scheme, which is used in some third generation wireless mobile standards. This time-space diversity scheme is designed for 2 by 1 antennas system, and might be generalized for more transmitting antennas as well.

Let us consider the scenario where two antennas are transmitting and only one is receiving. Hence, the received signal is:

$$y[m] = h_1[m]x_1[m] + h_2[m]x_2[m] + w[m], \tag{3.14}$$

where $h_i$ is the channel gain of transmitting antenna $i$. Alamouti scheme transmits two complex symbols $u_1$ and $u_2$ from two antennas over two transmission times in the following order:

1. At first symbol time we transmit $x_1[1] = u_1$, $x_2[1] = u_2$
2. At second symbol time we transmit $x_1[2] = -u_2^*$, $x_2[2] = u_1*$
3. We also assume that the channel remains constant over two symbol times: $h_1[1] = h_1[2] = h_1$, $h_2[1] = h_2[2] = h_2$

The equation (3.14) could be rewritten in a matrix form:

$$\begin{bmatrix} y[1] & y[2] \end{bmatrix} = \begin{bmatrix} h_1 & h_2 \end{bmatrix} \begin{bmatrix} u_1 & -u_2^* \\ u_2 & u_1^* \end{bmatrix} + \begin{bmatrix} w[1] & w[2] \end{bmatrix}, \tag{3.15}$$

or after some rearrangement,

$$\begin{bmatrix} y[1] \\ y[2]^* \end{bmatrix} = \begin{bmatrix} h_1 & h_2 \\ h_2^* & -h_1^* \end{bmatrix} \begin{bmatrix} u_1 \\ u_2 \end{bmatrix} + \begin{bmatrix} w[1] \\ w[2]^* \end{bmatrix} = \mathbf{Hu} + \mathbf{w} \tag{3.16}$$

The columns of the square matrix $\mathbf{H}$ are orthogonal, hence we may separate the equation (3.16) into two orthogonal problems. To decode information we project $\mathbf{y}$ onto each of the two columns of the matrix: $[h_1\ h_2^*]^t$, $[h_2\ -h_1^*]^t$:

$$r_i = ||\mathbf{h}||u_i + w_i, \qquad i = 1, 2 \tag{3.17}$$

where $\mathbf{h} = [h_1, h_2]^t$ and $w_i \sim CN(0, N_0)$ ($w_1$, $w_2$ are independent), and then we perform ML detection for each of the decoded signal. In this scheme two symbols are transmitted over two symbol times, and each time each symbol is transmitted with half a power. Effectively, both symbols are transmitted over two non-interfering parallel channels.

It is shown in [2], that bit error probability might be bounded using conditioned on fading gains $\mathbf{h}$ pairwise error probability of confusing a block of codeword $\mathbf{X}_B$ with $\mathbf{X}_A$, when $\mathbf{X}_A$ is transmitted, averaged over statistics of the channel:

$$\begin{aligned}
&\mathbb{P}\left\{\mathbf{X}_A \to \mathbf{X}_B\right\} = \\
&= \mathbb{E}\left[Q\left(\sqrt{\frac{\gamma\ \mathbf{h}^*(\mathbf{X}_A - \mathbf{X}_B)(\mathbf{X}_A - \mathbf{X}_B)^*\mathbf{h}}{2}}\right)\right] = \\
&= \mathbb{E}\left[\sqrt{\frac{\gamma \sum_{l=1}^{L} |\tilde{h}_l|^2 \lambda_l^2}{2}}\right]
\end{aligned} \tag{3.18}$$

Here $\mathbb{P}\{A\}$ represents probability of an event $A$ and $\lambda_l$ are singular values of the codeword difference matrix $(\mathbf{X}_A - \mathbf{X}_B)$. Second step was due to the fact that this matrix is Hermitian with thus diagonalizable by a unitary transformation $\mathbf{U}\mathbf{\Lambda}\mathbf{U}^*$, where $\mathbf{U}$ is unitary and $\mathbf{\Lambda} = diag\{\lambda_1^2, \ldots, \lambda_L^2\}$, therefore $\tilde{\mathbf{h}} = \mathbf{U}^*\mathbf{h}$. In Rayleigh fading model the above expression might be bounded by:

$$\mathbb{P}\{\mathbf{X}_A \to \mathbf{X}_B\} \leqslant \frac{4^2}{\gamma^2 \det\left[(\mathbf{X}_A - \mathbf{X}_B)(\mathbf{X}_A - \mathbf{X}_B)^*\right]} \tag{3.19}$$

In general, Alamouti scheme works for any constellation. In the following we are interested in BPSK case to isolate the effects of fading. The exact Bit Error Probability was derived by [10] as a limiting case for perfect CSI:

$$P_b = \frac{1}{4}\left(2 + \sqrt{\frac{\gamma}{\gamma+2}}\right)\left(1 - \sqrt{\frac{\gamma}{\gamma+2}}\right)^2 \sim \frac{1}{\gamma^2} \tag{3.20}$$

The last step in 3.20 is due to the fact that the first term in brackets converges to constant for high SNR and the second term could be approximated as:

$$\left(1-\sqrt{\frac{\gamma}{\gamma+2}}\right)^2=\left(1-\frac{1}{\sqrt{1+\frac{2}{\gamma}}}\right)^2\sim\left[1-\left(1-\frac{1}{\gamma}\right)\right]^2=\frac{1}{\gamma^2}, \tag{3.21}$$

what declares diversity gain of 2.

From the simulation results we may clearly see, that comparing to coherent detection of uncoded information Alamouti space-time coding scheme improves communication quality by decreasing Bit Error Probability, see Fig. 3.4. In this case $P_e$ converges to zero much faster than in uncoded case. Similarly the simulation results

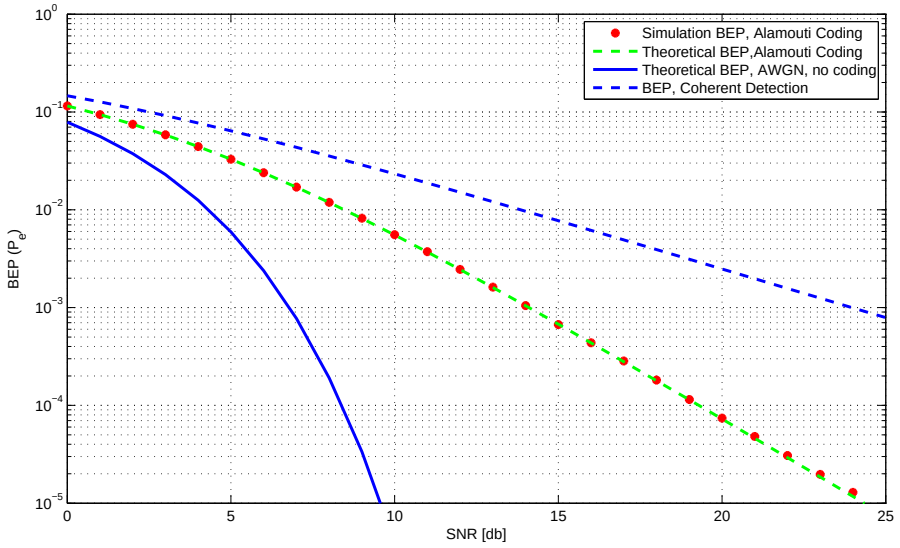


Figure 3.4: *Bit error probability, Alamouti Scheme, perfect CSI at the receiver side*

show, that SoS and MDPSS channel generators, discussed in Chapter2 demonstrate the same performance as Gaussian *i.i.d.* channel. As well known in ideal case of perfect CSI the performance of the system depends only on the first order statistics of the channel, and because in all cases channel gains are Gaussian distributed, we do not expect any differences in simulation results. See simulation verification is in Fig. 3.5.

However, in reality, the receiver does not possess perfect channel gains in-

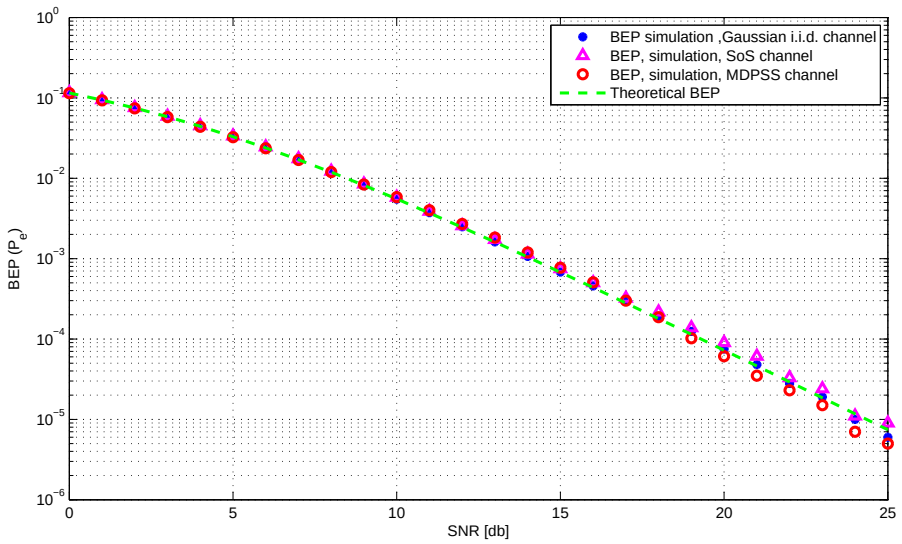


Figure 3.5: *Comparison of the system's performance when different channel generators were applied*

formation. Hence, we need to estimate the channel from the received data, and in this case the correlation between channel gains takes an important role, which makes possible to predict channel behavior at the receiver side in case of no CSI. The accuracy of estimation depends on the amount of available measurements, rate of channel change, noise at the receiver, *etc.*, and as the consequence, the decoded information is not perfect, what is expressed in estimation noise, which bounds the achievable rates. In our work we employ the pilot symbol assisted channel estimation scheme with Wiener filter as a pilot filter at the receiver side [25], [10].

## 3.2 No CSI at the Receiver, Channel Gains Estimation

As we mentioned before, the receiver usually does not possess any information about the current channel state. Therefore different estimation schemes could be employed, see [25] - [26], [10] for example. We adopt pilot-based estimation with Wiener filter at the receiver [14], [10] because of its simplicity and ubiquitousness in many com-

munication scenarios. In this section we introduce briefly the theory of Wiener filter and then we explain how we implement it in our transmission system. At the end we present simulational results which show how different system parameters affect the quality of estimation, and at the end we present different scenarios of mobile to base station or mobile to mobile communication.

### 3.2.1 Wiener Filter

According to [15] a linear discrete time filtering problem could be described as shown in Fig. 3.6. Linearity of the filter is assumed for convenience and ease of mathemat-

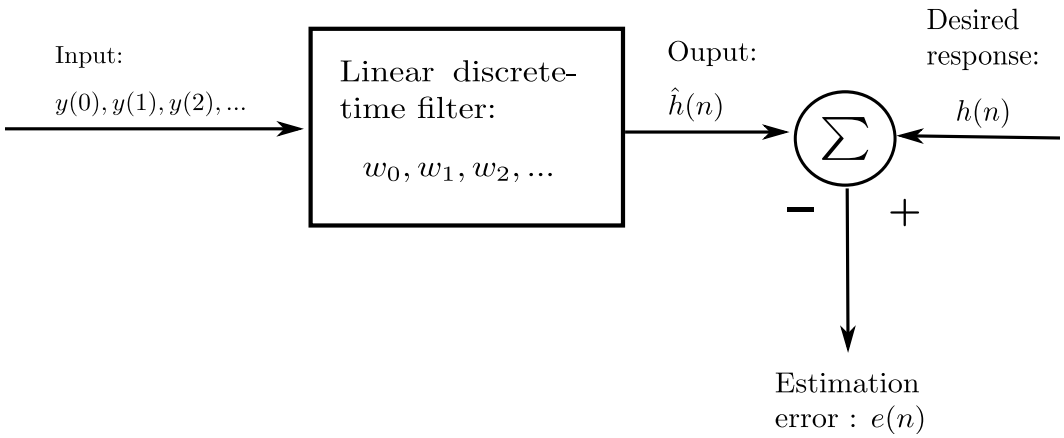


Figure 3.6: *Block scheme of a linear filtering problem*

ical analysis and assumption of discrete time is made for its applicability in digital hardware and software. Moreover this problem is assumed to be a *finite impulse response problem* (FIR), because it contains only forward filtering paths and hence it is stable (in contrary to an *infinite impulse response problem* (IIR), where both feedforward and feedback structures are involved, and therefore the output is prone to oscillate). The filter has an impulse response $w_0, w_1, w_2$, the input of the filter is a sequence of samples of a stochastic zero-mean process in time $y(0), y(1), y(2)...$, and the *actual output* is $\hat{h}(n)$ ($n$ denotes discrete time sample), which is then subtracted from the *desired output* at time $n$, $h(n)$ to produce an estimation error $e(n)$. If we denote the filter coefficients to be complex-valued (in case of a complex input), which

take form of:

$$w_k = a_k + jb_k, \quad k = 0, 1, 2, ... \tag{3.22}$$

the output of the filter could be expressed as follows:

$$\hat{h}(n) = \sum_{k=0}^{\infty} w_k^* y(n-k), \quad n = 0, 1, 2, ... \tag{3.23}$$

The goal here is to bring the mean-square value of the error $e(n)$ to the minimum [15]. Therefore one may define the cost function $J$ as follows:

$$J = E\left[e(n)e^*(n)\right] = E\left[|e(n)|^2\right] \tag{3.24}$$

where $E$ is an expectation operation and the error $e(n)$ is defined as the difference between estimated and desired processes:

$$e(n) = h(n) - \hat{h}(n) \tag{3.25}$$

It might be shown, that the necessary and sufficient condition to bring the cost function $J$ to its minimum is to find a special value of estimation error $e_0(n)$, which is orthogonal to each sample of the input process taken for the estimation of the desired process at time $n$. This is called the *principle of orthogonality* and this is one of the most important theorems in linear filtering theory. Therefore

$$E\left[y(n-k)e_0^*(n)\right] = 0, \qquad k = 0, 1, 2, ... \tag{3.26}$$

and

$$J_{min} = E\left[|e_0(n)|^2\right] \tag{3.27}$$

Following the principle of orthogonality, the next corollary could be attained:

$$E\left[\hat{h}_0(n)e_0^*(n)\right] = 0 \tag{3.28}$$

that means that the output of optimized in the mean-square error sense filter $\hat{h}_0(n)$ is orthogonal to the corresponding estimation error $e_n(n)$ at time $n$. The desired output process takes the form of:

$$h(n) = \hat{h}_0(n) + e_0(n) \tag{3.29}$$

Then if one evaluates mean of both sides and applies the principle of orthogonality, the following expression of the minimum value of the cost function could be derived:

$$J_{min} = \sigma_h^2 - \sigma_{\hat{h}}^2 \tag{3.30}$$

where $\sigma_h^2$ and $\sigma_{\hat{h}}^2$ are the variances of the desired and estimated processes respectively. The *normalized mean-square error* can be expressed as shown below:

$$\varepsilon = \frac{J_{min}}{\sigma_h^2} = 1 - \frac{\sigma_{\hat{h}^2}}{\sigma_h^2} \tag{3.31}$$

It is clear that $\varepsilon$ can never be negative and it takes values in the range of:

$$0 \leq \varepsilon \leq 1 \tag{3.32}$$

If $\varepsilon = 0$, the error-less estimation is achieved, *i.e.* filter's operation is perfect. If $\varepsilon = 1$, there is no correlation between input and output of the filter, what corresponds to the worst case scenario.

The optimality condition of the filter could be restated by substituting eq.(3.23) and eq.(3.25) into eq.(3.26):

$$E\left[y(n-k)\left(h^*(n) - \sum_{i=0}^{\infty} w_{0i} y^*(n-i)\right)\right] = 0, \quad k = 0, 1, 2, ... \tag{3.33}$$

what is equal to:

$$\sum_{i=0}^{\infty} w_{0i} E\left[y(n-k)y^*(n-i)\right] = E\left[y(n-k)h^*(n)\right] \tag{3.34}$$

We can define the auto-correlation of the input process for the lag $(i-k)$ as $E\left[y(n-k)y^*(n-i)\right] = r(i-k)$ (assuming $h$ being a stationary process) and $E\left[y(n-k)h^*(n)\right] = p(-k)$, the cross-correlation between input and the desired processes for a lag $-k$. Therefore eq.(3.34) takes a form of:

$$\sum_{i=0}^{\infty} w_{0i} r(i-k) = p(-k), \qquad k = 0, 1, 2, ... \tag{3.35}$$

and defines the most general representation of optimal filter coefficients in terms of two correlation functions in an infinite set of equations. They are called the *Wiener-Hopf equations* [15].

The simplified solution could be obtained in the special case of FIR filter (or linear transversal filter), which impulse response is finite. Its structure is shown in Fig. 3.7 and contains three main operations: storage, multiplication and addition. The storage operation is described by M-1 taps, or delay blocks. Therefore if the

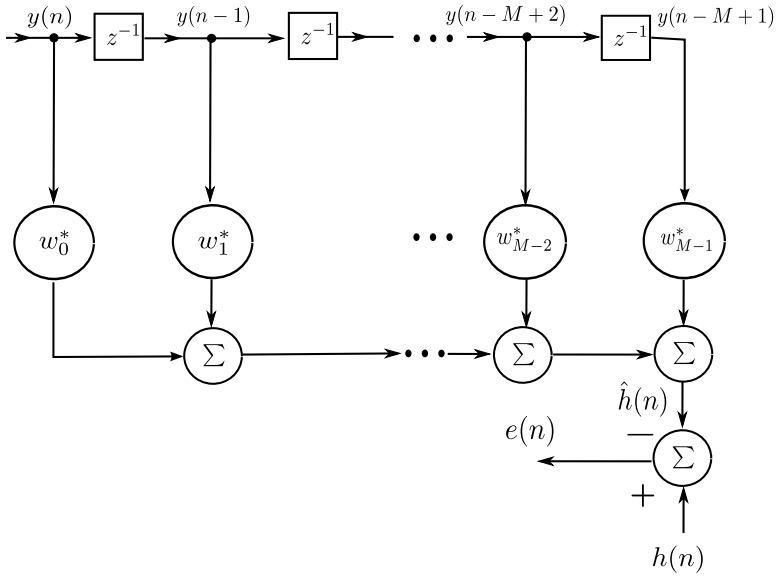


Figure 3.7: *Transversal filter*

current input of the filter is $y(n)$, there are $M-1$ past samples stored in taps, see Fig. 3.7, which are called tap inputs. Multiplication operation involves scalar inner products of $M$ tap outputs with appropriate tap gains $w_i$ $(i = 0, 1..., M-1)$. These blocks are denoted as $w_i^*$. Then adders sum up outputs of multipliers to form the filter

output at time $n$. Therefore Wiener-Hopf equations reduce to a set of $M$ equations only, *i.e.*:

$$\sum_{i=0}^{M-1} w_{0i} r(i-k) = p(-k), \qquad k = 0, 1, ..., M-1 \tag{3.36}$$

here $w_{0i}$ are the optimal filter weights.

Now one can formulate Wiener-Hopf equations in matrix form and find an explicit expression for the filter coefficients and the estimation error. Equation (3.36) could be represented as:

$$\mathbf{R}\mathbf{w}_0 = \mathbf{p}, \tag{3.37}$$

where $\mathbf{R}$ is denoted as an $M \times M$ correlation matrix of $M \times 1$ input vector $\mathbf{y}(n) = [y(n), y(n-1), ..., y(n-M+1)]^T$:

$$\mathbf{R} = E\left[y(n)y^H(n)\right] \tag{3.38}$$

or

$$\mathbf{R} = \begin{bmatrix} r(0) & r(1) & \cdots & r(M-1) \\ r^*(1) & r(0) & \cdots & r(M-2) \\ \vdots & \vdots & \ddots & \vdots \\ r^*(M-1) & r^*(M-2) & \cdots & r(0) \end{bmatrix} \tag{3.39}$$

Vector $\mathbf{p}$ is the correlation vector between output of the filter and the desired response:

$$\mathbf{p} = E\left[\mathbf{y}(n)h^*(n)\right] = [p(0), p(-1), ..., p(1-M)]^T \tag{3.40}$$

And $\mathbf{w}_0 = \left[w_{00}, w_{01}, ..., w_{0M-1}\right]^T$ is the $M \times 1$ vector of the optimal filter weights. Therefore assuming non-singularity of the correlation matrix $\mathbf{R}$, these coefficient could be calculated as:

$$\mathbf{w}_0 = \mathbf{R}^{-1}\mathbf{p} \tag{3.41}$$

From this equation it is clear that in order to calculate Wiener filer coefficients one is required to posses information about correlation matrix of the input vector and cross-correlation vector between the desired response and input vector.

The output of the filter could be expressed as:

$$\hat{h} = \mathbf{w}_0^H \mathbf{y}(n) \tag{3.42}$$

with variance:

$$\sigma_{\hat{h}}^2 = E\left[\mathbf{w}_0^H \mathbf{y}(n)\mathbf{y}^H(n)\mathbf{w}_0\right] = \mathbf{w}_0^H \mathbf{R}\mathbf{w}_0 = \mathbf{p}^H \mathbf{R}^{-1}\mathbf{p} \tag{3.43}$$

Therefore, following eq.(3.30) the estimation MMSE is:

$$J_{min} = \sigma_h^2 - \mathbf{w}_0^H \mathbf{R}\mathbf{w}_0 = \sigma_h^2 - \mathbf{p}^H \mathbf{R}^{-1}\mathbf{p} \tag{3.44}$$

### 3.2.2 Pilot-Based Channel Estimation Scheme Using Full Wiener Filter

As the perfect CSI is not available in real-life communication, estimation of channel gains at the receiver is always required. One of the most commonly used estimation schemes is pilot-assisted scheme with Wiener filter at the receiver [14], [15]. The information codewords (or blocks of two symbol times length each in Alamouti coding case) are divided into frames and interleaved with pilot symbols known to the receiver. Each frame contains $N_b+1$ blocks: $N_b$ blocks of information symbols and one block of pilot which is added at the beginning of the frame. The symbol time is $T_s$. We assume that the receiver possesses the information about channel statistics, bit rate and the frame length, and hence, it is able to extract pilot signals from the data stream and store them in the buffer of length $2M + 1$. Then, based on the information from the buffer and known correlation function between pilots, the receiver is able to perform channel estimation, decoding and decision. An example of a division into frames and pilot interleaving is visualized in Fig. 3.8. In addition to the baseband representation (3.14), we express the pilot signal $r_p$ (which has energy 1, *i.e.* 1/2 per antenna) and

the buffer $\vec{\mathbf{r}}_p$ for each antenna as follows [10]:

$$r_p^j[m] = \frac{1}{\sqrt{2}} h_j[m] + \xi_j[m], j = 1, 2 \tag{3.45}$$
$$\vec{\mathbf{r}}_p^j[m] = \left[ r_p^j[m-M] \cdots r_p^j[m] \cdots r_p^j[m+M] \right]^T$$

Here index $m$ represents time and index $j$ represents antenna. Since the receiver processes data at time $m$, we may consider first $M$ and last $M$ pilots in the buffer as "past" and "future" pilots, see Fig. 3.9. Therefore data processing of a certain frame is performed at delay of $2M(N_b + 1)$ symbol periods (in order to have needed amount of pilots in the buffer for estimation). On the other hand, greater number of pilots allows more accurate channel estimation, hence the trade-off between delay and accuracy of estimation can be reached based on the application needs.

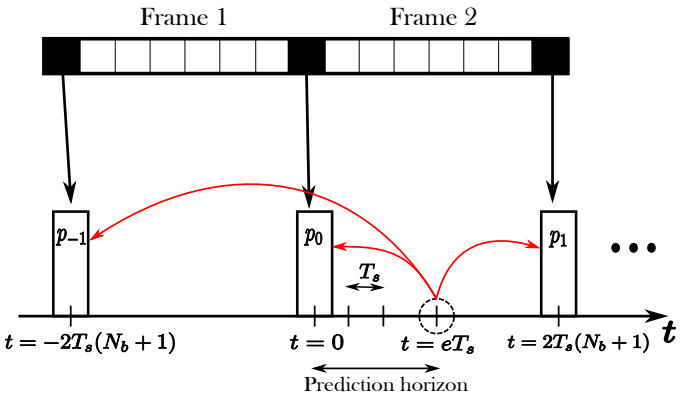


Figure 3.8: *An example of a stream with 3 pilot signals,* $M = 1$

Outputs of the filter are given by:

$$\hat{h}^1[i] = \mathbf{h}^H \mathbf{r}_p^1[i], \quad \hat{h}^2[i] = \mathbf{h}^H \mathbf{r}_p^2[i] \tag{3.46}$$

where $\hat{h}^j[i]$ represents estimated channel gain for antenna $j$, and the vector $\mathbf{h}$ represents pilots filter coefficients: $[h_M \ldots h_0 \ldots h_{-M}]^T$. Assuming, that channel does not

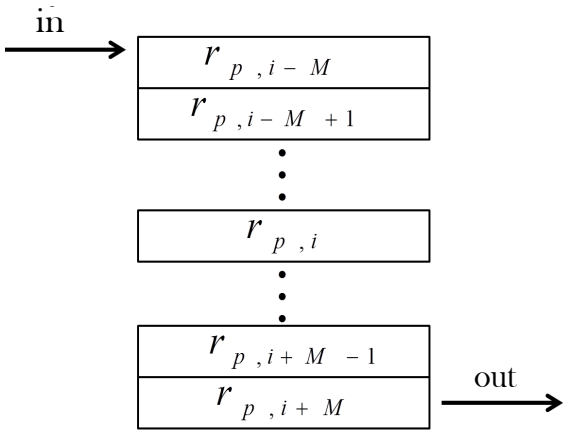


Figure 3.9: *The scheme of a buffer accumulating pilot signals*

change in the duration of the frame [10], these coefficients take a form of [15]:

$$\mathbf{h} = \frac{1}{\sqrt{2}} \left( \frac{\mathbf{D}_0}{2} + \bar{\gamma}_p^{-1} \mathbf{I}_{2M+1} \right)^{-1} \boldsymbol{\rho}_0 \tag{3.47}$$

Where $R$ is channel autocorrelation function, $\mathbf{D}_e$ denotes a square matrix of size $(2M+1)$ with entrances given by

$$\begin{aligned} \mathbf{D}_e(k,l) &= R(-eT_s + (k-l)T_s N), \\ & k,l = 1,\ldots,2M+1; \\ & e = 0,\ldots,2N_b+1 \end{aligned} \tag{3.48}$$

and $\boldsymbol{\rho}_e$ is the $(M+1)^{th}$ column of $\mathbf{D}_e$ (in a case of stationary channel during one frame we take $e=0$ for both $\mathbf{D}_e$ and $\mathbf{w}_e$), $\bar{\gamma}_p$ denotes the average pilot SNR or pilot $E_p/N_0$. $\mathbf{I}_{2M+1}$ is Identity matrix of size $(2M+1)$. Substituting (3.47) into (3.46) one may calculate channel gain estimates for the frame $i$. However, in our work we assume that channel gains have a slight variation in the duration of a frame, hence, based on the variation of the correlation function, the filter coefficients should be recalculated every symbol time in a frame duration. This will increase reliability of estimation scheme (in terms of smaller MMSE). Therefore we may express the coefficients for

each symbol time in the frame as follows

$$\mathbf{h}_e = \frac{1}{\sqrt{2}} \left( \frac{\mathbf{D}_0}{2} + \bar{\gamma}_p^{-1} \mathbf{I}_{2M+1} \right)^{-1} \boldsymbol{\rho}_e \tag{3.49}$$

Therefore

$$\hat{h}^1[i,e] = \mathbf{h}_e^H \mathbf{r}_p^1[i], \quad \hat{h}^2[i,e] = \mathbf{h}_e^H \mathbf{r}_p^2[i] \tag{3.50}$$

where index $i$ runs on frames' times with interval $2(N_b+1)T_s$ and index $e$ runs within a single frame with interval $T_s$. That means, that in the above scheme, matrix $\mathbf{D}_0$ is a covariance matrix between pilot signals given in a buffer, and $\boldsymbol{\rho}_e$ is a vector of correlations between a specific frame element at place $e$ and the nearest pilot signals, see Fig. 3.10 for visualization. For example, for $M = 1$, $\boldsymbol{\rho}_e$ for $e = 0, 1, 2$ $\boldsymbol{\rho}_e$ takes a

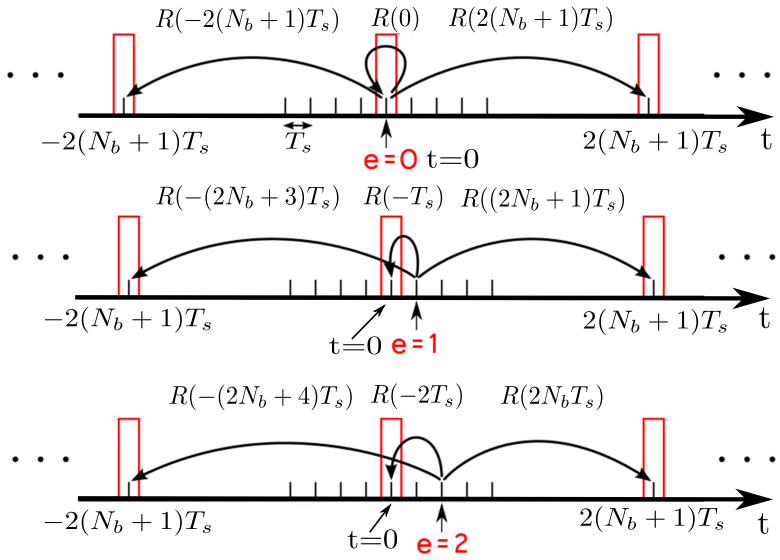


Figure 3.10: *Estimation scheme within a frame. $R(\cdot)$ is a Covariance Function between elements*

form:

$$\boldsymbol{\rho}_0 = \begin{pmatrix} R(2(N_b+1)T_s) \\ R(0) \\ R(-2(N_b+1)T_s) \end{pmatrix}$$

$$\boldsymbol{\rho}_1 = \begin{pmatrix} R((2N_b+1)T_s) \\ R(-T_s) \\ R(-(2N_b+3)T_s) \end{pmatrix}$$

$$\boldsymbol{\rho}_2 = \begin{pmatrix} R(2N_bT_s) \\ R(-2T_s) \\ R(-2(N_b+2)T_s) \end{pmatrix}$$

It is worth mentioning, that since we deal with Gaussian distributed channel gains, Wiener filter is the optimal estimation filter.

BER of this scheme has been derived in [10] and is a function of SNR and correlation between the pilots at $e = 0$ as the best-case scenario:

$$P_{e=0} = \frac{1}{4}(2+\Upsilon)(1-\Upsilon)^2 \tag{3.51}$$

Here

$$\Upsilon = \left( \frac{4\left(1+\bar{\gamma}_s^{-1}\right)}{\epsilon_0} - \left(\frac{\epsilon_1}{\epsilon_0}\right)^2 \right)^{-\frac{1}{2}} \tag{3.52}$$

and

$$\epsilon_0 = \boldsymbol{\rho}_0^H \left( \frac{\mathbf{D}_0}{2} + \bar{\gamma}_p^{-1}\mathbf{I}_{2M+1} \right)^{-1} \boldsymbol{\rho}_0 \tag{3.53}$$

$$\epsilon_1 = \boldsymbol{\rho}_1^H \left( \frac{\mathbf{D}_0}{2} + \bar{\gamma}_p^{-1}\mathbf{I}_{2M+1} \right)^{-1} \boldsymbol{\rho}_0$$

In case of perfect CSI, $R(\tau) = 1$, (3.51) reduces to (3.20). Theoretical MMSE is given by:

$$\sigma_e^2 = 1 - \boldsymbol{\rho}_e^H \left( \frac{\mathbf{D}_0}{2} + \bar{\gamma}_p^{-1}\mathbf{I}_{2M+1} \right)^{-1} \boldsymbol{\rho}_e \tag{3.54}$$

### 3.2.3 Simulation Evaluation of the System Performance

In this section we evaluate by numerical simulation the performance of the discussed transmission system and we observe how it depends on different channel and estimation scheme parameters. Further we look into different real-life scenarios of MS to Base Station (BS) or MS to MS transmission and check how environment can affect the quality of estimation in STTD system.

#### 3.2.3.1 General Evaluation of the System

In general simulational evaluation of the discussed transmission system we used SoS channel generator because of its simplicity and stationarity. We were interested in verifying how different parameters, for example, length of frame (or length of a buffer) or channel fading speed may affect the quality of estimation of the system. First we evaluated how number of pilots $M$ affects estimation. We run the simulation with normalizes bit rate $f_D T_s = 1.5 \cdot 10^{-3}$ and $N_b = 5$, the number of blocks per frame. Estimation error and BER are shown in Figs. 3.11 - 3.12. As we may see from

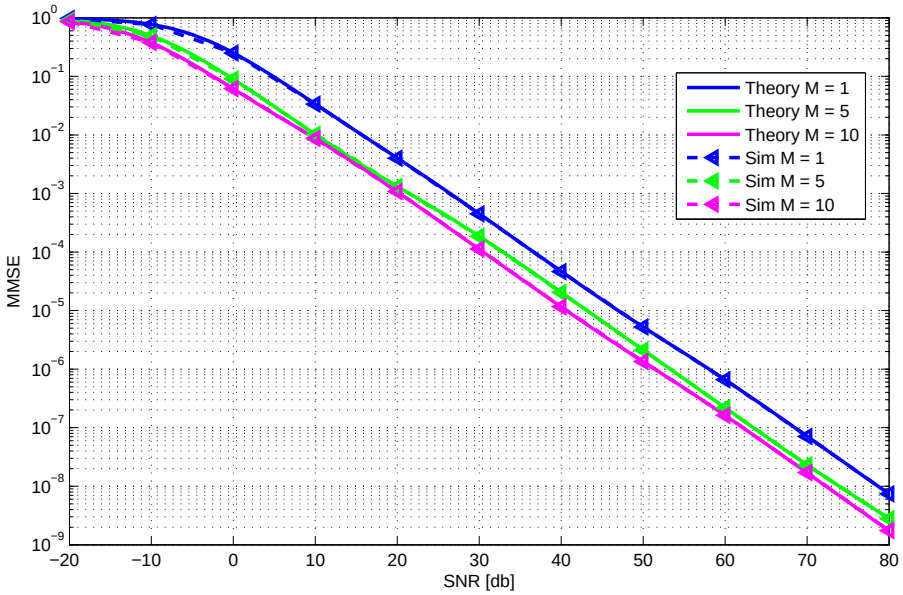


Figure 3.11: *Effect of a buffer length $M$ on quality of estimation. Estimation error $\sigma_e$ as a function of SNR and $M$, SoS channel*

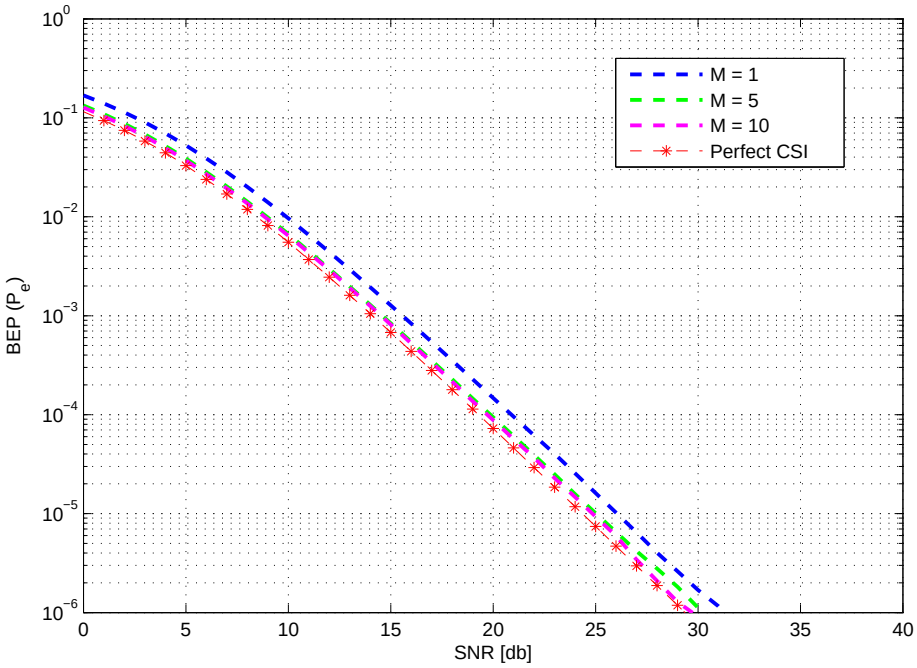


Figure 3.12: *Effect of a buffer length $M$ on quality of estimation. BEP as a function of SNR and $M$, SoS channel*

Fig. 3.11, the greater number of pilot signals in the buffer decreases estimation error. This is due to the fact that with more pilots available at the receiver, the coefficients of Wiener filter are calculated with better precision, hence the estimation is more rigorous. In all cases there is an excellent agreement with the theory. Increasing estimation error with decreasing number of pilots affects as well BEP of the system, see Fig. 3.12. With 10 pilots BEP curve is fairly close to curve in perfect CSI case, what is equivalent to a very good estimation.

In Figs. 3.13 - 3.14 we may see how frame length affects the quality of estimation. As we may infer from Fig. 3.13, with growing number of blocks in a frame MMSE increases. The reason is that with greater $N_b$, an effective number of pilots in a buffer decreases, *i.e.* the covariance function at $2\pi f_D T_s 2(N_b+1)M$ (corresponding to the farthest pilot in a scheme) has considerable attenuation, or $R(2\pi f_D T_s 2(N_b+1)M) \leq 0.5$, which is equivalent to less pilots in possession of the receiver, as pilots with low correlation do not add any additional information about

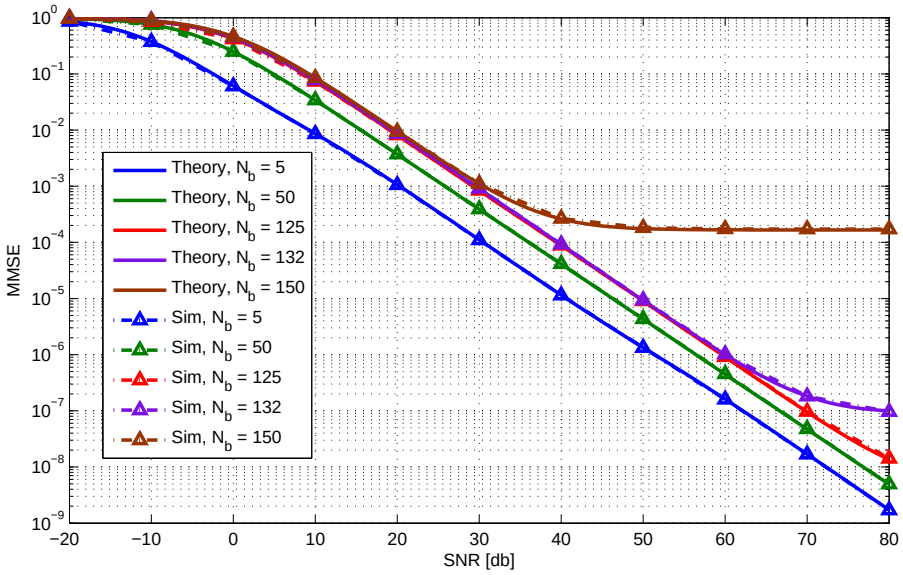


Figure 3.13: *$\sigma_e$ as a function of SNR and a number of blocks per frame $N_b$, SoS channel*

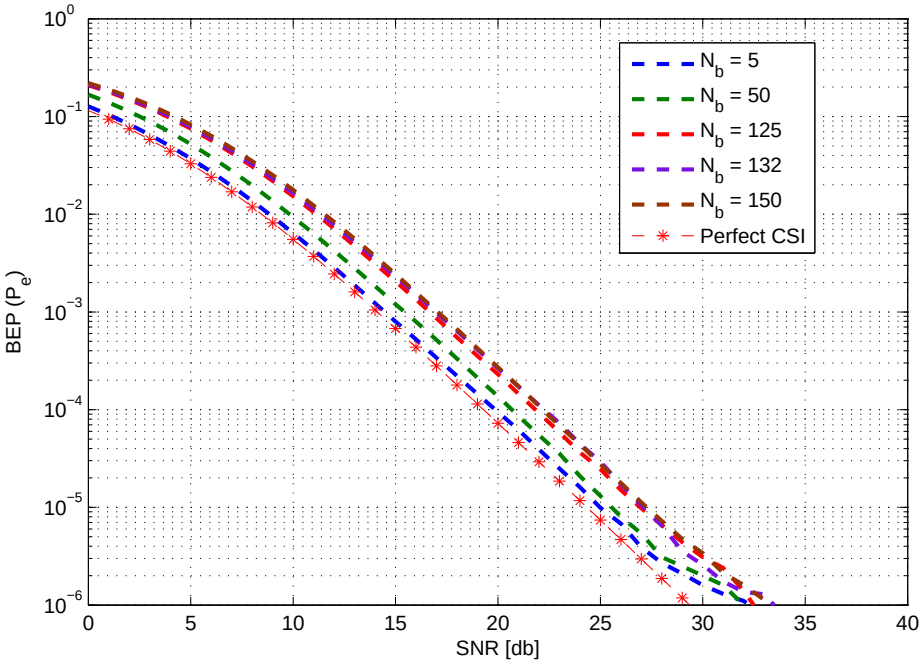


Figure 3.14: *BEP as a function of SNR and $N_b$, SoS channel*

the channel. Again, there is a very good agreement of simulation and theory. BEP is plotted in Fig. 3.14, where we may observe how growing estimation error (as a result of additional blocks per frame) decreases reliability of the system. In general, as the number of blocks increases, the better channel utilization is achieved, but on the other hand, as we see from the simulation it decreases reliability of the system and as a result the achievable rates. According to [25] an optimal frame length $N_b$ could be found numerically through simulation of the capacity of the system as a function of frame length at a desired SNR level. Also we may observe saturation floor effect for large $N_b$: when the number of effective pilots is one or $M_{eff} = 0$, and we estimate channel gain at the middle of the frame, $e = N_b$, it is equivalent to prediction of the point which is $N_b$ samples ahead in future from the pilot signal. Therefore, when the prediction error is greater than estimation one saturation occurs. The saturation thresholds are higher for longer frames, as the prediction point becomes less correlated to the effective pilot.

In Figs. 3.15 - 3.16 the estimation error and BEP are plotted as functions of SNR and rate of channel variation, $f_D T_s$. In Fig. 3.15 we may observe MMSE,

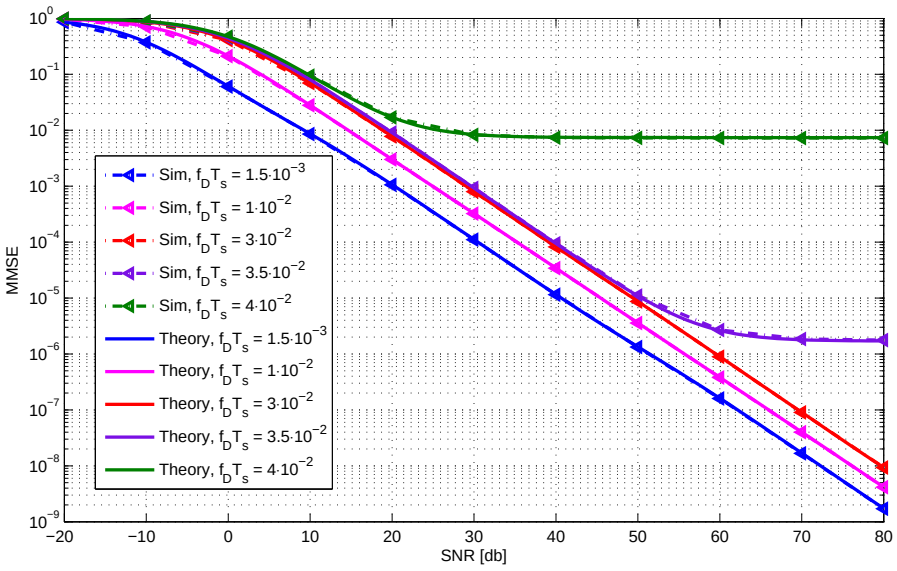


Figure 3.15: *$\sigma_e$ as a function of SNR and channel variation rate $f_D\tau_s$, SoS channel*

and we see good agreement with theory again. MMSE is sensitive to alterations in

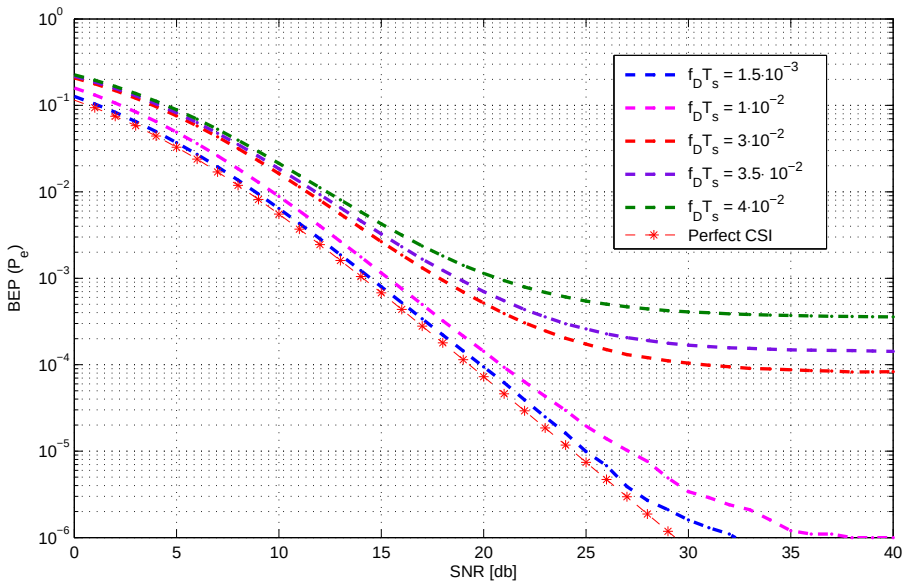


Figure 3.16: *BEP as a function of SNR and $f_D\tau_s$, SoS channel*

channel speed, what results in different saturation levels. We can explain it as follows: with faster channel rates elements within a frame become less correlated, and once the correlation between the pilot signals and estimated point in a frame is close to 1/2 or less (which we consider as a low correlation, or independence) MMSE saturates (estimation error is smaller than prediction error). BEP is plotted in Fig. 3.16. Saturation in BEP on high SNR levels is a result of two reasons: first is the saturation in MMSE due to rapidly varying channel and decaying correlation between pilots, as we discussed previously. Second, it is due to the fact that with faster channel alterations, Alamouti Coding assumption becomes not valid, *i.e.* $h_1[1] \neq h_1[2]$ and $h_2[1] \neq h_2[2]$. In order to check that, we simulated a case of perfect CSI at the receiver, when changing speed of cannel variations, see Fig. 3.17. As we assumed, in perfect CSI case with increasing fading speed BEP curves start saturating, as the Alamouti coding assumption becomes less accurate. We may clearly see, that saturation levels at high SNR in Fig. 3.17 are approximately the same as in case of no CSI at the reciver, Fig. 3.16, therefore we infer that in our estimation scheme inaccuracy of Alamouti coding makes the major contribution to saturation of BEP curves on high SNR. At the same time, increasing estimation error puts the curves further off

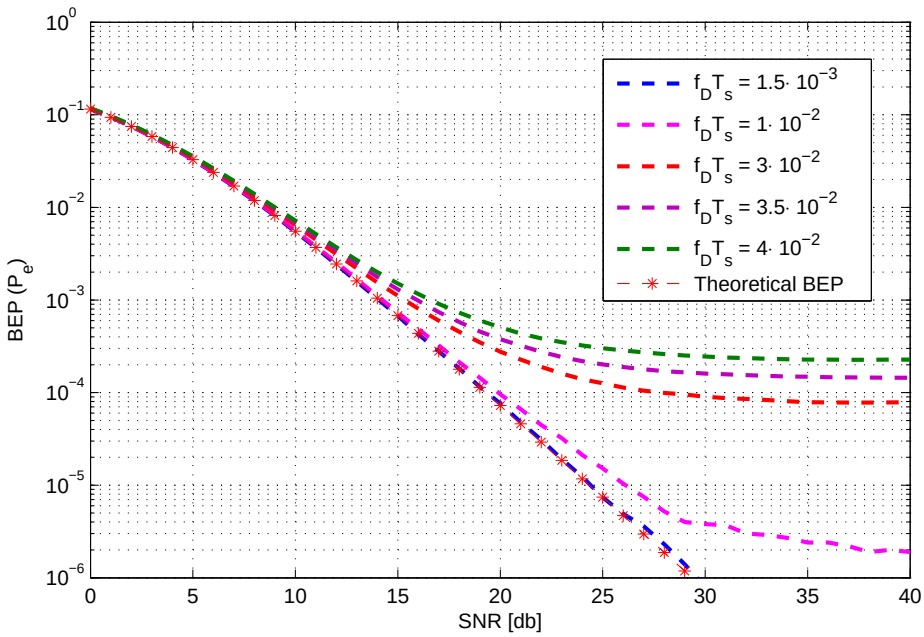


Figure 3.17: *BEP as a function of SNR and channel speed $f_DT_s$ in case of SoS channel and perfect CSI at $R_x$*

the theoretical perfect CSI case in low SNR.

#### 3.2.3.2 Effect of Scattering Environment on Performance of Alamouti Scheme with Imperfect Channel Estimation

In this section we analyze the influence of presence of one or more clusters in the transmission environment in different real-life scenarios. MDPSS channel model, which we discussed in section 2.2.5.2, is very flexible in definition of the geometry and location of different clusters that enables us to analyze various scattering scenarios of interest.

#### 3.2.3.3 Vehicle to Infrastructure Communications (V2I)

This type of communications is featured by the motion of one transmission side (Mobile Station) and stationarity of the other side (Base Station). We discuss two different scenarios where clusters are located on the way of the mobile or on the side of the road, and mobile is passing by. For visualization look up Figs. 3.19 and 3.23. Then we model a real-life scenario from one of the intersections in city of London, ON.

Reciprocally to the previous section, first we run some general simulations with use of MDPSS channel model to validate the performance of the system. Thus, for example, Fig. 3.18 shows how number of pilots $M$ used for estimation affects MMSE of the scheme. The simulation was performed for the rate of 50 Kbps, $N_b = 5$, $e = 0$ and cluster parameters given in Table 2.1. As we would expect, the greater number of pilots reduces estimation error for any SNR. It happens because larger number of pilots provides more information to the receiver about correlation of channel gains, therefore better estimation is achieved. There is a good convergence between theory and simulation.

At the first scenario we assume that a mobile, for example a car, is moving along the road and passing under a big road sign, as in Fig. 3.19. The base station is assumed to be far away. In this case the angular spread $\Delta\phi_r$ changes as a function of time (or distance to the cluster) and as we may see from the figure $\Delta\phi_r$ increases as the car approaches the cluster. The expression for the varying angular spread is

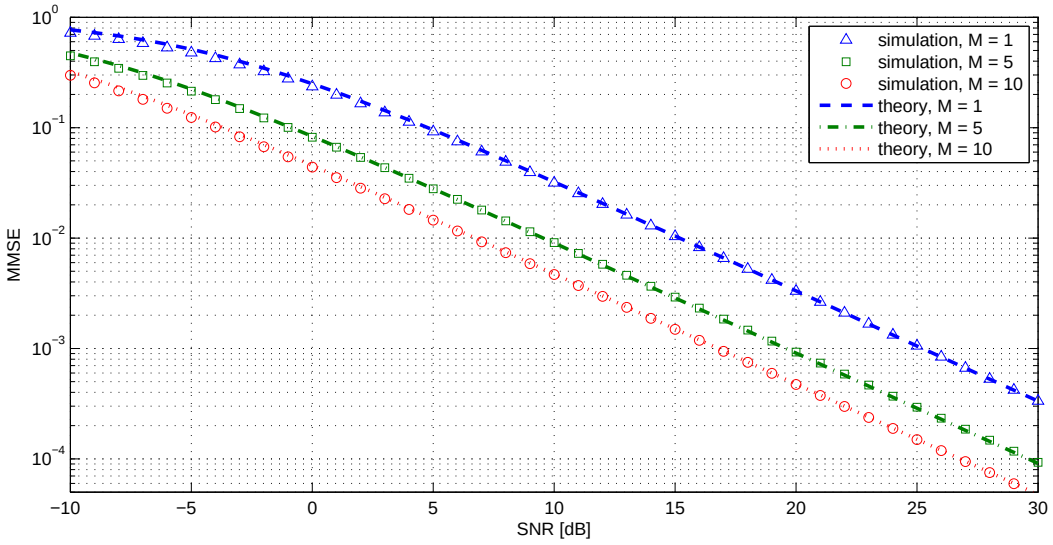


Figure 3.18: *Estimation quality as a function of SNR and number of pilot signals M*

then:

$$\Delta\phi_r(t) = 2\tan^{-1}\left(\frac{a\tan\left(\frac{\Delta\phi_{r0}}{2}\right)}{a - 2v_r t\cdot\tan\left(\frac{\Delta\phi_{r0}}{2}\right)}\right) \tag{3.55}$$

Here the initial angular spread is $\Delta\phi_{r0} = 5^0$, $\phi_r \approx 0^0$, $a = 5$ m is the width of the road sign and all the other parameters are as in Table 2.1. Fig. 3.20 shows behaviour of

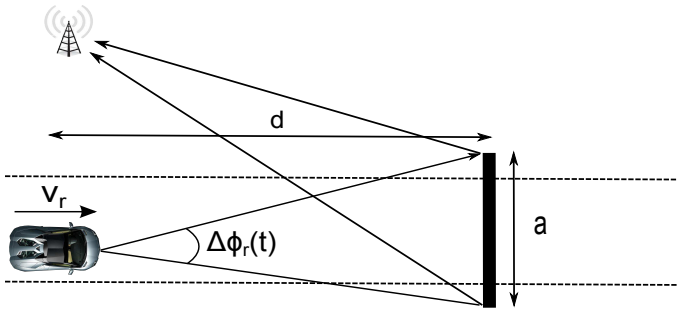


Figure 3.19: *Scenario 1, a mobile is moving under a big road sign*

absolute value of autocorrelation function of channel gains as a function of normalized delay time and a distance to the cluster. Negative distance implies that the mobile is located on the left side of the cluster (according to Fig. 3.19) and positive distance

implies that it is located to the right. The cluster is located at $d = 0$ m. It can be seen, that as the mobile gets closer to the cluster, autocorrelation function decays quicker. As a consequence, the pilot signals become less correlated, which results into higher estimation error. The behaviour of channel gains estimation MMSE as a

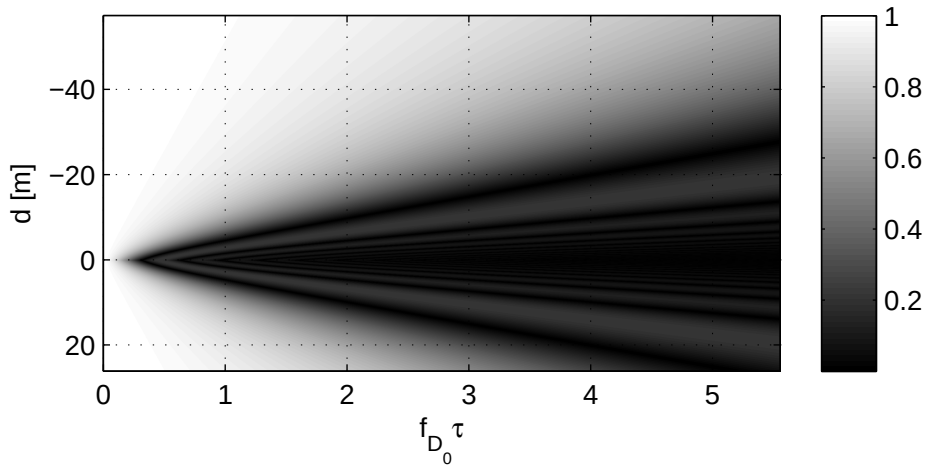


Figure 3.20: *Absolute value of autocorrelation function of channel gains,* $|R(d, f_{D_0\tau})|$*, Scenario 1*

function of distance to the cluster at SNR = 10 dB and 50 Kbps rate with $M = 1$ and $e = 0$ for the estimation is shown in Fig. 3.21 and the resulting BER is given in Fig. 3.22. If we compare BER curves to perfect CSI case (or error-free estimation) we may see that the initial increase of 4 dB in BER presents because of the estimation based on 3 pilots only. Further increase in BER is introduced as the car is nearing the cluster. As we may observe the effect of cluster's presence is more pronounced at longer frames. If the frame is built of more that 100 blocks, MMSE increases dramatically when the vehicle approaches the cluster. For example, for 200 blocks length frames the increase in MMSE is more than 10 times with resultant increase in BER by 4.7 dB (see Fig. 3.22) when the car is under the road sign. Therefore this kind of clusters produce significant shadowing effect on communication session. On the other hand this apparent decrease of communication quality is fleeting and does not last more than a couple of seconds.

The second scenario depicts a mobile passing by two significant clusters located on a side of the road, see Fig. 3.23. In this case we assume that clusters are far enough

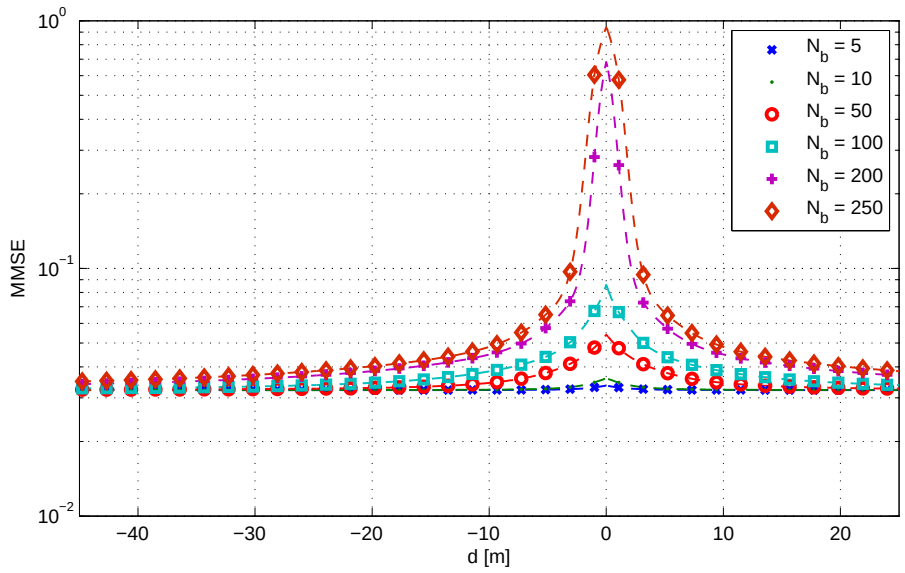


Figure 3.21: *Estimation MMSE as a function of distance to the cluster and frame length at $SNR = 10dB$, $50Kbps$ rate and 3 pilot-based estimation, Scenario 1*

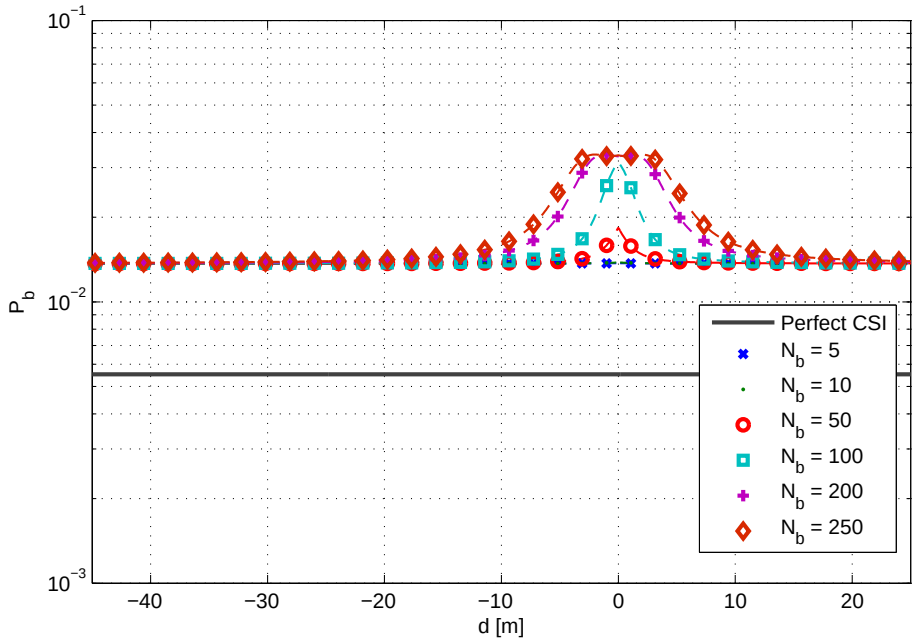


Figure 3.22: *BER as a function of distance to the cluster at $SNR = 10dB$, $50Kbps$ rate and 3 pilot-based estimation, Scenario 1*

so that their angular spread $\Delta\phi_{r1}$, $\Delta\phi_{r2}$ are small and do not change as a car passes by. The initial angle between the vector of movement and the first cluster's centre is $\phi_{r1_0} = 10^0$. Moreover we assume for simplicity that both clusters are located on the same perpendicular to the mobile movement vector with equal distances between each other and the road, $h = 10$ m, as shown in Fig. 3.23, and clusters' angular spreads do not change. Hence the initial angle of the second cluster with the receiving side equals

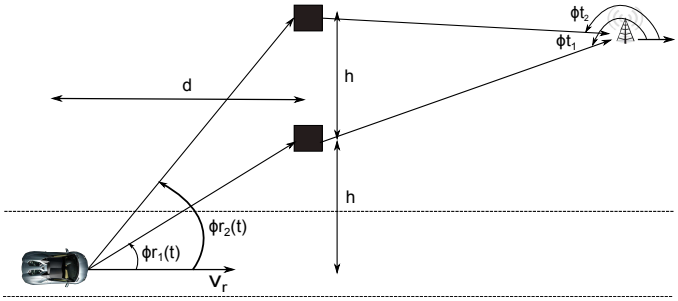


Figure 3.23: *Scenario 2, a mobile is passing by two significant clusters located on the side of the road*

$\phi_{r2_0} = \tan^{-1}(2\tan(\phi_{r1_0})) \approx 19^0$. The angles from the BS to clusters are arbitrary taken to be $\phi_{t1} = 185^0$, $\phi_{t2} = 175^0$ and they are constant. Each one of angels $\phi_{r1}(t)$, $\phi_{r2}(t)$ changes in accordance with distance change (as a function of time) between clusters and the car:

$$\phi_{r,i}(t) = \tan^{-1}\left(\frac{h\tan(\phi_{r0,i})}{h - vt\tan(\phi_{r0,i})}\right), \quad i = 1, 2 \tag{3.56}$$

The autocorrelation function of the channel in this scenario is shown in Fig. 3.24. Corresponding BER and MMSE graphs are shown in Figs. 3.25 - 3.26. As in previous case, there is an initial recession of 4 dB in BER because of estimation based on 3 pilot signals only (when comparing to perfect CSI). Furthermore, as we expected, autocorrelation function of the channel decays more rapidly in vicinity of clusters, what affects the performance of the system, increasing estimation error and thus BER by additional 3 dB. In contrast to the previous case, the increase in MMSE is not as sharp, but its duration is considerably longer, about 5 seconds. The notable attribute in this case is that when the mobile is located precisely at $d = 0$ m, *i.e.* perpendicular to clusters, autocorrelation function has an instant escalation (see Fig.

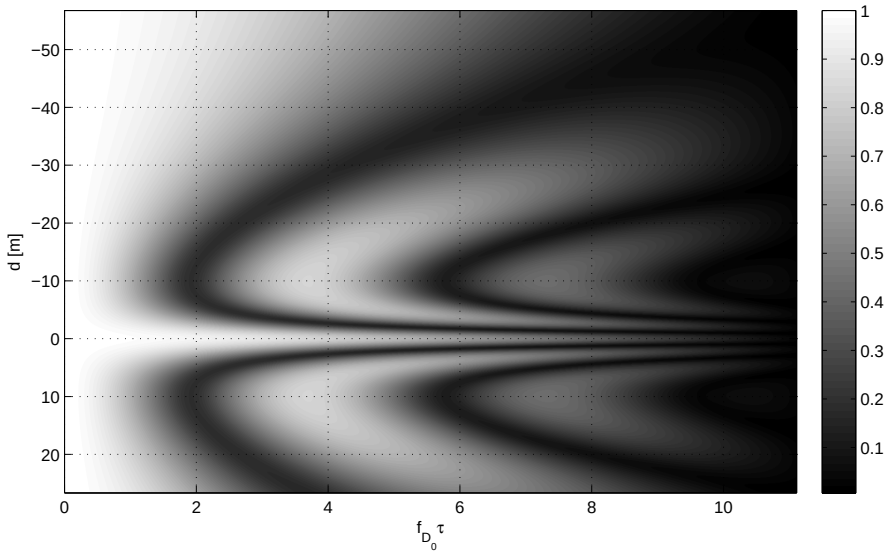


Figure 3.24: *Absolute value of autocorrelation function of channel gains,* $|R(d, f_{D_0\tau})|$*, Scenario 2*

3.24), what results in a notch in MMSE and BER curves around zero (Fig. 3.25 and Fig. 3.26). This behaviour has a simple explanation: when the mobile is located at $d = 0$ m, both clusters have equivalent angular parameters, what in terms of auto-correlation function equals to summation of two equally modulated sink functions, therefore when absolute value is taken it behaves like a one-cluster case: a very slow decay in correlation as an absolute value of a pure sink function. Or effectively the mobile "sees" one cluster with unity power.

Now we model a scenario from a real intersection in the city of London, Ontario. The picture in Fig. 3.27 was taken at the intersection of Wonderland Road and Oxford Street (East of Wonderland Road view to the North-West). The view on the same intersection, but from Google Maps Street Viewer ©, is shown in In Fig. 3.28.

Let us assume, that some mobile equipped with our system is passing through the intersection with speed of $30km/h$ and moving to the North along Wonderland Road. Let us assume as well that there is a downlink between the mobile and a Bell cellular tower located on the roof of one of the apartment buildings on the left-hand side of the road, at the address 720 Wonderland Rd., which is approximately 400 m to the North from the intersection, see Fig. 3.29. From the picture of the intersection, we

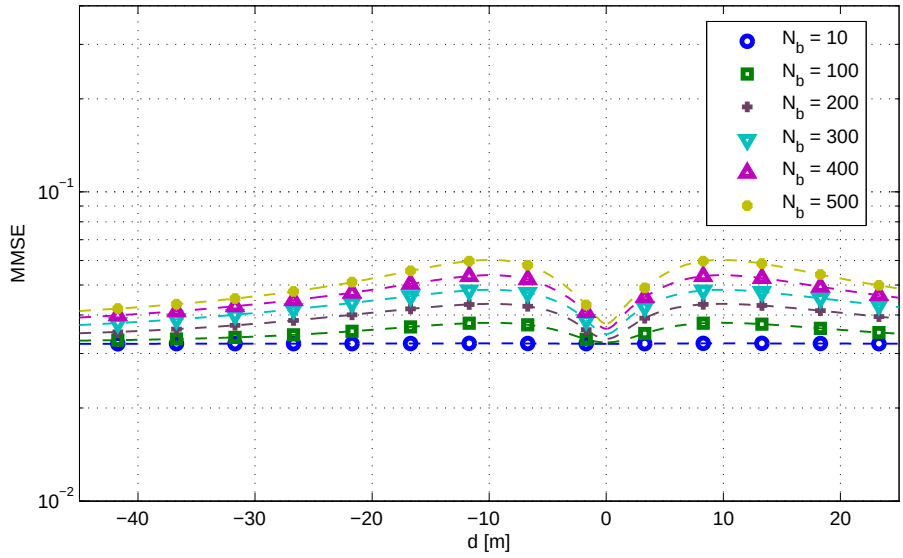


Figure 3.25: *Estimation MMSE as a function of distance to clusters and frame length at* $SNR = 10dB$, $50Kbps$ *rate and 3 pilot-based estimation, Scenario 2*

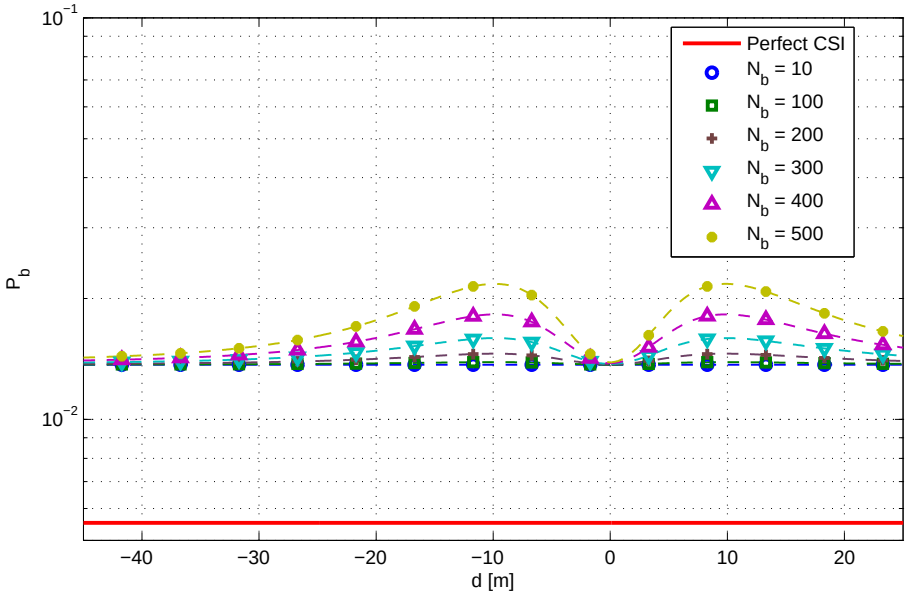


Figure 3.26: *BER as a function of distance to clusters at* $SNR = 10dB$, $50Kbps$ *rate and 3 pilot-based estimation, Scenario 2*

may clearly define several clusters in vicinity of the mobile station: Petro-Canada and Esso gas stations on the Western side of Wonderland Road (and on opposite sides

Figure 3.27: *Real Street View, Wonderland Rd. and Oxford St. intersection, London, Ontario, Canada, ON N6H*

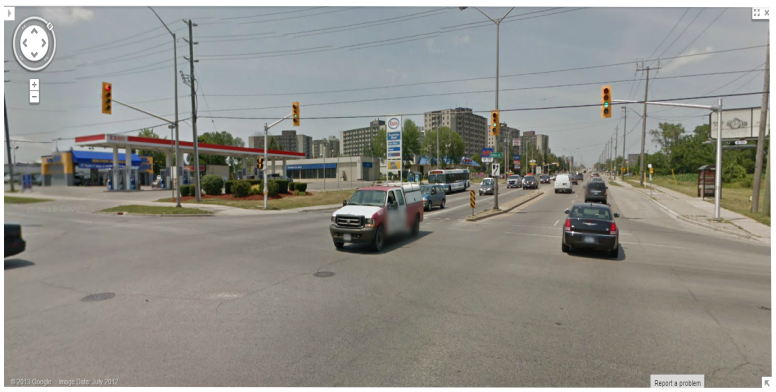

Figure 3.28: *Google Map Street View ©, Wonderland Rd. and Oxford St. intersection, London, Ontario, Canada, ON N6H*

of Oxford), a big metal poster, a convenience store near the Esso gas station, and Malibu Restaurant West Intc. to the North from Esso, see Fig. 3.30. All the rest of buildings and obstacles are either shadowed by these four clusters (for example, Cluster 5 on the picture) or approximately too far to contribute to the signal scattering with respect to the current mobile location, but might be taken into the consideration when recalculating the communication site layout as the mobile moves forward and approaches them. The distances, angles and angular spreads of each cluster can be

| | *Cluster 1* | *Cluster 2* | *Cluster 3* | *Cluster 4* |
|---|---|---|---|---|
| $\phi_r$ $[^0]$ | 121.3 | 46.1 | 26.3 | 22 |
| $\Delta\phi_r$ $[^0]$ | 25.7 | 35.7 | 2.4 | 16.7 |
| $\phi_t$ $[^0]$ | 134.8 | 143.9 | 134.3 | 134.9 |
| $\Delta\phi_t$ $[^0]$ | 3.4 | 5.1 | 0.6 | 6 |
| $\tau$ $[\mu sec]$ | 1.68 | 1.43 | 1.38 | 1.38 |
| $\Delta\tau$ $[\mu sec]$ | 0.09 | 0.08 | 0.003 | 0.01 |
| $h$ $[m]$ | 55.7 | 64.55 | 31.88 | 42.78 |
| $P$ | 0.3 | 0.3 | 0.1 | 0.3 |

Table 3.1: *Parameters of clusters in scenario on Wonderland Road and Oxford Street intersection*

easily measured and calculated using Google Distance Measurement Tool ©, see Fig 3.31. The parameters of each cluster are listed in Table. 3.1. Powers of clusters were chosen arbitrary for simplicity purposes, but could be verified through more elaborate calculations, for example with use of Radar Equation. Auto-correlation function of the channel in this scenario is shown in Fig. 3.33 as a function of normalized Doppler time and distance to cluster 2. As we may see, cluster 1 almost does not contribute to the fading, cluster 2 and cluster 4 make the major contribution and we may clearly distinguish them on the auto-covariance graph. Contribution of cluster 3 is merged with one of cluster 2, because this cluster is small and is located really close to the big cluster, therefore the mobile is not able to distinguish it. We may think that it adds up to the power of cluster 2. Overall, the correlation snapshot appears blurred with a lot of grey-level corresponding to correlation of 0.3-0.6 with no very pronounced dark areas (a very low correlation), as we saw in previous cases. The reason is that in this scenario the distances between the mobile and clusters are bigger than in previous cases (30-64 meters compared to 10-20 meters) as well as angular spreads ($2^0 - 35^0$ compared to $10^0 - 19^0$). An example of MMSE and BER for 200 blocks frame-length and with 3 pilot signals prediction at 50 *kbps* is shown in Fig. 3.34, where we can see the influence of clusters at 0 and around 40 meters (with respect to the second cluster).

In a similar way we may analyze communication in any type of terrain containing multiple obstacles. Of course, extension to more complicated scenarios

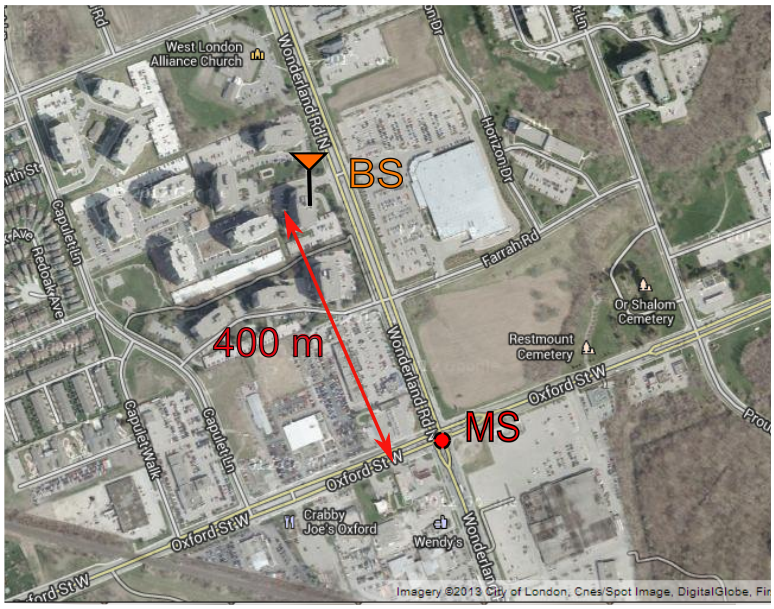


Figure 3.29: *Google Map Street View ©, locations of base station and mobile station*

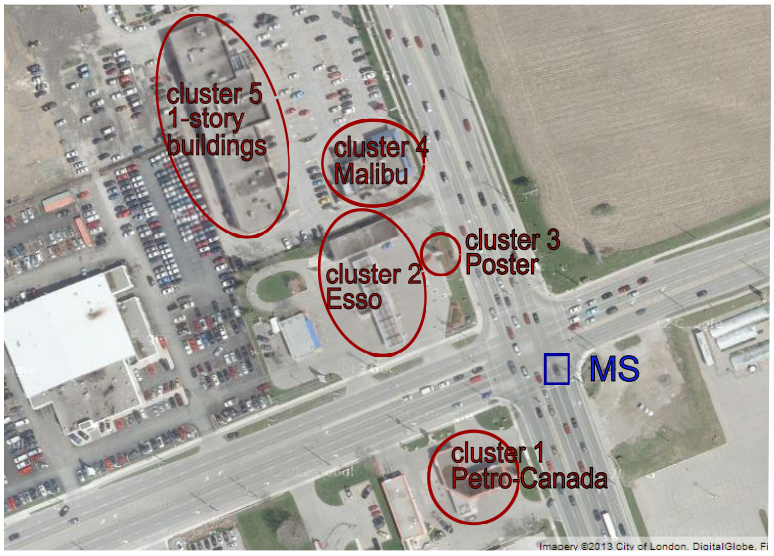


Figure 3.30: *Google Map Street View ©, clusters contributing to the signal diffusion around the mobile*

describing bigger number of clusters with non-symmetrical allocation is straightforward. Also another various kinds of modulation and transmission schemes could be evaluated to improve the overall performance of the system.

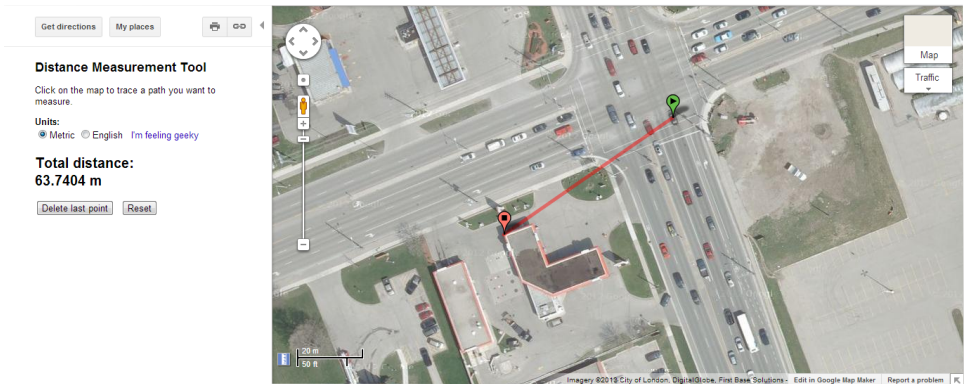


Figure 3.31: *Google Map Street View ©, Distance Measurement Tool*

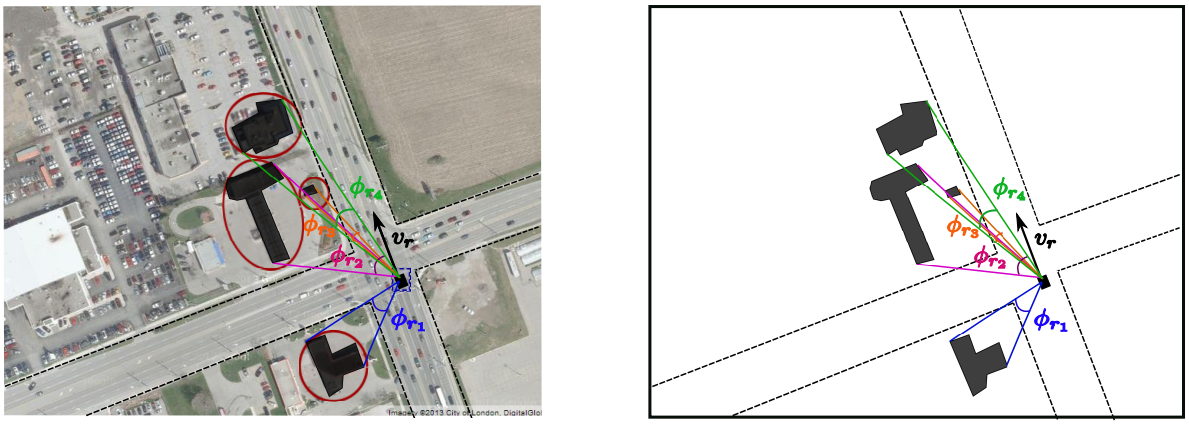


(a) (b)

Figure 3.32: *The geometry of the site around the mobile*

#### 3.2.3.4 Vehicle to Vehicle Communications (V2V)

Vehicle to Vehicle communication is currently a quickly developing area of wireless communications. Many new applications are designed in order to improve vehicular active safety, for example critical distancing between cars, collision warnings, alert about poor road conditions, *etc.*, other applications are in demand to enhance transportation systems efficiency, *i.e.* avoiding transport jamming or construction sites, as well as improving passengers comfort [16]. Realistic models for V2V physical channels characterization are essential for reliable design and testing of V2V systems. Since this kind of communication is accompanied by the motion of both receive and transmit

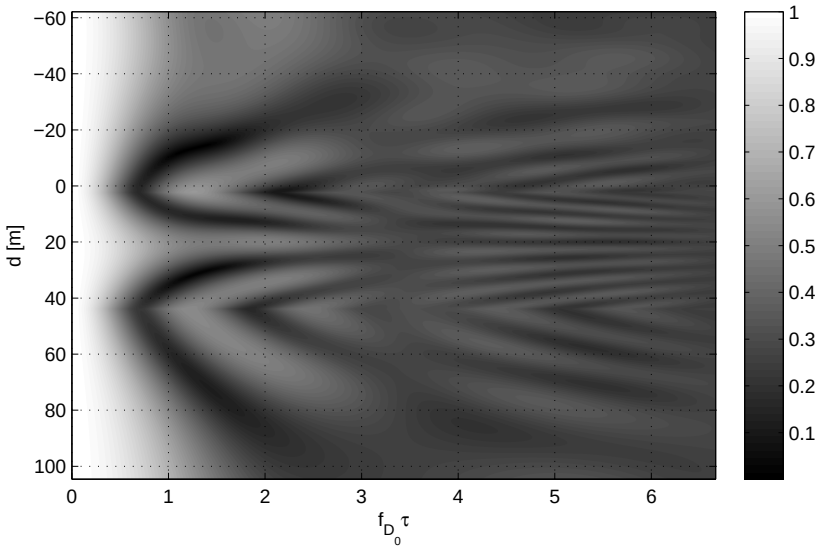


Figure 3.33: *Auto-correlation function in a real-life scenario, Oxford Street - Wonderland Road intersection, London ON*

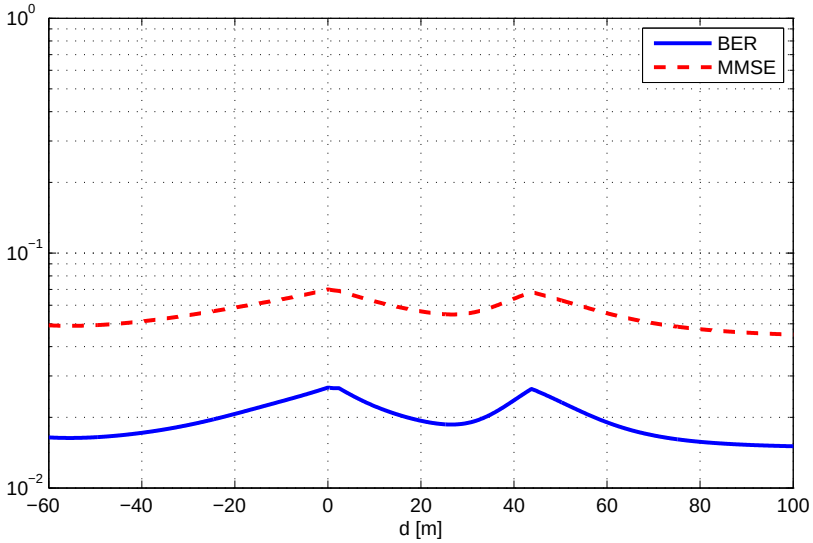


Figure 3.34: *Estimation Error and Bit Error Rate as a function of distance to the cluster, Oxford Street - Wonderland Road intersection, London ON*

sides with low elevation antennas and scatterers which are assumed to be located on perimeters of multiple co-focal ellipses (where the receiver and the transmitter are at ellipse's focals), the MDPSS channel model might be used as Regular-Shaped Geom-

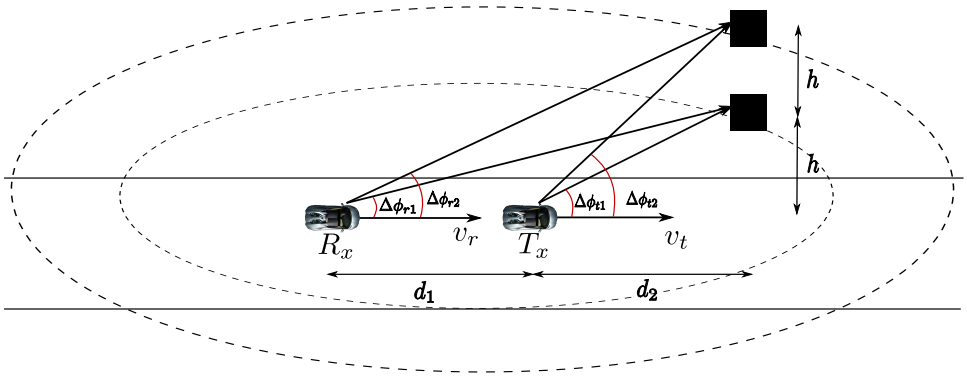


Figure 3.35: *V2V scenario with two clusters*

etry Based Stochastic Model (RS-GBSM) for the description of underlying physical channel between communicating sides in Moderate Spatial Scale (MSS) or Small Spatial Scale (SSS) scenarios. Assuming that the exact geometry description of clusters and obstacles is available through different accessible applications like Google Maps © for 3D street view or through different global navigation and positioning satellite systems like GPS [27], GLONASS [28] or QZSS [29], it is possible to model the geometry of any site of interest.

The scenario, shown in Fig. 3.35, is similar to scenario 2, but now both the receiver and the transmitter are moving at the same direction and are passing two identical clusters, which are located on the side of the road. Again, for simplicity, we assume that both clusters are located on the same perpendicular to the mobile movement vector with equal distance between each other and the road, $h = 10$ m. Also, we assume that the angular spread of both clusters is the same and approximately does not change as mobiles pass by, $\Delta\phi_1, \Delta\phi_2 \approx 5^0$. The initial angles between the first cluster's centre and the vectors of movement of the receiver and the transmitter respectively are $\phi_{r1_0} = 5^0, \phi_{t1_0} = 7^0$. Hence the angle between mobile's movement vectors and the center of the second cluster is calculated from: $\phi_{r2_0,t2_0} = \tan^{-1}(2\tan(\phi_{r1_0,t1_0}))$ and equal approximately $10^0$ and $14^0$. Each one of angels $\phi_{r1}(t)$, $\phi_{r2}(t)$, $\phi_{t1}(t)$, $\phi_{t2}(t)$ changes in accordance with distance change

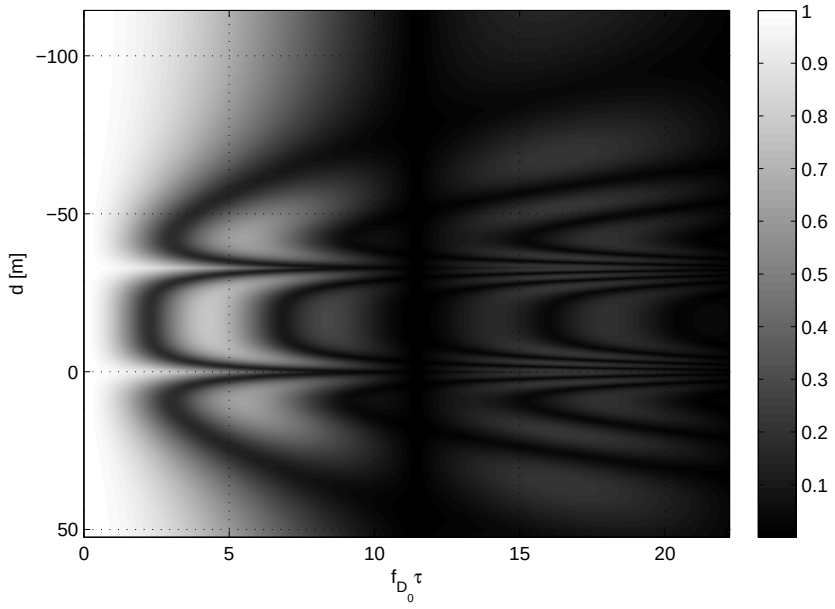


Figure 3.36: *Absolute value of autocorrelation function of channel gains,* $|R(d, f_{D_0\tau})|$*, V2V scenario*

between clusters and the car:

$$\phi_{r,t,i}(t) = \tan^{-1}\left(\frac{h\tan(\phi_{r0,t0,i})}{h - vt\tan(\phi_{r0,t0,i})}\right), i = 1, 2 \tag{3.57}$$

The snapshot of auto-covariance function in the case when both vehicles' speed equal $30km/h$ is shown in Fig. 3.36. Resulting estimation MMSE and BER are shown in Figs. 3.37 - 3.38. Fig. 3.37 shows the estimation error as a function of frame length $N_b$ and the distance from the cluster with respect to the receiver. As we can see, longer frames increase MMSE due to decreasing correlation between pilots. On the graph we can distinguish two notches at $d = -40m$ and $d = 0m$, where the system experiences quick decrease in estimation MMSE, corresponding to the vehicles' location strictly perpendicular to clusters, where the mobiles effectively "see" one cluster with the unity power (same explanation as in Sec. 3.2.3.3, scenario 2). In addition, the greatest estimation error is induced when vehicles are located from the different sides of the cluster ($-40m \leq d \leq 0m$ on the graph). From the graph of BER we see that, as in V2I case, there is an initial recession of 4 dB in BER because of estimation based

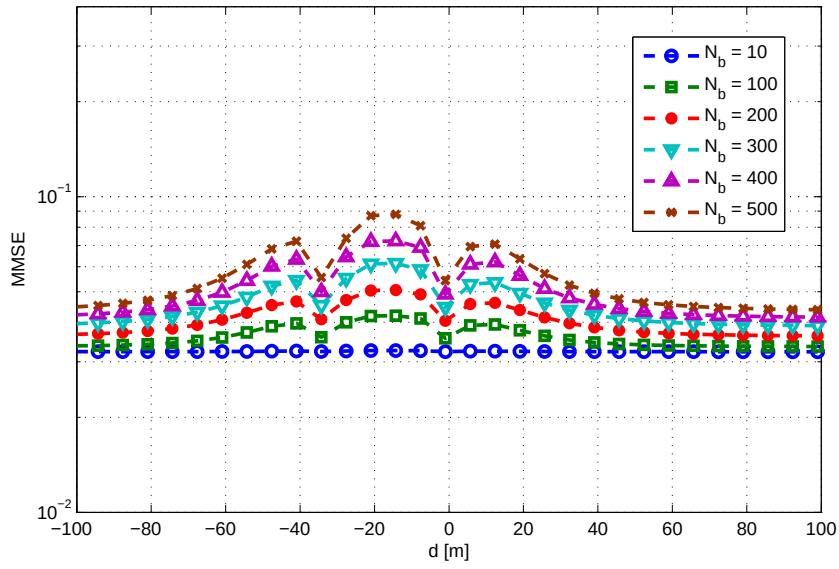


Figure 3.37: *Estimation MMSE as a function of distance to the cluster with respect to $R_x$ and a frame length $N_b$ at $SNR = 10db$ and 3 pilot-based estimation, V2V scenario*

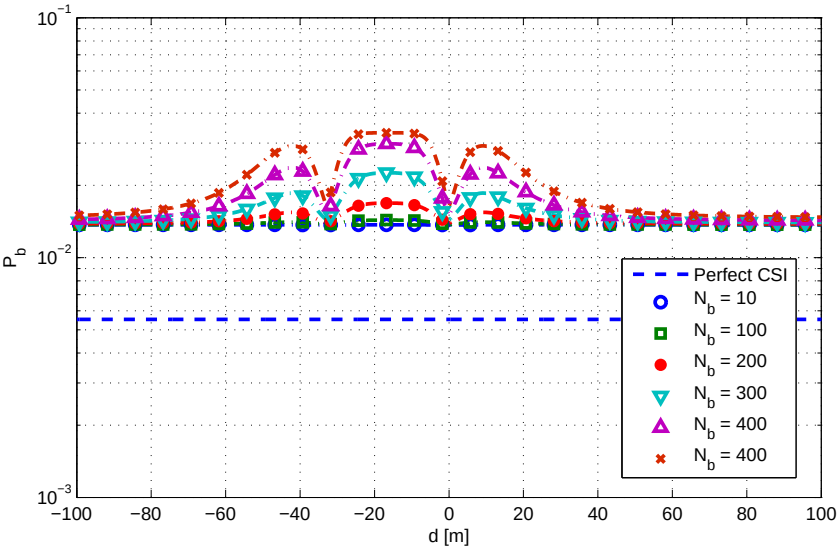


Figure 3.38: *BER as a function of distance to the cluster with respect to $R_x$ and a frame length $N_b$ at the rate $SNR = 10db$ and 3 pilot-based estimation, V2V scenario*

on 3 pilot signals only (when comparing to the perfect CSI), and further increase of 3.8 dB is introduced because of the clusters presence.

## 3.3 Summary

- Communication over a wireless channel includes different factors which corrupt the information sent over the medium. The most pronounced of them are noise and channel fluctuations in time and frequency. While the performance in AWGN channel in terms of BER improves exponentially with growing SNR, with presence of a random channel it improves only linearly, even with a perfect knowledge of CSI at the receiver. This happens because there is a probability greater than zero, that the channel is in a deep fading state. Therefore different diversity techniques should be applied in order to improve system's performance. In our work we focus on $2 \times 1$ STTD system with Alamouti coding.
- Alamouti scheme significantly relies on the channel knowledge at the receiver side. In a real-life communication system perfect CSI is not available and there is a need in channel estimation unit. One of the most popular estimation schemes is pilot-based estimation with Wiener filter for pilot signals at the receiver.
- It was shown trough the simulation, that different parameters of estimation system and the channel affect the quality of communications. Thus, the greater number of pilot signals (or length of the buffer) improves system's performance in terms of BER and estimation MMSE, since the receiver has more information about the channel. On the other hand bigger number of blocks per frame and faster channel fading were shown to deteriorate system's performance, because both of these factors decrease pilots correlation, making the effective buffer length smaller.
- A number of real-life scenarios of V2I communications was investigated: one of them includes a big cluster located on the way of a moving mobile, like a road sign. The other one consists of two similar clusters located on one side of the road and the mobile passes by, for example, houses or gas stations, or any other obstacles, which could be found on the side of a road. In both cases increase in estimation MMSE was detected in vicinity of clusters resulting in

degradation of system's performance in terms of BER. At the same time, the effect of performance's downgrading is bigger in cases of longer frames between pilot signals, as a straightforward result from quickly decaying autocorrelation function of channel gains in occurrence of clusters in the environment. In first scenario increase in MMSE and BER was higher, although with shorter duration, than in second scenario. A scenario, which describes the channel analysis from a real street, located in London, ON, is demonstrated as well, where we explain in detail how we can use different tools (like Google Maps ©) in order to calculate the parameters of clusters which contribute to signal scattering in vicinity of mobile during the communication session.

- We have shown how MDPSS model could be easily applied to mimic channels in mobile to mobile communications scenario, where we assume, that clusters are located on the perimeters of co-centric ellipses and their geometry can be calculated from available online resources.
- It is worth mentioning that due to flexibility of the MDPSS simulator the description of a vast variety of different scenarios is available, allowing one to easily test any kind of environment with different positioning of clusters.

# Chapter 4
# Light Wiener Filters for Channel Estimation of Slowly Varying Wireless Channels

As it was previously mentioned, classical Wiener filter (or full Wiener filter as we refer to it in this work) is an optimal filter for gaussian signals because it minimizes the estimation error [15], therefore it is optimal for pilot symbol assisted modulation (PSAM) as well [14], [15]. But in order to apply it, the receiver needs to know the statistics of the channel, *i.e.* the auto-covariance function. In real life communication this information is usually unavailable and its estimation is complicated. In the best case scenario, the receiver has some partial knowledge about the channel process, for example mean value and variance, but in many cases even this is not available. Therefore Wiener filters are not practical and other estimators are used, which are suboptimal, but do not require full knowledge of covariance function. Some of the interpolation filters used in previous works include lowpass and approximately Gaussian filters [14], [30], Least-Squares Estimates (LSE) [31], [32], James-Stein estimate [33], ML estimates [10] or Minimum Variance Unbiased (MVU) estimates [34], [35], [36]. The research in this topic is still relevant and new reduced complexity estimators are proposed, for example see [37].

Let us assume the case of downlink or uplink between the mobile and the base station. When data rates are relatively high, the channel features in slow fading. In this case, channel gains remain highly correlated during relatively long time slots, what leads to slowly change in auto-covariance function. We assert that in these communication conditions during the channel estimation stage via Wiener filter at the receiver it is unnecessarily to calculate the whole auto-covariance function, but it

is sufficient to provide its low order approximation. This can be useful when statistics of the channel are partially unknown, as the estimation of polynomial coefficients is much easier, than estimation of the precise covariance function. Moreover, this approach would reduce computational load of the receiver and would result in more efficient energy source utilization. In this chapter we provide theoretical derivations of Light Wiener filers, which are based on the approximated channel auto-covariance functions and support our assumption by the simulation. In our analysis we address both real-valued and complex covariance functions cases. Simulation is performed for channels discussed in Chapter 2 and with $2 \times 1$ narrowband MISO transmission system, discussed in Chapter 3.

## 4.1 Zero Order Approximation of Covariance Function

For simplicity we write the general representation for Wiener filter coefficients as follows (energy normalization between antennas is dropped for the same reason):

$$\mathbf{h}_e = \left(\mathbf{R} + \gamma_p^{-1}\mathbf{I}\right)^{-1} \boldsymbol{\rho}_e \tag{4.1}$$

Here $\mathbf{h}_e$ is the vector of filter coefficients for calculation of the channel gain at place $e$ at the frame (see Fig. 3.10), $\mathbf{R}$ and $\boldsymbol{\rho}_e$ are pilots correlation matrix and vector respectively. In the case of a very slow fading, channel covariance function might be approximated by a zero order polynomial (first term of Taylor Series expansion), *i.e.*

$$R(\tau) \approx 1 + O(\tau), \tag{4.2}$$

where $\tau = nT_s$. This approximation is valid for any kind of covariance functions (both real and complex). If we denote $N = 2M + 1$ to be the total number of pilots,

correlation matrix $\mathbf{R}$ can be written as a unit matrix:

$$\mathbf{R}_{N\times N} = \begin{bmatrix} 1 & 1 & \dots & 1 \\ 1 & 1 & \dots & 1 \\ . & . & . & . \\ 1 & 1 & \dots & 1 \end{bmatrix} = \vec{\mathbf{1}}_N \vec{\mathbf{1}}_N^H \tag{4.3}$$

where $\vec{\mathbf{1}}_N$ is $N \times 1$ unity vector:

$$\vec{\mathbf{1}}_N = \begin{bmatrix} 1 \\ 1 \\ \vdots \\ 1 \end{bmatrix}$$

Under similar conditions the correlation vector could be approximated as:

$$\boldsymbol{\rho}_e = \vec{\mathbf{1}}_N \tag{4.4}$$

Equation (4.1) now could be approximated as follows:

$$\mathbf{h}_{e_0} \approx \left(\vec{\mathbf{1}}_N \vec{\mathbf{1}}_N^H + \gamma_p^{-1}\mathbf{I}\right)^{-1} \vec{\mathbf{1}}_N \tag{4.5}$$

In order to evaluate (4.5) explicitly, we can use Sherman-Morrison identity [7]:

$$\left(\mathbf{A} + \mathbf{u}\mathbf{v}^T\right)^{-1} = \mathbf{A}^{-1} - \frac{\mathbf{A}^{-1}\mathbf{u}\mathbf{v}^T\mathbf{A}^{-1}}{1 + \mathbf{v}^T\mathbf{A}^{-1}\mathbf{u}} \tag{4.6}$$

where $\mathbf{A}$ is an invertible matrix and $\mathbf{u}\mathbf{v}^T$ is a product of a column vector $\mathbf{u}$ and a row vector $\mathbf{v}^T$. In our case:

$$\begin{aligned} &\mathbf{A} = \gamma_p^{-1}\mathbf{I} \;\Rightarrow\; \mathbf{A}^{-1} = \gamma_p\mathbf{I} \\ &\vec{\mathbf{u}} = \vec{\mathbf{v}} = \vec{\mathbf{1}}_N \end{aligned} \tag{4.7}$$

Therefore

$$\left(\vec{\mathbf{1}}_N\vec{\mathbf{1}}_N^H+\gamma_p^{-1}\mathbf{I}\right)^{-1}=\gamma_p\mathbf{I}-\frac{\gamma_p\mathbf{I}\ \vec{\mathbf{1}}_N\vec{\mathbf{1}}_N^H\ \gamma_p\mathbf{I}}{1+\vec{\mathbf{1}}_N^H\ \gamma_p\mathbf{I}\ \vec{\mathbf{1}}_N}=\gamma_p\mathbf{I}-\frac{\gamma_p^2\ \vec{\mathbf{1}}_N\vec{\mathbf{1}}_N^H}{1+N\gamma_p} \tag{4.8}$$

Substituting (4.8) into (4.5) one obtains the expression for the zero order approximation filter coefficients $\mathbf{h}_{e_0}$:

$$\mathbf{h}_{e_0}=\left(\gamma_p\mathbf{I}-\frac{\gamma_p^2\vec{\mathbf{1}}_N\vec{\mathbf{1}}_N^H}{1+N\gamma_p}\right)\vec{\mathbf{1}}_N= \tag{4.9a}$$

$$=\left(\gamma_p\vec{\mathbf{1}}_N-\frac{\gamma_p^2N}{1+N\gamma_p}\vec{\mathbf{1}}_N\right)= \tag{4.9b}$$

$$=\frac{\gamma_p}{1+N\gamma_p}\vec{\mathbf{1}}_N=\frac{N\gamma_p}{1+N\gamma_p}\ \frac{1}{N}\vec{\mathbf{1}}_N, \tag{4.9c}$$

where in the transition from (4.9a) to (4.9b) we used the identity

$$\vec{\mathbf{1}}_N\vec{\mathbf{1}}_N^H\vec{\mathbf{1}}_N=\begin{bmatrix}1&1&\dots&1\\1&1&\dots&1\\.&.&.&.\\1&1&\dots&1\end{bmatrix}\begin{bmatrix}1\\1\\.\\1\end{bmatrix}=N\begin{bmatrix}1\\1\\.\\1\end{bmatrix}=N\vec{\mathbf{1}}_N \tag{4.10}$$

If we define:

$$\mathbf{h}_{N0}=\frac{1}{N}\vec{\mathbf{1}}_N \tag{4.11}$$

the final expression for Wiener filter coefficients of zero order becomes as follows:

$$\mathbf{h}_{e_0}=\frac{N\gamma_p}{1+N\gamma_p}\mathbf{h}_{N0} \tag{4.12}$$

Thus the filter $\mathbf{h}_{N0}$ is simply an averaging filter with all weights equal to $1/N$ at high SNR. This could be expected, as the problem we consider is equivalent to noise reduction in constant channel for $T_s=0$. The scale coefficient $\dfrac{N\gamma_p}{1+N\gamma_p}$ reflects the property of MMSE estimators to account for variance of noise and prediction error.

The next step is to find the expression for the estimation error:

$$\begin{aligned}\sigma_{e_0}^2 &= 1 - \mathbf{h}_{e_0}^H \left(\mathbf{R} + \gamma_p^{-1}\mathbf{I}\right)\mathbf{h}_{e_0} = \\ &= 1 - \frac{\gamma_p^2}{(1+N\gamma_p)^2}\vec{\mathbf{1}}_N^H \left(\vec{\mathbf{1}}_N\vec{\mathbf{1}}_N^H + \gamma_p^{-1}\mathbf{I}\right)\vec{\mathbf{1}}_N = \\ &= 1 - \frac{\gamma_p^2}{(1+N\gamma_p)^2}\vec{\mathbf{1}}_N^H \left(N\vec{\mathbf{1}}_N + \gamma_p^{-1}\vec{\mathbf{1}}_N\right) = \\ &= 1 - \frac{\gamma_p}{1+N\gamma_p}\vec{\mathbf{1}}_N^H\vec{\mathbf{1}}_N = 1 - \frac{N\gamma_p}{1+N\gamma_p}\end{aligned} \tag{4.13}$$

Therefore:

$$\sigma_{e_0}^2 = 1 - \frac{N\gamma_p}{1+N\gamma_p} \tag{4.14}$$

Thus, as we may see, if $\gamma_p \to 0$ so $\sigma_{e_0}^2 \to 1$, and if $\gamma_p \to \infty$ so $\sigma_{e_0}^2 \to 0$. Moreover this filter improves SNR by factor of $N$, as $\gamma_p$ in (4.14) is multiplied by $N$.

## 4.2 Real Covariance Functions Case: Second Order Approximation

Any real-valued covariance function could be approximated to the second order polynomial:

$$\begin{aligned}R(\tau) &\approx 1 + \frac{R^{'}(0)}{1!}\tau + \frac{R^{''}(0)}{2!}\tau^2 + O(\tau^3) = \\ &= 1 - \frac{a}{2}\tau^2 + O(\tau^3)\end{aligned} \tag{4.15}$$

Here $a$ is a real constant. Estimation of this constant is much easier than calculation of full covariance function, what significantly reduces processing effort. Note, that in case of real covariance functions the first order polynomial term in (4.15) is dropped, since in this case $R^{'}(0) = 0$.

Therefore approximation of the channel covariance matrix $\mathbf{R}$ in (4.1) is given by

$$\mathbf{R} \approx \begin{pmatrix} 1 & 1 & \cdots & 1 \\ 1 & 1 & \cdots & 1 \\ \vdots & & \ddots & \vdots \\ 1 & 1 & \cdots & 1 \end{pmatrix} - 2a(N_b+1)^2 T_s^2 \begin{pmatrix} (0)^2 & (1)^2 & \dots & (N-1)^2 \\ (-1)^2 & (0)^2 & \dots & (N)^2 \\ \vdots & & \ddots & \vdots \\ (-N+1)^2 & \dots & & (0)^2 \end{pmatrix}$$

This could be written as:

$$\mathbf{R} \approx \vec{\mathbf{1}}_N \vec{\mathbf{1}}_N^H + \Delta\underline{\mathcal{E}} \tag{4.16}$$

where

$$\begin{aligned} \Delta\underline{\mathcal{E}} &= -2a(N_b+1)^2 T_s^2 \mathbf{E} \\ \mathbf{E}_{kl} &= (l-k)^2, \quad k,l = 1 \cdots N \end{aligned} \tag{4.17}$$

Here $\mathbf{E}$ is a full rank Hermitian matrix, hence the inverse of this matrix always exists. Furthermore, vector $\boldsymbol{\rho}_e$ in (4.1) could be then approximated as:

$$\boldsymbol{\rho}_e \approx \begin{pmatrix} 1 \\ 1 \\ \vdots \\ 1 \\ \vdots \\ 1 \\ 1 \end{pmatrix} - \frac{a}{2} T_s^2 \begin{pmatrix} (2N_b M - e)^2 \\ (2N_b(M-1) - e)^2 \\ \vdots \\ (-e)^2 \\ \vdots \\ (-2N_b(M-1) - e)^2 \\ (-2N_b M - e)^2 \end{pmatrix} \tag{4.18}$$

or:

$$\begin{aligned} \boldsymbol{\rho}_e &\approx \vec{\mathbf{1}}_N - \frac{a}{2} T_s^2 \mathbf{k} = \vec{\mathbf{1}}_N + \Delta\underline{\boldsymbol{\rho}_e} \\ \mathbf{k}_k &= \left[ 2(N_b+1)\left(\frac{N-1}{2} + 1 - k\right) - e \right]^2 \\ k &= 1, \dots N \end{aligned} \tag{4.19}$$

### 4.2.1 Wiener Filter Coefficients

Substituting $\mathbf{R}$ and $\boldsymbol{\rho}_e$ into eq. (4.1) and after some algebra, the expression for the second order Wiener filter coefficients takes the following form:

$$\mathbf{h}_{e_2} = (\mathbf{I} + \mathbf{A}\Delta\underline{\mathcal{E}})^{-1} \cdot \left( \frac{N\gamma_p}{1 + N\gamma_p} \mathbf{h}_{N_0} + \mathbf{A}\Delta\underline{\boldsymbol{\rho}_e} \right) \tag{4.20}$$

where

$$\mathbf{A} = \left( \gamma_p \mathbf{I} - \frac{\gamma_p^2}{1 + N\gamma_p} \vec{\mathbf{1}}_N \vec{\mathbf{1}}_N^H \right) \tag{4.21}$$

and

$$\mathbf{h}_{N_0} = \frac{1}{N} \vec{\mathbf{1}}_N \tag{4.22}$$

See Appendix A for step by step derivation. If we assume, that

$$\| \mathbf{A}\Delta\underline{\mathcal{E}} \| \ll 1 \tag{4.23}$$

equation (4.20) could be further simplified by using the following identity [7]:

$$(\mathbf{I} + \mathbf{A}\Delta\underline{\mathcal{E}})^{-1} \approx \mathbf{I} - \mathbf{A}\Delta\underline{\mathcal{E}} \tag{4.24}$$

After cancelling higher order terms as insignificant eq. (4.20) takes a form of:

$$\mathbf{h}_{e_2} = \frac{N\gamma_p}{1 + N\gamma_p} \mathbf{h}_{N_0} + \mathbf{A} \left( \Delta\underline{\boldsymbol{\rho}_e} - \frac{N\gamma_p}{1 + N\gamma_p} \Delta\underline{\mathcal{E}} \mathbf{h}_{N_0} \right) \tag{4.25}$$

It is important to note, that given $a$ and for a predetermined length of the filter and the frame we may easily calculate all constants in (4.25), which do not change from one communication session to another. This significantly simplifies calculations and decreases computational effort. Also, if correction terms $\Delta\underline{\mathcal{E}}$ and $\Delta\underline{\boldsymbol{\rho}_e}$ equal zero, equations (4.25) and (4.20) reduce to zero order approximation case (4.12).

### 4.2.2 Estimation Error

Now we can find an expression for MMSE by using covariance function approximated to the second order. In this case MMSE is given by:

$$\sigma_{e_2}^2 = 1 - \mathbf{h}_{e_2}^H \left( \vec{\mathbf{1}}_N \vec{\mathbf{1}}_N^H + \Delta\underline{\mathcal{E}} + \gamma_p^{-1}\mathbf{I} \right) \mathbf{h}_{e_2} \tag{4.26}$$

If we substitute $\mathbf{h}_{e_2}$ and $\Delta\underline{\mathcal{E}}$ which were calculated in eqs. (4.25) and (4.17) into (4.26), after some algebra, which is described in detail in Appendix B, one may find the expression for MMSE:

$$\sigma_e^2 = 1 - \frac{N\gamma_p}{1+N\gamma_p} - 2\frac{\gamma_p}{1+N\gamma_p}\vec{\mathbf{1}}_N^H \Delta\underline{\boldsymbol{\rho}_e} + \frac{\gamma_p^2}{\left(1+N\gamma_p\right)^2}\vec{\mathbf{1}}_N^H \Delta\underline{\mathcal{E}}\vec{\mathbf{1}}_N \tag{4.27}$$

Here again we may clearly see, that if the correction terms $\Delta\underline{\boldsymbol{\rho}_e}$ and $\Delta\underline{\mathcal{E}}$ equal zero, the expression reduces to zero order approximation. We can rewrite the equation (4.27) in explicit way:

$$\sigma_{e_2}^2 = 1 - NC(\gamma_p)\left(1 - aT_s^2e^2\right) + \frac{4aMNT_s^2C(\gamma_p)}{3}(N_b+1)^2(M+1)(1-NC(\gamma_p)) \tag{4.28}$$

where

$$C(\gamma_p) = \frac{\gamma_p}{1+N\gamma_p}$$

When $\gamma \to 0$, $\sigma_{e_2}^2 \to 1$, and when $\gamma \to \infty$, $\sigma_{e_2}^2 \to aT_s^2e^2$, where the estimation error saturates. Therefore, if we estimate at $e = 0$, estimation error would not have a saturation threshold.

### 4.2.3 Zero Order and Second Order Approximations

From our theoretical results we can conclude that in order to satisfy zero order approximation assumption (4.2), the actual channel must be very slow (or equivalently data rates have to be high), so that the correlation between pilots is approximately unity. Moreover, for the same reason filter length should be short (one or two pilots), so that the first and the last pilot signals in the buffer are still highly correlated. The

last condition is often satisfied as the usual number of pilots in use for STTD schemes with estimation does not exceed more than three pilots for optimality reasons. Moreover, it has been mentioned at the end of Sec. 4.1, that theoretical zero order MMSE should decay to zero with growing SNR and it does not depend on channel speed or on frame length. In the reality, these factors make pilots less correlated, what leads to inaccuracy of the assumption and as a result, MMSE practical curves (obtained by simulation) saturate, whereas theoretical curve continues to decay. Assumption of the second order approximation of covariance function reliefs the tight condition of unity correlation between pilots and allows us to work with faster channels or slower bit rates. The most general analytical expression for second order coefficients is obtained in (4.20) and the corresponding MMSE is obtained by substitution of (4.20) into (4.26). Furthermore, in order to simplify the expression, we make an assumption (4.23), which is valid only when pilot signals are highly correlated. Nevertheless, according to our simulation results, it gives us a very precise theoretical description of MMSE at a marginal case of zero-order filter coefficients derived in (4.12). Therefore we refer to this expression as to a corrected zero order MMSE and mark it as *corrected* $\sigma_{e_0}$ in our simulations.

## 4.3 Simulation Results in Real Covariance Function Case - Bit Error Probability and Estimation Error Evaluation

In this section we validate the quality of estimation by means of simulation in cases of full Wiener filter, zero and second order approximations for different channel fading rates. In our simulation we used SoS channel model, described in Section 2.1, because it is well known that its covariance function is real-valued Bessel function of first kind and zero order. We start with the case of full filter in order to provide a reference of performance of STTD scheme with estimation at the receiver side. In Fig. 4.1 estimation MMSE is shown as a function of SNR and normalized Doppler time $f_D T_s$. Corresponding BER is shown in Fig. 4.2. The simulation parameters are: $N_b = 5$

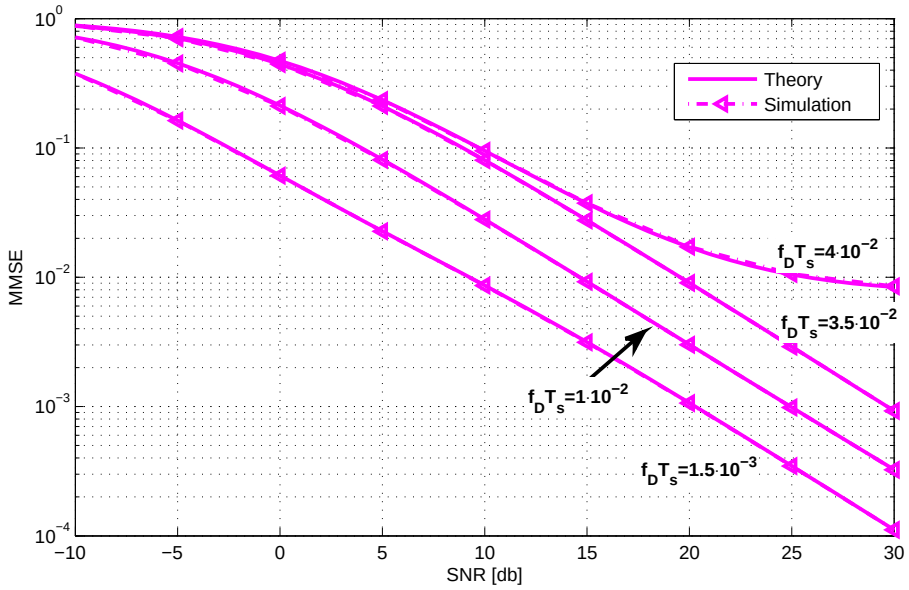


Figure 4.1: *MMSE in a case of estimation with full Wiener filter as a function of SNR and* $f_DT_s$, $M = 10$, $N_b = 5$

blocks per frame and $M = 10$, averaging is performed over $10^6$ bits. Prediction point was set to $e = N_b$, in the middle of the frame, what represents the worst case scenario. As we can see, the higher fading rates increase estimation error which translates to a higher BER. It happens due to the fact, that faster channels lead to quicker decay in correlation between symbols, and as a result estimation is performed on effectively smaller number of pilots what induces less precise estimation. There is a perfect agreement between theory and simulation.

In Fig. 4.3 theoretical and simulational results are shown for different channel fading rates in case of zero order approximation. The coefficient $a$ is obtained from the second derivation of Bessel function at $\tau = 0$, and equals $a = 2\pi^2 f_D^2$. In order to assure that condition (4.2) is valid, we run the simulation at relatively high channel rates with $M = 1$ pilots and $N_b = 5$ information blocks and $e = 5$ (middle of the frame). As we expect, with higher fading rates the approximation becomes less precise and simulational MMSE curves saturate (this is called fading floor), whereas theoretical one, based on equation (4.14), does not (theory $\sigma_{e0}$ at the graph). Also, corrected version of estimation error (4.28) allows us to track precisely the MMSE in

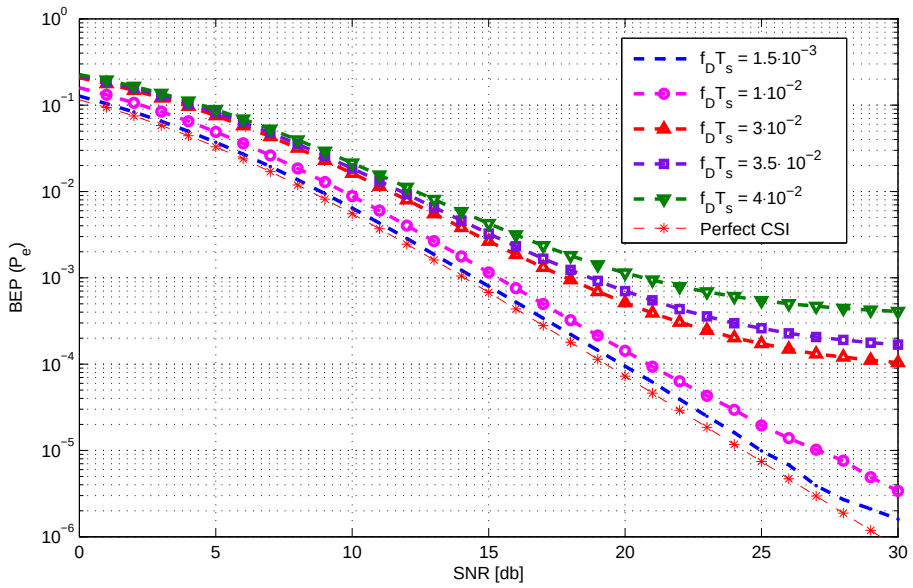


Figure 4.2: *BER in a case of full Wiener filter as a function of SNR and* $f_DT_s$, $M = 10$, $N_b = 5$

marginal channel rates, where zero order approximation becomes less accurate.

The simulation of a general equation of second order approximation (4.20) is

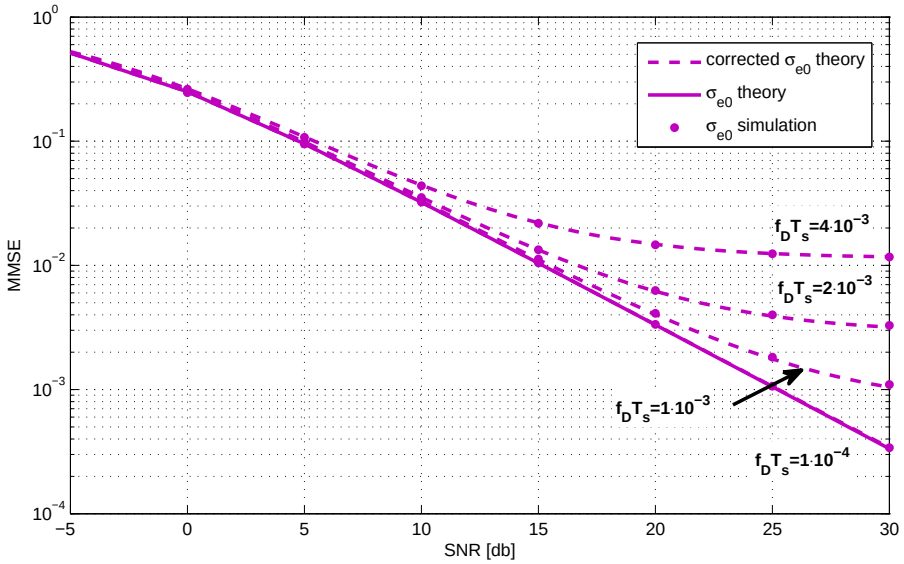


Figure 4.3: *Theoretical, corrected theoretical and simulational zero order approximation MMSE,* $\sigma_{e_0}$. *Effect of channel fading rate on quality of estimation,* $M = 1$, $N_b = 5$

shown in Fig. 4.4, from which we can see fading rates, at which the approximation works well, and when it starts increasing the MMSE due to inaccuracy. Failing of approximation is well-pronounced at high SNR as it is where the error is due to a lack of accuracy in the receiver's knowledge of statistics and not due to the noise. Therefore we may infer that this scheme works very well with channel rates up to about $f_D T_s = 6 \cdot 10^{-3}$. In a case of slow fading channels simulation shows that the approximation works precisely and theory matches simulation.

In Fig. 4.5 we compare performance of second order approximation with the zero order approximation schemes. As we expect, the second order approximation

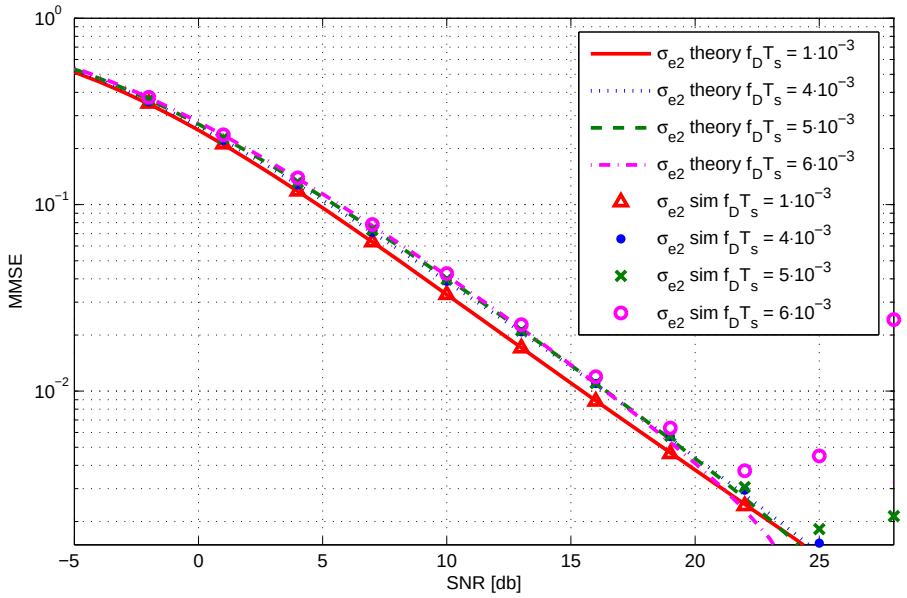


Figure 4.4: *Theoretical and simulational second order approximation MMSE, $\sigma_{e_2}$. Effect of channel fading rate on quality of estimation, $M = 1$, $N_b = 5$*

performs more precise estimation than zero order on higher SNR, what enables us to work with faster channels. It is important to mention that for these channel rates (and lower) second order approximation performs as good as estimator with full Wiener filter (see Fig. 4.5). Increasing order of approximation of covariance function increases accuracy of estimation for higher rates, but it also enlarges computational effort.

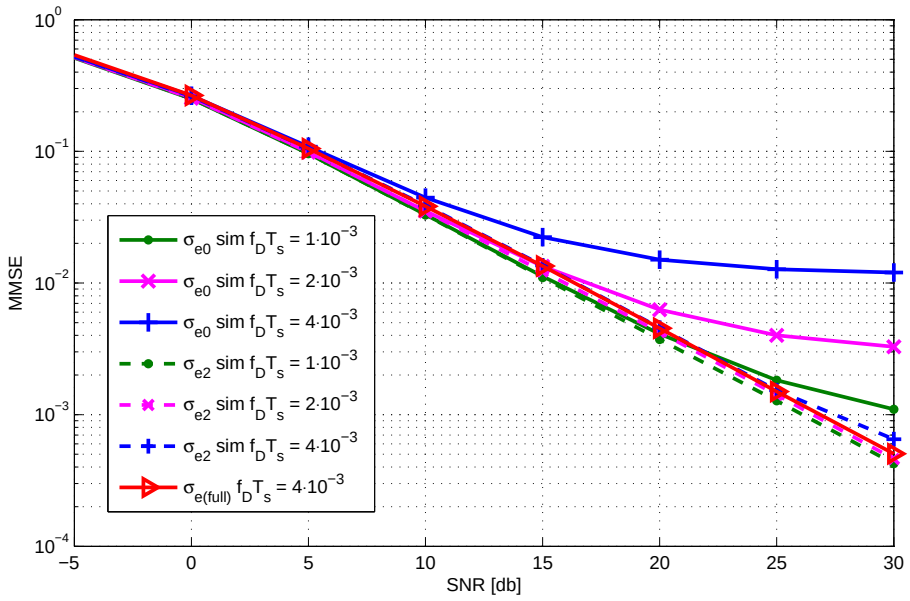


Figure 4.5: *Comparison between performances of zero and second order approximations,* $\sigma_{e_0}$ *versus* $\sigma_{e_2}$*,* $M = 1$*,* $N_b = 5$

## 4.4 Light Wiener Filters for Estimation of Channels with Complex Covariance Functions

In this section we extend our work to a case of channels with complex covariance functions. Any complex auto-correlation function can be approximated by second order Taylor series as follows [38]:

$$R(\tau) \approx 1 + \frac{R^{'}(0)}{1!}\tau + \frac{R^{''}(0)}{2!}\tau^2 + O(\tau^3) = \tag{4.29}$$
$$= 1 + ja\tau - \frac{b}{2}\tau^2 + O(\tau^3)$$

As we may see from the above equation, this could be reduced to a case of real auto-covariance functions by posing $a = 0$. Therefore the following coefficients and MMSE derivation are a generalization for any kind of covariance functions. In a similar way as we derived Winer filter coefficients in previous sections, we found coefficients for the general case, when we approximated $\mathbf{R}(\tau)$ is given by 4.29 and they take a form

of:

$$\mathbf{h}_{e_2} = (\mathbf{I} + \mathbf{A}\Delta\underline{\mathcal{E}})^{-1} \cdot \left( \frac{N\gamma_p}{1+N\gamma_p}\mathbf{h}_{N_0} + \mathbf{A}\Delta\underline{\boldsymbol{\rho}_e} \right) \tag{4.30}$$

when

$$\begin{aligned} \mathbf{A} &= \left( \gamma_p \mathbf{I} - \frac{\gamma_p^2}{1+N\gamma_p}\vec{\mathbf{1}}_N \vec{\mathbf{1}}_N^H \right) \\ \mathbf{h}_{N_0} &= \frac{1}{N}\vec{\mathbf{1}}_N \end{aligned} \tag{4.31}$$

and

$$\begin{aligned} \Delta\underline{\mathcal{E}} &= j\Delta\underline{\mathcal{E}}_{Im} + \Delta\underline{\mathcal{E}}_{Re} \\ \Delta\underline{\boldsymbol{\rho}_e} &= j\Delta\underline{\boldsymbol{\rho}}_{e_{Im}} + \Delta\underline{\boldsymbol{\rho}}_{e_{Re}} \end{aligned} \tag{4.32}$$

$\Delta\underline{\mathcal{E}}_{Re}$ and $\Delta\underline{\boldsymbol{\rho}}_{e_{Re}}$ are given by:

$$\begin{aligned} \Delta\underline{\mathcal{E}}_{Re} &= -2b(N_b+1)^2 T_s^2 \mathbf{E_2} \\ \mathbf{E_2}_{(kl)} &= (l-k)^2, \quad k,l = 1 \cdots N \end{aligned} \tag{4.33}$$

and

$$\begin{aligned} \Delta\underline{\boldsymbol{\rho}}_{e_{Re}} &= -\frac{b}{2}T_s^2 \mathbf{k_2} \\ \mathbf{k_2}_k &= \left[ 2(N_b+1)\left(\frac{N-1}{2} + 1 - k\right) - e \right]^2 \\ k &= 1, \ldots N \end{aligned} \tag{4.34}$$

It is important to note that $\mathbf{E_2}$ and $\mathbf{k_2}$ are exactly as described in equations (4.17) and (4.20). $\Delta\underline{\mathcal{E}}_{Im}$ and $\Delta\underline{\boldsymbol{\rho}}_{e_{Im}}$ are defined below:

$$\Delta\underline{\mathcal{E}}_{Im} = 2a(N_b+1)T_s \begin{pmatrix} 0 & 1 & \ldots & N-1 \\ -1 & 0 & \ldots & N \\ \vdots & & \ddots & \vdots \\ -N+1 & \ldots & & 0 \end{pmatrix} \tag{4.35}$$

or

$$\begin{aligned} \Delta\underline{\mathcal{E}}_{Im} &= 2a(N_b+1)T_s\mathbf{E_1} \\ \mathbf{E_1}_{(kl)} &= (l-k), \quad k,l = 1\cdots N \end{aligned} \tag{4.36}$$

and:

$$\Delta\underline{\boldsymbol{\rho}}_{e_{Im}} = aT_s \begin{pmatrix} 2N_bM - e \\ 2N_b(M-1) - e \\ \vdots \\ -e \\ \vdots \\ -2N_b(M-1) - e \\ -2N_bM - e \end{pmatrix} \tag{4.37}$$

or

$$\begin{aligned} \Delta\underline{\boldsymbol{\rho}}_{e_{Im}} &= aT_s\mathbf{k_1} \\ \mathbf{k_1}_k &= \left[2(N_b+1)(\frac{N-1}{2}+1-k) - e\right] \\ k &= 1,\dots N \end{aligned} \tag{4.38}$$

With further assumption of:

$$\| \mathbf{A}\Delta\underline{\mathcal{E}} \| \ll 1 \tag{4.39}$$

filter coefficients in equation (4.30) take a form:

$$\begin{aligned} \mathbf{h}_{e_2} = \frac{N\gamma_p}{1+N\gamma_p}\mathbf{h}_{N_0} + \mathbf{A}\left(\Delta\underline{\boldsymbol{\rho}}_{e_{Re}} - \frac{N\gamma_p}{1+N\gamma_p}\Delta\underline{\mathcal{E}}_{Re}\mathbf{h}_{N_0}\right) + \\ + j\mathbf{A}\left(\Delta\underline{\boldsymbol{\rho}}_{e_{Im}} - \frac{N\gamma_p}{1+N\gamma_p}\Delta\underline{\mathcal{E}}_{Im}\mathbf{h}_{N_0}\right) \end{aligned} \tag{4.40}$$

and the MMSE is:

$$\begin{aligned} \sigma^2_{e_2} = 1 - NC(\gamma_p)\left(1 - bT_s^2e^2\right) + \\ + \frac{4MbT_s^2NC(\gamma_p)}{3}(N_b+1)^2(M+1)\left(1-NC(\gamma_p)\right) \end{aligned} \tag{4.41}$$

where

$$C(\gamma_p) = \frac{\gamma_p}{1 + N\gamma_p}$$

For the detailed derivation, please look at the Appendix C. When $\gamma_p \to 0$, $\sigma^2_{e2} \to 1$, and when $\gamma_p \to \infty$, $\sigma^2_{e_2} \to bT_s^2e^2$,*i.e.* estimation error reaches saturation floor. As in previous case with real covariance functions this result is shown to accurately track the behaviour of zero order filter in conditions when the approximation is already not precise (saturation mode). Therefore in our simulation we refer to it as corrected zero order filter and denote it as $\sigma_{e0}$ *corrected*.

## 4.5 Simulation Results - MMSE in Estimation of Channels with Complex Covariance Function Approximated to Zero, First and Second Orders

In this section we verify analytical expressions/derivations of Section 4.4 by simulation. As previously, we test estimation quality of a system, described in Chapter 3, in environment which contains clusters and scatterers, what induces non-symmetric Doppler Spectrum and complex covariance function of channel gains. Therefore the MDPSS channel model, discussed in Section 2.2.5.2, was taken for the simulation.

For simplicity we take a case with a single cluster. As it was discussed previously, auto-covariance function of the channel is:

$$R(\tau) = P \exp(j2\pi f_D \tau)\mathrm{sinc}(\Delta f_D \tau) \tag{4.42}$$

where we take the power $P$ of the cluster to be 1. All other parameters are specified in Table 2.1. Polynomial coefficients in 4.29 can be easily found by derivation of the covariance function at $\tau = 0$, therefore $a = 2\pi f_D$ and $b = \left(\frac{1}{3}\Delta^2 + 4\pi^2 f_D^2\right)$. Furthermore, we run the simulation for estimation with 3 pilot signals ($M = 1$) and for $N_b = 5$ frame length.

In Fig. 4.6 we show the performance of zero-order approximation filter. As in the case of real covariance functions, MMSE curves saturate, because the approximation is not accurate for higher rates, whereas zero order theoretical curve does not depend on neither on data or channel rates nor on frame length (see eq. (4.14)). On the other hand the corrected theoretical curve $\sigma_{e0}$ *corrected*, which is an approximation of the second order filter, tracks accurately the saturation of zero order approximation.

In Fig. 4.7 we can observe rates at which second order Wiener filter achieves

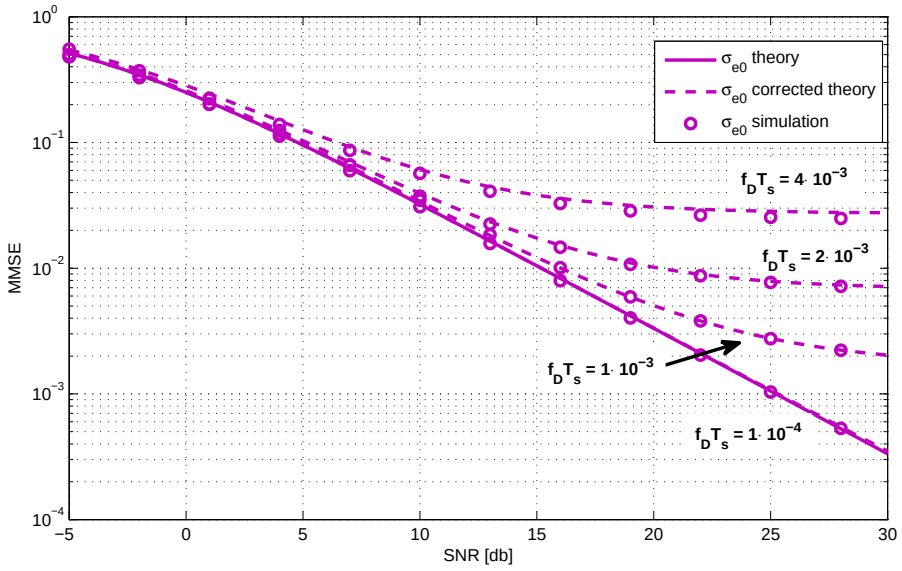


Figure 4.6: *Theoretical, corrected theoretical and simulational zero order approximation MMSE, $\sigma_{e_0}$. Effect of channel fading rate on quality of estimation, $M = 1$, $N_b = 5$, complex covariance function case*

good performance in terms of MMSE and when it starts behave not adequately due to the lack of positive definiteness property of polynomial covariance function. As it may be seen from the graph, MMSE becomes unstable at higher SNRs at $f_D T_s \approx 2 \cdot 10^{-3}$.

In Fig. 4.8 we compare zero order and second order filters, where we see, that at higher SNRs second order filter shows considerably better performance (up to $25dB$ improvement) than zero order one. Again, the reason is that at higher rates zero order approximation becomes not valid, whereas, second order approximation still holds very well. Furthermore, up to rates of $f_D T_s \approx 1.5 \cdot 10^{-3}$ second order

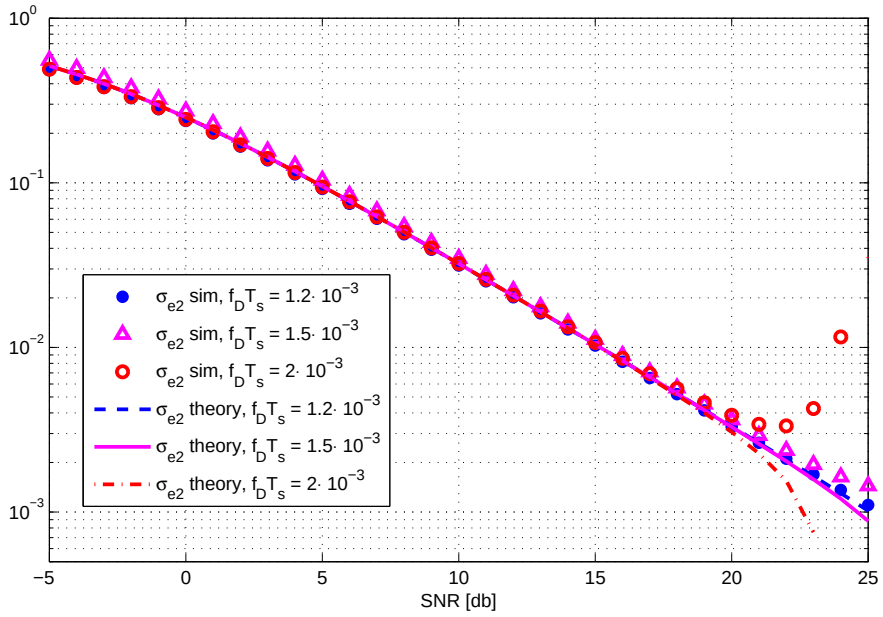


Figure 4.7: *Theoretical and simulational second order approximation MMSE, $\sigma_{e_2}$. Effect of channel fading rate on quality of estimation, $M = 1$, $N_b = 5$, complex covariance function case*

approximation performs as good as full Wiener filter (see the figure), while zero order approximation is already saturating. With increasing filter order one may achieve better performances for higher rates in expense of complexity.

## 4.6 Non-Uniform Scattering Effect on Estimation with Light Wiener Filter

As we have derived in previous sections, the estimation error for a second order filter is given by:

$$\sigma_{e_2}^2 = 1 - NC(\gamma_p)\left(1 - bT_s^2 e^2\right) + \\ + \frac{4MbT_s^2 NC(\gamma_p)}{3}(N_b+1)^2(M+1)\left(1 - NC(\gamma_p)\right) \tag{4.43}$$

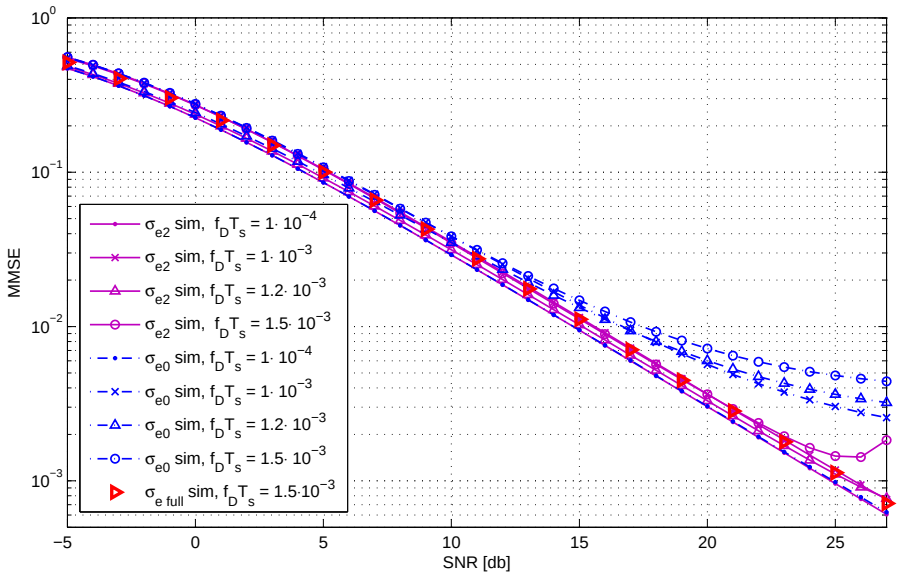


Figure 4.8: *Comparison between performances of zero and second order approximations,* $\sigma_{e_0}$ *versus* $\sigma_{e_2}$*,* $M = 1$*,* $N_b = 5$*, complex covariance function case*

With a slight rearrangement of terms we can write this equation as follows:

$$\begin{aligned}\sigma_{e_2}^2 &= 1 - NC(\gamma_p) + \\ &+ bT_s^2 NC(\gamma_p)\left(e^2 + \frac{4}{3}M(N_b+1)^2(M+1)\left(1 - NC(\gamma_p)\right)\right)\end{aligned} \tag{4.44}$$

Here the value $b$ is a function of clusters geometrical parameters. For example, for two clusters scenario, which is shown in Fig. 2.22, $b$ is equal:

$$b = P_1\left(\frac{1}{3}\Delta f_{D_1}^2 + 4\pi^2 f_{D_1}^2\right) + P_2\left(\frac{1}{3}\Delta f_{D_2}^2 + 4\pi^2 f_{D_2}^2\right) \tag{4.45}$$

and

$$\begin{aligned}f_{D_i} &= \frac{f_c}{c}\left(v_{t_i}\cos(\phi_{t0_i}) + v_{r_i}\cos(\phi_{r0_i})\right) \\ \Delta f_{D_i} &= \frac{f_c}{c}\left(v_{t_i}\Delta\phi_{t_i}|\sin(\phi_{t0_i})| + v_{r_i}\Delta\phi_{r_i}|\sin(\phi_{r0_i})|\right),\end{aligned} \tag{4.46}$$

for $i = 1, 2$.

It can be seen from equation (4.44), that parameter $b$ affects the estimation error. As $b$ becomes larger, MMSE grows as well. Moreover, if we know the geometry of clusters, this parameter (along with parameter $a$) can be calculated very easily and no covariance function estimation will be needed.

## 4.7 Summary

- In the case of highly correlated pilots it is not necessarily to know full correlation function in order to achieve a good quality of estimation, and it is enough to assume its low order polynomial approximation. Such approach allows us to work with scenarios where statistics of the channel are partially unknown and significantly reduces computational effort of the estimator at the receiver and hence saves the battery energy of the mobile.
- Theoretical representation for zero order and second order Light Wiener filter coefficients and estimation errors for channels with real-valued and complex covariance functions have been provided.
- All theoretical results are verified by the simulations. It is shown, that in the case of highly correlated pilots, zero and second order approximations work as good as full Wiener filter.
- As channel fading rates increase, zero order approximation becomes inaccurate what results in saturation of MMSE on high SNRs, whereas second order approximation still achieves a rather good performance (compared to that of full Wiener filter). This allows us to work with faster channels while keeping low filter complexity.
- As order of approximation is increased, we reach a better estimation, but with the price of higher computational load. Therefore the trade off should be achieved based on the environment, demands of the application and the expected battery life.
- It is possible to calculate polynomial coefficients if the geometry of clusters and their location is known. Therefore channel estimation could be performed with no channel statistical knowledge or its estimation at the receiver.

# Chapter 5
# Conclusion

Wireless channels modeling and simulation techniques have been discussed. Two main approaches had been implemented: channels which describe environment with rich scattering around the mobile (*i.e.* uniform AoA distribution) and channels which describe scattering from one or more clusters with rough surfaces, resulting in specular components with angular and delay spread. Combination of these scenarios is sufficient to describe majority of urban or suburban environments. First scenario was simulated with use of SoS simulational model with correct higher order statistics, and the second scenario can be simulated with MDPSS channel model. Both channel simulators were studied in detail, and verified by simulation.

As the next step we have studied a realistic $2 \times 1$ transmission system with Alamouti coding and pilot assisted noisy channel estimation. BPSK modulation was adopted for simplicity. At the receiver Wiener filter was used as pilots filter. The correlation function of channel gains was assumed to be known to the receiver. The evaluation of the system was performed via simulation, when influence of different parameters was tested: length of pilot sequence, channel fading rates, length of frames. It was shown that with longer pilot sequence the receiver provides better estimation. When the number of pilot signals is infinitely long, the system achieves perfect CSI case performance. In practice, 10 pilot signals is enough to achieve this performance. Increasing number of information blocks per frame increases MMSE, because pilot signals become less correlated, hence the receiver possesses effectively smaller number of pilots, what results in worse estimation, and hence larger bit error rates. Also, saturation floor effect has been observed as a consequence of estimation of a point in the middle of the frame with only one effective pilot signal in present ($M = 0$), what

is equivalent to prediction of a channel gain $N_b$ samples ahead from the known pilot. In this case prediction error is greater than estimation one and saturation occurs. As we increase channel fading rate $f_D T_s$, the system shows poorer performance. In this case the reasons are lower correlation between pilot signals as well as invalidity of Alamouti coding assumption about slow fading rate of the channel (two consequent channel gains should be equal). This results in saturation thresholds. Simulation has shown that in this case the main reason of saturation is inaccuracy of Alamouti coding condition.

Several real-life scenarios of V2I and V2V communications in urban environment were simulated to evaluate how clusters geometry and location can affect the performance of Alamouti scheme with imperfect channel estimation. The channel was simulated with use of MDPSS channel simulation model, discussed in Chapter 2. The flexibility of this model in definition of clusters geometry and the direction of movement of both communication sides allows us to simulate any site and mobile configuration of interest. It was shown by simulation that nearing clusters, located on a side of the movement trajectory of the mobile increases MMSE and BER due to quick decay of covariance function of pilot signals in vicinity of clusters. The effect was shown to be prolonged in time and increasing with nearing clusters. Another scenario described a cluster, located on the mobile movement direction (for example, a big road-directions poster above the road). In this case the simulation has shown a dramatic increase in MMSE and BER, when the mobile is passing under the cluster. Though this effect is fleeting and does not last more than a couple of seconds. In addition, a site from one of city's intersections was simulated to show how we can apply this model in real life. In another case we showed how this channel model could be easily adopted to mock mobile to mobile communications in urban area, when clusters are assumed to be located on the perimeters of co-centric ellipses, when two mobiles are located at ellipses focuses. This approach is important since V2V communications is currently a new and developing area of communications and novel channel models which can mimic realistic environments in this type of communications are on demand. Since MDPSS model requires manual adjustment of the site geometry (*i.e.* clusters locations and their angular and delay spreads), which might be easily calcu-

lated through online applications like Google Maps ©, it can pose some unsuitability in dynamic recalculation of the site (with the mobile movement, the environment is very likely to change), therefore one of the future projects in this topic should include the development of a specific software, which will be able to automatically recalculate clusters geometry, based on available mobile location (via GPS, for instance) and the current city map.

Finally we have developed reduced complexity Wiener filters for estimation of slowly time-varying narrowband channels. These light filters are based on approximation of channel auto-covariance function by a zero and second order Taylor series. This approach is useful when the statistics of the channel are partially unknown, and the receiver needs to estimate the correlation function in order to perform channel estimation. Moreover, reduced complexity filters are beneficial for lowering energy consumption in order to extend the battery life of the mobile. The coefficients of the polynomial can be estimated through spectrum analysis, which is much easier than estimation of the whole covariance function. We derived equations for Wiener filter coefficients and estimation error for both real and complex covariance functions cases. Furthermore, we run the simulation to verify at what data/channel rates approximations becomes invalid (as the correlation between pilots decays). In simulation of reduced order estimation of channels with real covariance function we used SoS model. The covariance function of this model is known to be real-valued Bessel function of first kind and zero order. For the simulation of estimation of channels with complex covariance functions we adopted MDPSS model, whose covariance function is a *sinc* function modulated by complex exponent (or a linear combination of several alike multiplications). For now we have assumed that the receiver perfectly knows the coefficients of the polynomial approximation, and leave the estimation of these coefficients and its influence on the system performance to the future work. In both cases Second order filters showed superiority over Zero order filters in performance in terms of MMSE (and consequently in BER) at higher channel rates. At low channel rates (*i.e.* high data rates), both filters perform as good as full Wiener filter. Accu-

rate performance tracing in case of practical saturation of Zero order filter (at higher rates) was derived through additional approximation of Second order filter. Also the additional simulation was performed to determine at what channel fading rates the Second order filters become unstable due to the lack of an important condition of positive definiteness in polynomial covariance function. In a particular case of a channel with one or more clusters, the coefficients of approximation can be derived from direct analysis of clusters geometry, therefore spectral analysis will not be necessary. As the complexity of the filter increases, one can achieve better performance for higher channel rates, but in expense of greater computational load. Future fork should include investigation of the trade-off between the complexity of the filter and desirable system performance (of course with consideration of required channel and/or data rates). As it was mentioned before, the estimation of the polynomial covariance function coefficients should be investigated in depth and a case of non-stationary processes should be considered. We believe that our approach could be extended to MIMO systems to investigate their performance in more realistic scattering scenarios.

# References


[1] S. Rappaport, *Wireless Communication, principle and Practice.* Prentice Hall PTR, 2002. 1, 7

[2] D. Tse and P. Viswanath, *Fundamentals of Wireless Communication.* Cambridge University Press, 2005. 1, 2, 3, 6, 7, 41, 42, 44, 46

[3] W. C. Jakes, *Microwave Mobile Communications.* Wiley-IEEE Press, 1994. 1, 9

[4] Yahong Rosa Zheng and Chengshan Xiao, "Simulation Models With Correct Statistical Properties for Rayleigh Fading Channels," *IEEE Transactions on Communications*, vol. 51, June 2003. 1, 6, 10, 11, 12

[5] C. S. Patel, G.L.Stuber, and T.G.Pratt, "Simulation of Rayleigh-Faded Mobile-to-Mobile Communication Channels," *IEEE Trans. Communications*, vol. 53, pp. 1876–1884, November 2005. 1

[6] Sahar Javaher Haghighi, Serguei Primak, Valeri Kontorovich, and Ervin Sejdic, "Wireless Communications and Multitiper Analysis: Applications to Channel Modeling and Estimation," in *Mobile and Wireless Communications Physical layer development and implementation.* InTech Publishing, 2010. 2, 6

[7] H. van Trees, *Detection, Estimation and Modulation Theory: Part1*, 1st ed. New York: John Wiley & Sons, Ltd., 2001. 2, 24, 84, 88

[8] K. M. Almustafa and S. L. Primak, *Performance of MIMO Systems in Partially Known Channels.* LAP LAMBERT Academic Publishing, 2011. 2, 3

[9] S. M. Alamouti, "A simple Transmit Diversity Technique for Wireless Communications," *Journal on Select Areas in Communications*, vol. 16, pp. 1451–1458, October 1998. 2

[10] Jittra Jootar, J. R. Zeidler, and J. G. Proakis, "Performance of Alamouti Space-Time Code in Time-Varying Channels with Noisy Channel Estimates," *IEEE*, 2005. 2, 3, 42, 46, 48, 55, 56, 58, 82

[11] J. P. McGeehan and A. J. Bateman, "Phase Locked Transparent Tone-in-Band (TTIB): a New Spectrum Configuration Particularly Suited to the Transmission

od Data Over SSB Mobile Radio Networks," *IEEE Trans. Communications*, vol. COM-32, pp. 81–87, January 1984. 3

[12] P. M. M. *et al*, "The Implementation of a 16-QAM Mobile Data System Using TTIB-Based Fading Correction Techniques," *Proc. IEEE Veh. Technol. Conf.*, pp. 71–76, 1988. 3

[13] J. Baltersee, G. Fock, and H. Meyr, "Achievable Rate of MIMO Channels With Data-Aided Channel Estimation and Perfect Interleaving," *IEEE Journal on Selected Areas in Communications*, vol. 19, pp. 2358–2368, December 2001. 3

[14] J. K. Cavers, "An analysis of Pilot Symbol Assisted Modulation for Rayleigh Fading Channels," *IEEE Transactions on Vehicular Technology*, vol. 40, November 1991. 3, 48, 54, 82

[15] S. Haykin, *Adaptive Filter Theory*, 4th ed. Prentice Hall, September 2001. 3, 4, 49, 50, 52, 54, 56, 82

[16] Cheng-Xiang Wang and Xiang Cheng, "Vehicle-to-Vehicle Channel Modeling and Measurements: Recent Advances and Future Challenges," *IEEE Communications Magazine*, pp. 96–103, November 2009. 3, 75

[17] J. G. Proakis, *Digital Communications*, 4th ed. McGraw-Hill, 2000. 4, 40

[18] M. Patzold, *Mobile Radio Channels*. John Wiley & Sons, Ltd., 2012. 6

[19] R. H. Clarke, "A statistical theory of mobile-radio reception," *Bell Syst. Tech. J.*, pp. 957–1000, Jul-August 1968. 9, 10

[20] G. S. Stuber, *Principles of Mobile Communication*, 2nd ed. Norwell, MA: Kluwer, 2001. 10

[21] M.Patzold, U.Killat, F.Laue, and Y.Li, "On the Statistical Properties of Deterministic Simulation Models for Mobile Fading Channels," *IEEE Trans. Veh. Technol.*, vol. 47, pp. 254–269, February 1998. 10

[22] M.F.Pop and N.C.Buleau, "Limitations of Sum-of-Sinusoids Fading Channel Simulators ," *IEEE Trans. Communications*, vol. 49, pp. 600–708, April 2001. 10

[23] S. A. F.Adachi, *Mobile and Wireless Communications Physical Layer Development and Implementatiom*. InTech, 2010. 20

[24] S. Primak, V. Kontorovich, and V. Lyandres, *Stochastic Methods and their Applications to Communications, Stochastic Differential Equations Approach*. John Wiley & Sons, Ltd, 2004. 39

[25] Khaled Almustafa, Serguei Primak, Tricia Willink, and Kareem Baddour, "On Achievable Data Rates and Optimal Power Allocation in Fading Channels with Imperfect Channel State Information," *Kluwer Academic Publishers*, 2008. 48, 62

[26] C. Komninakis, C. Fragouli, A. H.Sayed, and R. D.Wesel, "Multi-Input Multi-Output Fading Channel Tracking and Equalization Using Kalman Estimation," *IEEE TRANSACTIONS ON SIGNAL PROCESSING*, vol. 50, pp. 1065–1075, 2002. 48

[27] GPS.gov. Global Positioning System. [Online]. Available: http://www.gps.gov/ 77

[28] Information-Analytical Centre. Global Navigation Satellite System. [Online]. Available: http://glonass-iac.ru/en/ 77

[29] JAXA Japan Aerospace Exploration Agency. Quasi-Zenith Satellite System. [Online]. Available: http://glonass-iac.ru/en/ 77

[30] S. Sampei and T.Sunaga, "Rayleigh Fading Compensation Method for 16QAM in Digital and Mobile Radio Channels," *Proc. IEEE Veh. Technol. Conf.*, pp. 640–646, May 1989. 82

[31] V. Buchoux, O.Cappe, E.Moulines, and A.Gorokhov, "On the Performance of Semi-Blind Subspace-Based Channel Estimation," *IEEE Transactions on Signal Processing*, vol. 48, pp. 1750–1759, June 2000. 82

[32] Jia-Chil Lin, "Leat-Squares Channel Estimation for Mobile OFDM Communication on Time-Varying Frequency-Selective Fading Channels," *IEEE Transactions on Vehicular Technology*, vol. 57, pp. 3538–3550, November 2008. 82

[33] J.H.Manton, V.Krishnamurthy, and H.V.Poor, "JamesStein state filtering algorithms," *IEEE Transactions on Signal Processing*, vol. 46, p. 24312447, September 1998. 82

[34] J.H.Manton, "Optimal Training Sequences and Pilot Tones for OFDM Systems," *IEEE Communications Letters*, vol. 5, pp. 151–153, April 2001. 82

[35] J. R. Magnus and H. Neudecker, *Matrix Differential Calculus with Applications in Statistics and Econometrics.* New York: Wiley, 1994. 82

[36] S. Kay, *Fundamentals of Statistical Signal Processing: Estimation Theory.* Prentice Hall, 1993. 82

[37] Nafisheh Shariati, Emil Bjornson, Mats Bengtsson, and Merouane Debbah, "Low-Complexity Channel Estimation in Large-Scale MIMO Using Polynomial

Expansion," *IEEE International Symposium on Personal, Indoor and Mobile Radio Communications*, April 2013. 82

[38] A. Papoulis, *Probability, Random Variables, and Stochastic Processes*, 3rd ed. Mcgraw-Hill College Division, 1993. 94

[39] Guan Gui, Abolfazi Mehbodniya, and Fumiyuki Adachi, "Least Mean Square/Fourth Algorithm with Application to Sparse Channel Estimation," 2013. 110

[40] S.Saleh Hosseini Bidaki, Siamak Talebi, and Mostafa Shahabinejad, "A Full-Rate Full-Diversity 2×2 Space-Time Block code with Linear Complexity for the Maximum Likelihood Receiver," *IEEE COMMUNICATION LETTERS*, vol. 15, pp. 842–844, August 2011. 110

[41] Rodrigo Carvajal, Kaushik Mahata, and J. C. Aguero, "Low Complexity Wiener Filtering in CDMA Systems Using a Class of Pseudo-Noise Spreading Codes," *IEEE COMMUNICATION LETTERS*, vol. 16, pp. 1357–1360, September 2012. 110

[42] Chengshan Xiao, Yahong Rosa Zheng, and N. C. Beaulieu, "Novel Sum-of-Sinusoids Simulation Models for Rayleigh and Rician Fading Channels," *IEEE Transactions on Wireless Communications*, vol. 5, December 2006. 110

[43] Huiling Zhu, Bin Xia, and Zhenhui Tan, "Performance Analysis of Alamouti Transmit Diversity with QAM in Imperfect Channel Estimation," *IEEE JOURNAL ON SELECTED AREAS IN COMMUNICATIONS*, vol. 29, pp. 1242–1248, June 2011. 110

[44] Naofal Al-Dhahir and A. H.Sayed, "The Finite-Length Multi-Input Multi-Output MMSE-DFE," *IEEE TRANSACTIONS ON SIGNAL PROCESSING*, vol. 48, pp. 2921–2936, October 2000. 110

[45] K. E.Baddour and N. C.Beaulieu, "Autoregressive Modeling for Fading Channel Simlation," *IEEE TRANSACTIONS ON WIRELESS COMMUNICATIOS*, vol. 4, pp. 1650–1662, July 2005. 110

[46] D. S.Baum and Helmut Bolcskei, "Information-Teoretic Analysis of MIMO Channel Sounding," *IEEE TRANSACTIONS ON IFORMATION THEORY*, vol. 57, pp. 7555–7577, November 2011. 110

[47] Werner Weichselberger, Markus Herdin, Huseyin Ozcelik, and Ernst Bonek, "A Stochastic MIMO Channel Model With Joint Correlation of Both Link Ends," *IEEE Transactions on Wireless Communications*, vol. 5, pp. 90–100, January 2006. 110

# Appendix A
# Wiener Filter Coefficients, Second Order Approximation

Substituting $\mathbf{R}$ and $\boldsymbol{\rho}_e$ from (4.16) and (4.20) accordingly into (4.1) one may derive:

$$\begin{aligned}
&\left(\mathbf{R}+\gamma_p^{-1}\mathbf{I}\right)\mathbf{h}_{e_2}=\boldsymbol{\rho}_e \\
&\left(\vec{\mathbf{1}}_N\vec{\mathbf{1}}_N^H+\Delta\underline{\mathcal{E}}+\gamma_p^{-1}\mathbf{I}\right)\mathbf{h}_{e_2}=\vec{\mathbf{1}}_N+\Delta\underline{\boldsymbol{\rho}_e} \\
&\left(\vec{\mathbf{1}}_N\vec{\mathbf{1}}_N^H+\gamma_p^{-1}\mathbf{I}\right)\mathbf{h}_{e_2}+\Delta\underline{\mathcal{E}}\mathbf{h}_{e_2}=\vec{\mathbf{1}}_N+\Delta\underline{\boldsymbol{\rho}_e} \\
&\left(\vec{\mathbf{1}}_N\vec{\mathbf{1}}_N^H+\gamma_p^{-1}\mathbf{I}\right)\mathbf{h}_{e_2}=\vec{\mathbf{1}}_N+\Delta\underline{\boldsymbol{\rho}_e}-\Delta\underline{\mathcal{E}}\mathbf{h}_{e_2}
\end{aligned} \tag{A.1}$$

Now we multiply both sides by $\left(\vec{\mathbf{1}}_N\vec{\mathbf{1}}_N^H+\gamma_p^{-1}\mathbf{I}\right)^{-1}$ from the left:

$$\mathbf{h}_{e_2}=\left(\vec{\mathbf{1}}_N\vec{\mathbf{1}}_N^H+\gamma_p^{-1}\mathbf{I}\right)^{-1}\left(\vec{\mathbf{1}}_N+\Delta\underline{\boldsymbol{\rho}_e}-\Delta\underline{\mathcal{E}}\mathbf{h}_{e_2}\right) \tag{A.2}$$

If we flip sides of the equation and open the brackets:

$$\begin{aligned}
&\left(\vec{\mathbf{1}}_N\vec{\mathbf{1}}_N^H+\gamma_p^{-1}\mathbf{I}\right)^{-1}\left(\vec{\mathbf{1}}_N+\Delta\underline{\boldsymbol{\rho}_e}\right)-\left(\vec{\mathbf{1}}_N\vec{\mathbf{1}}_N^H+\gamma_p^{-1}\mathbf{I}\right)^{-1}\Delta\underline{\mathcal{E}}\mathbf{h}_{e_2}=\mathbf{h}_{e_2} \\
&\left(\vec{\mathbf{1}}_N\vec{\mathbf{1}}_N^H+\gamma_p^{-1}\mathbf{I}\right)^{-1}\left(\vec{\mathbf{1}}_N+\Delta\underline{\boldsymbol{\rho}_e}\right)=\left(\left(\vec{\mathbf{1}}_N\vec{\mathbf{1}}_N^H+\gamma_p^{-1}\mathbf{I}\right)^{-1}\Delta\underline{\mathcal{E}}+\mathbf{I}\right)\mathbf{h}_{e_2}
\end{aligned} \tag{A.3}$$

As in section 4.1 we may again apply Sherman-Morrison identity:

$$\left(\vec{\mathbf{1}}_N\vec{\mathbf{1}}_N^H+\gamma_p^{-1}\mathbf{I}\right)^{-1}=\left(\gamma_p\mathbf{I}-\frac{\gamma_p^2}{1+N\gamma_p}\vec{\mathbf{1}}_N\vec{\mathbf{1}}_N^H\right) \tag{A.4}$$

Therefore the equation (A.3) becomes:

$$\left(\gamma_p \mathbf{I} - \frac{\gamma_p^2}{1+N\gamma_p}\vec{\mathbf{1}}_N\vec{\mathbf{1}}_N^H\right)\left(\vec{\mathbf{1}}_N + \Delta\underline{\boldsymbol{\rho}_e}\right) = \tag{A.5}$$
$$= \left(\left(\gamma_p \mathbf{I} - \frac{\gamma_p^2}{1+N\gamma_p}\vec{\mathbf{1}}_N\vec{\mathbf{1}}_N^H\right)\Delta\underline{\mathcal{E}} + \mathbf{I}\right)\mathbf{h}_{e_2}$$

$$\mathbf{h}_{e_2} = \left(\mathbf{I} + \left(\gamma_p \mathbf{I} - \frac{\gamma_p^2}{1+N\gamma_p}\vec{\mathbf{1}}_N\vec{\mathbf{1}}_N^H\right)\Delta\underline{\mathcal{E}}\right)^{-1} \cdot \tag{A.6}$$
$$\cdot \left(\frac{\gamma_p}{1+N\gamma_p}\vec{\mathbf{1}}_N + \left(\gamma_p \mathbf{I} - \frac{\gamma_p^2}{1+N\gamma_p}\vec{\mathbf{1}}_N\vec{\mathbf{1}}_N^H\right)\Delta\underline{\boldsymbol{\rho}_e}\right)$$

If we denote $\mathbf{A}$ as follows:

$$\mathbf{A} = \left(\gamma_p \mathbf{I} - \frac{\gamma_p^2}{1+N\gamma_p}\vec{\mathbf{1}}_N\vec{\mathbf{1}}_N^H\right) \tag{A.7}$$

and

$$\mathbf{h}_{N_0} = \frac{1}{N}\vec{\mathbf{1}}_N \tag{A.8}$$

equation (A.6) takes a form of:

$$\mathbf{h}_{e_2} = (\mathbf{I} + \mathbf{A}\Delta\underline{\mathcal{E}})^{-1} \cdot \left(\frac{N\gamma_p}{1+N\gamma_p}\mathbf{h}_{N_0} + \mathbf{A}\Delta\underline{\boldsymbol{\rho}_e}\right) \tag{A.9}$$

If we assume, that

$$\| \mathbf{A}\Delta\underline{\mathcal{E}} \| \ll 1 \tag{A.10}$$

equation (A.9) could be further simplified by using the following identity:

$$(\mathbf{I} + \mathbf{A}\Delta\underline{\mathcal{E}})^{-1} \approx \mathbf{I} - \mathbf{A}\Delta\underline{\mathcal{E}} \tag{A.11}$$

Hence (A.9) equals:

$$\begin{aligned}\mathbf{h}_{e_2} = &\left(\mathbf{I} - \left(\gamma_p\mathbf{I} - \frac{\gamma_p^2}{1+N\gamma_p}\vec{\mathbf{1}}_N\vec{\mathbf{1}}_N^H\right)\Delta\underline{\mathcal{E}}\right)\cdot \\ &\cdot\left(\frac{N\gamma_p}{1+N\gamma_p}\mathbf{h}_{N_0} + \left(\gamma_p\mathbf{I} - \frac{\gamma_p^2}{1+N\gamma_p}\vec{\mathbf{1}}_N\vec{\mathbf{1}}_N^H\right)\Delta\underline{\boldsymbol{\rho}_e}\right) = \\ &= \frac{N\gamma_p}{1+N\gamma_p}\mathbf{h}_{N_0} + \left(\gamma_p\mathbf{I} - \frac{\gamma_p^2}{1+N\gamma_p}\vec{\mathbf{1}}_N\vec{\mathbf{1}}_N^H\right)\Delta\underline{\boldsymbol{\rho}_e} - \\ &- \left(\gamma_p\mathbf{I} - \frac{\gamma_p^2}{1+N\gamma_p}\vec{\mathbf{1}}_N\vec{\mathbf{1}}_N^H\right)\Delta\underline{\mathcal{E}}\cdot\frac{N\gamma_p}{1+N\gamma_p}\mathbf{h}_{N_0} + \\ &+ \cancel{\left(\gamma_p\mathbf{I} - \frac{\gamma_p^2}{1+N\gamma_p}\vec{\mathbf{1}}_N\vec{\mathbf{1}}_N^H\right)^2}\Delta\underline{\mathcal{E}}\Delta\underline{\boldsymbol{\rho}_e}\end{aligned} \tag{A.12}$$

The last part of the equation is canceled because the multiplication $\Delta\underline{\mathcal{E}}\Delta\underline{\boldsymbol{\rho}_e}$ defines higher order term which might be neglected. After a little reorganization of terms Wiener coefficients are:

$$\mathbf{h}_{e_2} = \frac{N\gamma_p}{1+N\gamma_p}\mathbf{h}_{N_0} + \left(\gamma_p\mathbf{I} - \frac{\gamma_p^2}{1+N\gamma_p}\vec{\mathbf{1}}_N\vec{\mathbf{1}}_N^H\right)\left(\Delta\underline{\boldsymbol{\rho}_e} - \frac{N\gamma_p}{1+N\gamma_p}\Delta\underline{\mathcal{E}}\mathbf{h}_{N_0}\right) \tag{A.13}$$

or

$$\mathbf{h}_{e_2} = \frac{N\gamma_p}{1+N\gamma_p}\mathbf{h}_{N_0} + \mathbf{A}\left(\Delta\underline{\boldsymbol{\rho}_e} - \frac{N\gamma_p}{1+N\gamma_p}\Delta\underline{\mathcal{E}}\mathbf{h}_{N_0}\right) \tag{A.14}$$

# Appendix B
# Estimation Error, Second Order Approximation

We want to calculate estimation error for the second order approximation case, which is given by:

$$\sigma_{e_2}^2 = 1 - \mathbf{h}_{e_2}^H \left( \vec{\mathbf{1}}_N \vec{\mathbf{1}}_N^H + \Delta\underline{\mathcal{E}} + \gamma_p^{-1}\mathbf{I} \right) \mathbf{h}_{e_2} \tag{B.1}$$

when the expressions for $\mathbf{h}_{e_2}$ and $\Delta\underline{\mathcal{E}}$ are given by equations (4.25) and (4.17). Lets calculate first the multiplication of a column vector $\mathbf{h}_{e_2}$ from the right side of the noisy approximated matrix:

$$\begin{aligned}
&\left( \vec{\mathbf{1}}_N \vec{\mathbf{1}}_N^H + \Delta\underline{\mathcal{E}} + \gamma_p^{-1}\mathbf{I} \right) \mathbf{h}_{e_2} = \qquad (B.2)\\
&= \left( \vec{\mathbf{1}}_N \vec{\mathbf{1}}_N^H + \Delta\underline{\mathcal{E}} + \gamma_p^{-1}\mathbf{I} \right) \left[ \frac{N\gamma_p}{1+N\gamma_p}\mathbf{h}_{N_0} + \right.\\
&\left. + \left( \gamma_p\mathbf{I} - \frac{\gamma_p^2}{1+N\gamma_p}\vec{\mathbf{1}}_N\vec{\mathbf{1}}_N^H \right) \left( \Delta\underline{\boldsymbol{\rho}_e} - \frac{N\gamma_p}{1+N\gamma_p}\Delta\underline{\mathcal{E}}\mathbf{h}_{N_0} \right) \right] =\\
&= \underbrace{\frac{N\gamma_p}{1+N\gamma_p}\vec{\mathbf{1}}_N\vec{\mathbf{1}}_N^H\mathbf{h}_{N_0}}_{1^*} +\\
&+ \underbrace{\vec{\mathbf{1}}_N\vec{\mathbf{1}}_N^H \left( \gamma_p\mathbf{I} - \frac{\gamma_p^2}{1+N\gamma_p}\vec{\mathbf{1}}_N\vec{\mathbf{1}}_N^H \right)}_{2^*} \left( \Delta\underline{\boldsymbol{\rho}_e} - \frac{N\gamma_p}{1+N\gamma_p}\Delta\underline{\mathcal{E}}\mathbf{h}_{N_0} \right) +\\
&+ \frac{N\gamma_p}{1+N\gamma_p}\Delta\underline{\mathcal{E}}\mathbf{h}_{N_0} +\\
&+ \underbrace{\Delta\underline{\mathcal{E}} \left( \gamma_p\mathbf{I} - \frac{\gamma_p^2}{1+N\gamma_p}\vec{\mathbf{1}}_N\vec{\mathbf{1}}_N^H \right) \left( \Delta\underline{\boldsymbol{\rho}_e} - \frac{N\gamma_p}{1+N\gamma_p}\Delta\underline{\mathcal{E}}\mathbf{h}_{N_0} \right)}_{3^*} +
\end{aligned}$$

$$
\begin{aligned}
&+\frac{1}{\gamma_p}\frac{N\gamma_p}{1+N\gamma_p}\mathbf{h}_{N_0}+\\
&+\frac{1}{\gamma_p}\left(\gamma_p\mathbf{I}-\frac{\gamma_p^2}{1+N\gamma_p}\vec{\mathbf{1}}_N\vec{\mathbf{1}}_N^H\right)\left(\Delta\underline{\boldsymbol{\rho}_e}-\frac{N\gamma_p}{1+N\gamma_p}\Delta\underline{\mathcal{E}}\mathbf{h}_{N_0}\right)=\\
&=\frac{N\gamma_p}{1+N\gamma_p}\vec{\mathbf{1}}_N+\vec{\mathbf{1}}_N\vec{\mathbf{1}}_N^H\frac{\gamma_p}{1+N\gamma_p}\left(\Delta\underline{\boldsymbol{\rho}_e}-\frac{N\gamma_p}{1+N\gamma_p}\Delta\underline{\mathcal{E}}\mathbf{h}_{N_0}\right)+\\
&+\frac{N\gamma_p}{1+N\gamma_p}\Delta\underline{\mathcal{E}}\mathbf{h}_{N_0}+\frac{1}{\gamma_p}\frac{N\gamma_p}{1+N\gamma_p}\mathbf{h}_{N_0}+\\
&+\left(\mathbf{I}-\frac{\gamma_p}{1+N\gamma_p}\vec{\mathbf{1}}_N\vec{\mathbf{1}}_N^H\right)\left(\Delta\underline{\boldsymbol{\rho}_e}-\frac{N\gamma_p}{1+N\gamma_p}\Delta\underline{\mathcal{E}}\mathbf{h}_{N_0}\right)=\\
&=\frac{N\gamma_p}{1+N\gamma_p}\vec{\mathbf{1}}_N+\vec{\mathbf{1}}_N\vec{\mathbf{1}}_N^H\frac{\gamma_p}{1+N\gamma_p}\Delta\underline{\boldsymbol{\rho}_e}-\vec{\mathbf{1}}_N\vec{\mathbf{1}}_N^H\frac{N\gamma_p^2}{\left(1+N\gamma_p\right)^2}\Delta\underline{\mathcal{E}}\mathbf{h}_{N_0}+\\
&+\frac{N\gamma_p}{1+N\gamma_p}\Delta\underline{\mathcal{E}}\mathbf{h}_{N_0}+\frac{N}{1+N\gamma_p}\mathbf{h}_{N_0}+\Delta\underline{\boldsymbol{\rho}_e}-\frac{N\gamma_p}{1+N\gamma_p}\Delta\underline{\mathcal{E}}\mathbf{h}_{N_0}-\\
&-\frac{\gamma_p}{1+N\gamma_p}\vec{\mathbf{1}}_N\vec{\mathbf{1}}_N^H\Delta\underline{\boldsymbol{\rho}_e}+\frac{N\gamma_p^2}{\left(1+N\gamma_p\right)^2}\vec{\mathbf{1}}_N\vec{\mathbf{1}}_N^H\Delta\underline{\mathcal{E}}\mathbf{h}_{N_0}=\\
&=\frac{N\gamma_p}{1+N\gamma_p}\vec{\mathbf{1}}_N+\frac{1}{1+N\gamma_p}\vec{\mathbf{1}}_N+\Delta\underline{\boldsymbol{\rho}_e}=\frac{N\gamma_p+1}{1+N\gamma_p}\vec{\mathbf{1}}_N+\Delta\underline{\boldsymbol{\rho}_e}=\vec{\mathbf{1}}_N+\Delta\underline{\boldsymbol{\rho}_e}
\end{aligned}
$$

1*

$$
\frac{N\gamma_p}{1+N\gamma_p}\vec{\mathbf{1}}_N\vec{\mathbf{1}}_N^H\mathbf{h}_{N_0}=\vec{\mathbf{1}}_N\vec{\mathbf{1}}_N^H\vec{\mathbf{1}}_N\frac{N\gamma_p}{1+N\gamma_p}\frac{1}{N}=\frac{N\gamma_p}{1+N\gamma_p}\vec{\mathbf{1}}_N \tag{B.3}
$$

2*

$$
\begin{aligned}
&\vec{\mathbf{1}}_N\vec{\mathbf{1}}_N^H\left(\gamma_p\mathbf{I}-\frac{\gamma_p^2}{1+N\gamma_p}\vec{\mathbf{1}}_N\vec{\mathbf{1}}_N^H\right)= \qquad (B.4)\\
&=\gamma_p\vec{\mathbf{1}}_N\vec{\mathbf{1}}_N^H-\frac{\gamma_p^2\vec{\mathbf{1}}_N\vec{\mathbf{1}}_N^H\vec{\mathbf{1}}_N\vec{\mathbf{1}}_N^H}{1+N\gamma_p}=\gamma_p\vec{\mathbf{1}}_N\vec{\mathbf{1}}_N^H-\frac{\gamma_p^2N\vec{\mathbf{1}}_N\vec{\mathbf{1}}_N^H}{1+N\gamma_p}=\\
&=\vec{\mathbf{1}}_N\vec{\mathbf{1}}_N^H\frac{\gamma_p+N\gamma_p^2-N\gamma_p^2}{1+N\gamma_p}=\vec{\mathbf{1}}_N\vec{\mathbf{1}}_N^H\frac{\gamma_p}{1+N\gamma_p}
\end{aligned}
$$

3* This part is neglected as a multiplication of higher order terms

Therefore:

$$\left(\vec{\mathbf{1}}_N\vec{\mathbf{1}}_N^H + \Delta\underline{\mathcal{E}} + \gamma_p^{-1}\mathbf{I}\right)\mathbf{h}_{e_2} = \vec{\mathbf{1}}_N + \Delta\underline{\boldsymbol{\rho}_e} \tag{B.5}$$

Now we can calculate the left-hand multiplication of the equation (B.1):

$$\begin{aligned}
&\mathbf{h}_{e_2}^H\left(\vec{\mathbf{1}}_N\vec{\mathbf{1}}_N^H + \Delta\underline{\mathcal{E}} + \gamma_p^{-1}\mathbf{I}\right)\mathbf{h}_{e_2} = \mathbf{h}_{e_2}^H\left(\vec{\mathbf{1}}_N + \Delta\underline{\boldsymbol{\rho}_e}\right) = \qquad \text{(B.6)}\\
&= \left[\frac{N\gamma_p}{1+N\gamma_p}\frac{1}{N}\vec{\mathbf{1}}_N^H + \right.\\
&\left. + \left(\Delta\underline{\boldsymbol{\rho}_e} - \frac{N\gamma_p}{1+N\gamma_p}\Delta\underline{\mathcal{E}}\mathbf{h}_{N_0}\right)^H\left(\gamma_p\mathbf{I} - \frac{\gamma_p^2}{1+N\gamma_p}\vec{\mathbf{1}}_N\vec{\mathbf{1}}_N^H\right)^H\right]\cdot\\
&\cdot\left(\vec{\mathbf{1}}_N + \Delta\underline{\boldsymbol{\rho}_e}\right) = \frac{\gamma_p}{1+N\gamma_p}\vec{\mathbf{1}}_N^H\vec{\mathbf{1}}_N + \\
&+ \underbrace{\left(\Delta\underline{\boldsymbol{\rho}_e}^H - \frac{\gamma_p}{1+N\gamma_p}\vec{\mathbf{1}}_N^H\Delta\underline{\mathcal{E}}^H\right)\left(\gamma_p\mathbf{I} - \frac{\gamma_p^2}{1+N\gamma_p}\vec{\mathbf{1}}_N\vec{\mathbf{1}}_N^H\right)\vec{\mathbf{1}}_N}_{4^*} + \\
&+ \frac{\gamma_p}{1+N\gamma_p}\vec{\mathbf{1}}_N^H\Delta\underline{\boldsymbol{\rho}_e} + \\
&+ \underbrace{\left(\Delta\underline{\boldsymbol{\rho}_e}^H - \frac{\gamma_p}{1+N\gamma_p}\vec{\mathbf{1}}_N^H\Delta\underline{\mathcal{E}}^H\right)\left(\gamma_p\mathbf{I} - \frac{\gamma_p^2}{1+N\gamma_p}\vec{\mathbf{1}}_N\vec{\mathbf{1}}_N^H\right)\Delta\underline{\boldsymbol{\rho}_e}}_{5^*} = \\
&= \frac{N\gamma_p}{1+N\gamma_p} + \frac{\gamma_p}{1+N\gamma_p}\Delta\underline{\boldsymbol{\rho}_e}^H\vec{\mathbf{1}}_N - \frac{\gamma_p^2}{\left(1+N\gamma_p\right)^2}\vec{\mathbf{1}}_N^H\Delta\underline{\mathcal{E}}\vec{\mathbf{1}}_N + \\
&+ \frac{\gamma_p}{1+N\gamma_p}\vec{\mathbf{1}}_N^H\Delta\underline{\boldsymbol{\rho}_e} = \\
&= \frac{N\gamma_p}{1+N\gamma_p} + \frac{\gamma_p}{1+N\gamma_p}\left(\Delta\underline{\boldsymbol{\rho}_e}^H\vec{\mathbf{1}}_N + \vec{\mathbf{1}}_N^H\Delta\underline{\boldsymbol{\rho}_e}\right) - \qquad \text{(B.7a)}\\
&- \frac{\gamma_p^2}{\left(1+N\gamma_p\right)^2}\vec{\mathbf{1}}_N^H\Delta\underline{\mathcal{E}}\vec{\mathbf{1}}_N = \\
&= \frac{N\gamma_p}{1+N\gamma_p} + 2\frac{\gamma_p}{1+N\gamma_p}\vec{\mathbf{1}}_N^H\Delta\underline{\boldsymbol{\rho}_e} - \frac{\gamma_p^2}{\left(1+N\gamma_p\right)^2}\vec{\mathbf{1}}_N^H\Delta\underline{\mathcal{E}}\vec{\mathbf{1}}_N
\end{aligned}$$

In (B.7a) we used the fact that $\Delta\underline{\boldsymbol{\rho}_e}$ and $\vec{\mathbf{1}}_N$ are real, therefore their conjugate transpose equals to their regular transpose, therefore the following statement is valid: $\Delta\underline{\boldsymbol{\rho}_e}^H\vec{\mathbf{1}}_N = \vec{\mathbf{1}}_N^H\Delta\underline{\boldsymbol{\rho}_e}$.

4*

$$\left(\Delta\underline{\boldsymbol{\rho}_e}^H - \frac{\gamma_p}{1+N\gamma_p}\vec{\mathbf{1}}_N^H\Delta\underline{\mathcal{E}}^H\right)\left(\gamma_p\mathbf{I} - \frac{\gamma_p^2}{1+N\gamma_p}\vec{\mathbf{1}}_N\vec{\mathbf{1}}_N^H\right)\vec{\mathbf{1}}_N = \tag{B.8a}$$

$$= \left(\Delta\underline{\boldsymbol{\rho}_e}^H - \frac{\gamma_p}{1+N\gamma_p}\vec{\mathbf{1}}_N^H\Delta\underline{\mathcal{E}}^H\right)\left(\gamma_p\vec{\mathbf{1}}_N - \frac{N\gamma_p^2\vec{\mathbf{1}}_N}{1+N\gamma_p}\right) =$$

$$\left(\Delta\underline{\boldsymbol{\rho}_e}^H - \frac{\gamma_p}{1+N\gamma_p}\vec{\mathbf{1}}_N^H\Delta\underline{\mathcal{E}}^H\right)\frac{\gamma_p}{1+N\gamma_p}\vec{\mathbf{1}}_N =$$

$$= \frac{\gamma_p}{1+N\gamma_p}\Delta\underline{\boldsymbol{\rho}_e}^H\vec{\mathbf{1}}_N - \frac{\gamma_p^2}{\left(1+N\gamma_p\right)^2}\vec{\mathbf{1}}_N^H\Delta\underline{\mathcal{E}}\vec{\mathbf{1}}_N$$

Where we used the fact, that $\Delta\underline{\mathcal{E}}^H = \Delta\underline{\mathcal{E}}$, because it is real and symmetric.

5* This part is neglected as a multiplication of higher order terms.

Therefore the expression for the estimation error is:

$$\sigma_{e_2}^2 = 1 - \frac{N\gamma_p}{1+N\gamma_p} - 2\frac{\gamma_p}{1+N\gamma_p}\vec{\mathbf{1}}_N^H\Delta\underline{\boldsymbol{\rho}_e} + \frac{\gamma_p^2}{\left(1+N\gamma_p\right)^2}\vec{\mathbf{1}}_N^H\Delta\underline{\mathcal{E}}\vec{\mathbf{1}}_N \tag{B.9}$$

which we can write in explicit way as follows:

$$\sigma_{e_2}^2 = 1 - NC(\gamma_p) + aT_s^2C(\gamma_p)\left[Ne^2 + 8(N_b+1)^2\cdot\right. \tag{B.10}$$

$$\left.\cdot\sum_{n=0}^{M-1}(M-n)^2\right] - 2aT_s^2C^2(\gamma_p)(N_b+1)^2\sum_{k=0}^{2M}\sum_{l=0}^{2M}(l-k)^2 =$$

$$= 1 - NC(\gamma_p) + aT_s^2NC(\gamma_p)\left[e^2 + \frac{4M}{3}(N_b+1)^2(M+1)\right] -$$

$$- \frac{4aMT_s^2N^2}{3}C^2(\gamma_p)(N_b+1)^2(M+1) =$$

$$= 1 - NC(\gamma_p)\left(1 - aT_s^2e^2\right) + \frac{4aT_s^2MNC(\gamma_p)}{3}(N_b+1)^2(M+1)(1-NC(\gamma_p))$$

or

$$\sigma_{e_2}^2 = 1 - NC(\gamma_p)\left(1 - aT_s^2 e^2\right) + \frac{4aMNT_s^2 C(\gamma_p)}{3}(N_b+1)^2(M+1)(1 - NC(\gamma_p)) \tag{B.11}$$

where

$$C(\gamma_p) = \frac{\gamma_p}{1 + N\gamma_p}$$

# Appendix C
# Extension to Complex Covariance Functions - Wiener Filter Coefficients

Any complex-valued covariance function has Taylor series expansion as follows:

$$R(\tau) \approx 1 + \frac{R^{'}(0)}{1!}\tau + \frac{R^{''}(0)}{2!}\tau^2 + O(\tau^3) = \\ = 1 + aj\tau - \frac{b}{2}\tau^2 + O(\tau^3) \tag{C.1}$$

Therefore correlation matrix $\mathbf{R}$ could be expressed as:

$$\mathbf{R} \approx \vec{\mathbf{1}}_N \vec{\mathbf{1}}_N^H + \Delta\underline{\mathcal{E}} = \vec{\mathbf{1}}_N \vec{\mathbf{1}}_N^H + \Delta\underline{\mathcal{E}}_{Re} + j\Delta\underline{\mathcal{E}}_{Im} \tag{C.2}$$

Where

$$\Delta\underline{\mathcal{E}}_{Im} = 2a(N_b+1)T_s\mathbf{E_1} \\ \mathbf{E_1}_{(kl)} = (l-k), \quad k,l = 1\cdots N \tag{C.3}$$

and

$$\Delta\underline{\mathcal{E}}_{Re} = -2b(N_b+1)^2T_s^2\mathbf{E_2} \\ \mathbf{E_2}_{(kl)} = (l-k)^2, \quad k,l = 1\cdots N \tag{C.4}$$

Vector $\boldsymbol{\rho}_e$ could be approximated then as follows:

$$\boldsymbol{\rho}_e \approx \vec{\mathbf{1}}_N + \Delta\underline{\boldsymbol{\rho}_e} = \vec{\mathbf{1}}_N + \Delta\underline{\boldsymbol{\rho}}_{e_{Re}} + j\Delta\underline{\boldsymbol{\rho}}_{e_{Im}} \tag{C.5}$$

where:

$$\begin{aligned} \Delta\underline{\boldsymbol{\rho}}_{e_{Im}} &= aT_s\mathbf{k_1} \\ \mathbf{k_1}_k &= \left[2(N_b+1)(\frac{N-1}{2}+1-k)-e\right] \\ k &= 1,\dots N \end{aligned} \tag{C.6}$$

and

$$\begin{aligned} \Delta\underline{\boldsymbol{\rho}}_{e_{Re}} &= -\frac{b}{2}T_s^2\mathbf{k_2} \\ \mathbf{k_2}_k &= \left[2(N_b+1)(\frac{N-1}{2}+1-k)-e\right]^2 \\ k &= 1,\dots N \end{aligned} \tag{C.7}$$

In order to find Wiener filter coefficients we use the result for real-valued covariance functions case, (A.9):

$$\mathbf{h}_{e_2} = (\mathbf{I}+\mathbf{A}\Delta\underline{\mathcal{E}})^{-1}\cdot\left(\frac{N\gamma_p}{1+N\gamma_p}\mathbf{h}_{N_0}+\mathbf{A}\Delta\underline{\boldsymbol{\rho}_e}\right) \tag{C.8}$$

where

$$\begin{aligned} \mathbf{A} &= \left(\gamma_p\mathbf{I}-\frac{\gamma_p^2}{1+N\gamma_p}\vec{\mathbf{1}}_N\vec{\mathbf{1}}_N^H\right) \\ \mathbf{h}_{N_0} &= \frac{1}{N}\vec{\mathbf{1}}_N \end{aligned} \tag{C.9}$$

and now:

$$\begin{aligned} \Delta\underline{\mathcal{E}} &= \Delta\underline{\mathcal{E}}_{Re}+j\Delta\underline{\mathcal{E}}_{Im} \\ \Delta\underline{\boldsymbol{\rho}_e} &= \Delta\underline{\boldsymbol{\rho}}_{e_{Re}}+j\Delta\underline{\boldsymbol{\rho}}_{e_{Im}} \end{aligned} \tag{C.10}$$

As previously, we can use the approximation:

$$\parallel \mathbf{A}\Delta\underline{\mathcal{E}} \parallel \ll 1 \tag{C.11}$$

And the equation (C.8) becomes:

$$\begin{aligned}\mathbf{h}_{e_2} &= \frac{N\gamma_p}{1+N\gamma_p}\mathbf{h}_{N_0} + \mathbf{A}\left(\Delta\underline{\boldsymbol{\rho}_e} - \frac{N\gamma_p}{1+N\gamma_p}\Delta\underline{\mathcal{E}}\mathbf{h}_{N_0}\right) = \\ &= \frac{N\gamma_p}{1+N\gamma_p}\mathbf{h}_{N_0} + \mathbf{A}\left(j\Delta\underline{\boldsymbol{\rho}}_{e_{Im}} + \Delta\underline{\boldsymbol{\rho}}_{e_{Re}} - \frac{N\gamma_p}{1+N\gamma_p}\left(j\Delta\underline{\mathcal{E}}_{Im} + \Delta\underline{\mathcal{E}}_{Re}\right)\mathbf{h}_{N_0}\right)\end{aligned} \tag{C.12}$$

or:

$$\begin{aligned}\mathbf{h}_{e_2} = \frac{N\gamma_p}{1+N\gamma_p}\mathbf{h}_{N_0} &+ \mathbf{A}\left(\Delta\underline{\boldsymbol{\rho}}_{e_{Re}} - \frac{N\gamma_p}{1+N\gamma_p}\Delta\underline{\mathcal{E}}_{Re}\mathbf{h}_{N_0}\right) + \\ &+ j\mathbf{A}\left(\Delta\underline{\boldsymbol{\rho}}_{e_{Im}} - \frac{N\gamma_p}{1+N\gamma_p}\Delta\underline{\mathcal{E}}_{Im}\mathbf{h}_{N_0}\right)\end{aligned} \tag{C.13}$$

# Appendix D
# Extension to Complex Covariance Functions - Estimation Error

Estimation error derivation is very similar to one that we done for real covariance functions in B, but now we need to keep in mind that matrices $\Delta\underline{\mathcal{E}}$ and $\Delta\underline{\boldsymbol{\rho}_e}$ are complex. The expression for MMSE is:

$$\sigma_{e_2}^2 = 1 - \mathbf{h}_{e_2}^H \left(\vec{\mathbf{1}}_N \vec{\mathbf{1}}_N^H + \Delta\underline{\mathcal{E}} + \gamma_p^{-1}\mathbf{I}\right) \mathbf{h}_{e_2} \tag{D.1}$$

when $\mathbf{h}_{e_2}$ was found in (C.13), and $\Delta\underline{\mathcal{E}}$ and $\Delta\underline{\boldsymbol{\rho}_e}$ are given by (C.2) - (C.4) and (C.5) - (C.7) respectively. The right hand side multiplication is exactly the same as we calculated in (B.2)-(B.5), therefore:

$$\left(\vec{\mathbf{1}}_N \vec{\mathbf{1}}_N^H + \Delta\underline{\mathcal{E}} + \gamma_p^{-1}\mathbf{I}\right) \mathbf{h}_{e_2} = \vec{\mathbf{1}}_N + \Delta\underline{\boldsymbol{\rho}_e} \tag{D.2}$$

Note, that $\Delta\underline{\boldsymbol{\rho}_e}$ is complex now. Left hand side multiplication takes the form of:

$$\mathbf{h}_{e_2}^H\left(\vec{\mathbf{1}}_N\vec{\mathbf{1}}_N^H+\Delta\underline{\mathcal{E}}+\gamma_p^{-1}\mathbf{I}\right)\mathbf{h}_{e_2}=\mathbf{h}_{e_2}^H\left(\vec{\mathbf{1}}_N+\Delta\underline{\boldsymbol{\rho}_e}\right)= \tag{D.3}$$

$$=\left[\frac{N\gamma_p}{1+N\gamma_p}\frac{1}{N}\vec{\mathbf{1}}_N^H+\right.$$

$$\left.+\left(\Delta\underline{\boldsymbol{\rho}_e}-\frac{N\gamma_p}{1+N\gamma_p}\Delta\underline{\mathcal{E}}\mathbf{h}_{N_0}\right)^H\left(\gamma_p\mathbf{I}-\frac{\gamma_p^2}{1+N\gamma_p}\vec{\mathbf{1}}_N\vec{\mathbf{1}}_N^H\right)^H\right]\cdot$$

$$\cdot\left(\vec{\mathbf{1}}_N+\Delta\underline{\boldsymbol{\rho}_e}\right)=\frac{\gamma_p}{1+N\gamma_p}\vec{\mathbf{1}}_N^H\vec{\mathbf{1}}_N+$$

$$+\left(\Delta\underline{\boldsymbol{\rho}_e}^H-\frac{\gamma_p}{1+N\gamma_p}\vec{\mathbf{1}}_N^H\Delta\underline{\mathcal{E}}^H\right)\left(\gamma_p\mathbf{I}-\frac{\gamma_p^2}{1+N\gamma_p}\vec{\mathbf{1}}_N\vec{\mathbf{1}}_N^H\right)\vec{\mathbf{1}}_N+$$

$$+\frac{\gamma_p}{1+N\gamma_p}\vec{\mathbf{1}}_N^H\Delta\underline{\boldsymbol{\rho}_e}+$$

$$+\underbrace{\left(\Delta\underline{\boldsymbol{\rho}_e}^H-\frac{\gamma_p}{1+N\gamma_p}\vec{\mathbf{1}}_N^H\Delta\underline{\mathcal{E}}^H\right)\left(\gamma_p\mathbf{I}-\frac{\gamma_p^2}{1+N\gamma_p}\vec{\mathbf{1}}_N\vec{\mathbf{1}}_N^H\right)\Delta\underline{\boldsymbol{\rho}_e}}_{\text{higher order term}}=$$

$$=\frac{N\gamma_p}{1+N\gamma_p}+\left(\Delta\underline{\boldsymbol{\rho}_e}^H-\frac{\gamma_p}{1+N\gamma_p}\vec{\mathbf{1}}_N^H\Delta\underline{\mathcal{E}}^H\right)\left(\gamma_p\vec{\mathbf{1}}_N-\frac{\gamma_p^2N\vec{\mathbf{1}}_N}{1+N\gamma_p}\right)+$$

$$+\frac{\gamma_p}{1+N\gamma_p}\vec{\mathbf{1}}_N^H\Delta\underline{\boldsymbol{\rho}_e}=$$

$$=\frac{N\gamma_p}{1+N\gamma_p}+\left(\Delta\underline{\boldsymbol{\rho}_e}^H-\frac{\gamma_p}{1+N\gamma_p}\vec{\mathbf{1}}_N^H\Delta\underline{\mathcal{E}}^H\right)\frac{\gamma_p}{1+N\gamma_p}\vec{\mathbf{1}}_N+\frac{\gamma_p}{1+N\gamma_p}\vec{\mathbf{1}}_N^H\Delta\underline{\boldsymbol{\rho}_e}=$$

$$=\frac{N\gamma_p}{1+N\gamma_p}+\frac{\gamma_p}{1+N\gamma_p}\left(\Delta\underline{\boldsymbol{\rho}_e}^H\vec{\mathbf{1}}_N+\vec{\mathbf{1}}_N^H\Delta\underline{\boldsymbol{\rho}_e}\right)-\frac{\gamma_p^2}{\left(1+N\gamma_p\right)^2}\vec{\mathbf{1}}_N^H\Delta\underline{\mathcal{E}}^H\vec{\mathbf{1}}_N=$$

$$=\frac{N\gamma_p}{1+N\gamma_p}+2\frac{\gamma_p}{1+N\gamma_p}\vec{\mathbf{1}}_N^H\Delta\underline{\boldsymbol{\rho}}_{e_{Re}}-\frac{\gamma_p^2}{\left(1+N\gamma_p\right)^2}\vec{\mathbf{1}}_N^H\Delta\underline{\mathcal{E}}_{Re}^H\vec{\mathbf{1}}_N+$$

$$+j\frac{\gamma_p^2}{\left(1+N\gamma_p\right)^2}\underbrace{\vec{\mathbf{1}}_N^H\Delta\underline{\mathcal{E}}_{Im}^H\vec{\mathbf{1}}_N}_{0}=$$

$$=\frac{N\gamma_p}{1+N\gamma_p}+2\frac{\gamma_p}{1+N\gamma_p}\vec{\mathbf{1}}_N^H\Delta\underline{\boldsymbol{\rho}}_{e_{Re}}-\frac{\gamma_p^2}{\left(1+N\gamma_p\right)^2}\vec{\mathbf{1}}_N^H\Delta\underline{\mathcal{E}}_{Re}^H\vec{\mathbf{1}}_N$$

Hence:

$$\sigma_{e_2}^2 = 1 - \frac{N\gamma_p}{1+N\gamma_p} - 2\frac{\gamma_p}{1+N\gamma_p}\vec{\mathbf{1}}_N^H \Delta\underline{\boldsymbol{\rho}}_{e_{Re}} + \frac{\gamma_p^2}{\left(1+N\gamma_p\right)^2}\vec{\mathbf{1}}_N^H \Delta\underline{\mathcal{E}}_{Re}^H \vec{\mathbf{1}}_N \tag{D.4}$$

Note, that the resulting estimation error is real, as it was expected. We may further expand the formula (D.4) and find the analytical representation of matrix and vectors multiplications. Thus:

$$\begin{aligned}\vec{\mathbf{1}}_N^H \Delta\underline{\mathcal{E}}_{Re}\vec{\mathbf{1}}_N &= -2bT_s^2(N_b+1)^2 \cdot \sum_{k=0}^{2M}\sum_{n=0}^{2M}(n-k)^2 = \\ &= -\frac{4bT_s^2MN^2}{3}(N_b+1)^2(M+1)\end{aligned} \tag{D.5}$$

$$\begin{aligned}\vec{\mathbf{1}}_N^H \Delta\underline{\boldsymbol{\rho}}_{e_{Re}} &= -\frac{bT_s^2}{2}\left[\sum_{k=0}^{M}((M-k)2(N_b+1)-e)^2 + \right. \\ &\left. + \sum_{k=0}^{M-1}(-(M-k)2(N_b+1)-e)^2\right] = \\ &= -\frac{bT_s^2}{2}\left[Ne^2 + 8(N_b+1)^2\sum_{k=0}^{M-1}(M-k)^2\right] = \\ &= -\frac{bT_s^2N}{2}\left[e^2 + \frac{4M}{3}(N_b+1)^2(M+1)\right]\end{aligned} \tag{D.6}$$

Therefore:

$$\begin{aligned}\sigma_{e_2}^2 &= 1 - NC(\gamma_p) + C(\gamma_p)bT_s^2Ne^2 + C(\gamma_p)bT_s^2N\frac{4M}{3}(N_b+1)^2(M+1) - \\ &- C^2(\gamma_p)\frac{4bT_s^2MN^2}{3}(N_b+1)^2(M+1) = \\ &= 1 - NC(\gamma_p)\left(1 - bT_s^2e^2\right) + \\ &+ \frac{4MbT_s^2NC(\gamma_p)}{3}(N_b+1)^2(M+1)\left(1 - NC(\gamma_p)\right)\end{aligned} \tag{D.7}$$

$$\sigma_{e_2}^2 = 1 - NC(\gamma_p)\left(1 - bT_s^2 e^2\right) + \\ + \frac{4MbT_s^2 NC(\gamma_p)}{3}(N_b+1)^2(M+1)\left(1 - NC(\gamma_p)\right) \tag{D.8}$$

where

$$C(\gamma_p) = \frac{\gamma_p}{1 + N\gamma_p}$$

# Curriculum Vitae

**Name:** Elena A. Uchiteleva

**Post-secondary Education and Degrees:**

2011-2013 M.E.Sc.
Wireless Communications Engineering
The University of Western Ontario
London, Ontario, Canada

2006-2010 B.Sc.
Electrical Engineering
The Technion - Israel Institute of Technology
Haifa, Israel

**Related Work Experience**

2011-2013
Teaching Assistance
The University of Western Ontario
London, Ontario, Canada

ECE 3374 - Introduction to Electronics for Mechanical Engineering
ECE 2240 - Electrical Laboratory
ECE 3374 - Electromagnetics Theory

**Honours and Awards**

June 2012
Outstanding Presentation in Graduate Symposium 2012
Communication Systems and Data Networking Presentations
The University of Western Ontario
London, Ontario, Canada